



**HAL**  
open science

## Surface assisted self-assembly of peptides

Cécile Vigier-Carriere

► **To cite this version:**

Cécile Vigier-Carriere. Surface assisted self-assembly of peptides. Theoretical and/or physical chemistry. Université de Strasbourg, 2016. English. NNT : 2016STRAE013 . tel-01585566

**HAL Id: tel-01585566**

**<https://theses.hal.science/tel-01585566v1>**

Submitted on 11 Sep 2017

**HAL** is a multi-disciplinary open access archive for the deposit and dissemination of scientific research documents, whether they are published or not. The documents may come from teaching and research institutions in France or abroad, or from public or private research centers.

L'archive ouverte pluridisciplinaire **HAL**, est destinée au dépôt et à la diffusion de documents scientifiques de niveau recherche, publiés ou non, émanant des établissements d'enseignement et de recherche français ou étrangers, des laboratoires publics ou privés.



*ECOLE DOCTORALE Physique et Chimie Physique*

Institut Charles Sadron, CNRS-UPR22

## THESE

pour obtenir le grade de :

**Docteur de l'Université de Strasbourg**

Discipline: Chimie-Physique

Présentée et soutenue le **05 septembre 2016** par :

**Cécile VIGIER-CARRIERE**

# Contrôle de l'auto-assemblage de peptides par une surface modifiée

**Surface assisted self-assembly of peptides**

---

### Membres du jury

<i>Directrice :</i>	Fouzia BOULMEDAIS	Chargée de recherches, HDR, CNRS, Strasbourg
<i>Rapporteurs :</i>	Thibaud CORADIN	Directeur de recherches, Collège de France, CNRS, Paris
	Sophie DEMOUSTIER	Professeur, Ecole Polytechnique de Louvain, Belgique
<i>Examineur :</i>	Mir Wais HOSSEINI	Professeur, Université de Strasbourg
<i>Invités :</i>	Pierre SCHAAF	Professeur, Université de Strasbourg
	Loïc JIERRY	Maître de conférences, Université de Strasbourg





# Remerciements

Je souhaite tout d'abord remercier, Fouzia Boulmedais, Loïc Jierry et Pierre Schaaf pour la confiance qu'ils m'ont accordée dès le début de cette aventure.

Merci Fouzia pour ta disponibilité, ta patience, ton implication au quotidien et tes précieux conseils. Ton expérience m'a permis de comprendre la physico-chimie et beaucoup d'autres choses. Je remercie également Loïc Jierry pour son dynamisme, son enthousiasme et sa grande pédagogie scientifique qui ont rendu ces trois ans de thèse simple. Enfin je tiens à remercier le charismatique Pierre Schaaf d'avoir pris le temps de suivre ce projet de près. Merci à lui d'avoir partagé sa passion pour la science, sa précieuse expérience et sa créativité.

Je remercie les membres de mon jury le Pr. Mir Wais Hosseini, Dr. Thibaud Coradin et le Pr. Sophie Demoustier, qui ont accepté de juger ces trois années de recherche.

Je voudrais également remercier l'ensemble de l'unité Inserm U1121 « Biomatériaux et Bioingénierie » pour son accueil : Merci à Sarah Zaouani, Angela Mutsliher, Florian Ponzio et Philippe Laval. Un très grand merci à Morgane Rabineau pour la réalisation de mesures en microscopie confocale, Joseph Hemmerlé pour la réalisation de mesures AFM, MEB et TEM, enfin merci à Bernard Senger d'avoir apporté son analyse sur certains résultats.

Je remercie tous mes collègues de l'institut Charles Sadron pour leur aide, notamment Marc Schmutz pour son travail en cryo-MEB.

Merci à l'équipe Lutz du 3<sup>ème</sup> étage Guillaume, Niklas, Gianni, Roza, Sophia, Aziz, Denise, Eliot, Benoit pour leur sympathie, et surtout un grand merci à Chloé une belle rencontre qui a partagé sa bonne humeur et m'a accordé son oreille attentive au quotidien.

J'aimerais remercier tous mes collègues/amis de l'équipe IMI avec qui j'ai partagé ces trois dernières années : merci à Pauline, Mélodie, Fabien, Johan, Lydie, Elodie, Véro, Alexandre,

Janwa et Lionel et à mes colocataires de laboratoires : To<sup>2</sup> qui a partagé son savoir mais aussi toutes ses anecdotes incroyables, Baptiste le roi de la blague, Julien pour sa bonne humeur qui a beaucoup participé à l'ambiance du laboratoire et Paolo pour son soutien et avec qui j'ai partagé toutes ces discussions sur tout et rien.

Je voudrais tout spécialement remercier Déborah Wagner sans qui cette thèse n'aurait pas été pareille et à qui je dois énormément.

MERCI Clément, mon binôme « Doctorants 2013 ! » qui est devenu mon ami au fil de ces années. Nous avons vécu ensemble les joies et les difficultés de la thèse. Ta bonne humeur et ton humour sans faille rendent la vie simple. Merci pour ta « zénitude », ton soutien et tes conseils.

Un grand merci à mes parents, mes grands-parents et mon frère pour leur soutien pendant ces longues études et mes amis strasbourgeois avec qui j'ai partagé ces 8 années : Lulu, Thomas, Marie, Marion, Marine, Badou. Merci Pit pour cette curiosité sans fin qui mène toujours à de belles discussions. Enfin, je souhaite remercier trois personnes très importantes : Julie, Morgane et Solène ont été pour moi une seconde famille strasbourgeoise ; Merci pour votre présence quoi qu'il arrive, vous m'avez beaucoup apporté, tous ces après-midis, week-end, et soirées passés ensemble sont de très beaux souvenirs.

# Table of Contents

<b>List of abbreviations</b>	<b>iv</b>
<b>General Introduction</b>	<b>1</b>
<b>Chapter 1: Bibliographic review</b>	<b>7</b>
<b>1.1 Supramolecular hydrogels of small molecules</b>	<b>10</b>
1.1.1 Classification of gels	10
1.1.2 Low molecular weight gelation process	11
1.1.3 Peptide based hydrogels	12
1.1.3.1 Amino acid building blocks and their classification	13
1.1.3.2 Peptide sequences for the design of efficient hydrogelators	15
1.1.4 Toward the design of responsive hydrogels based on aromatic PA	20
1.1.4.1 Gelation of LMWG triggered by physical stimuli	21
1.1.4.2 Gelation of LMWG triggered by chemical stimuli	21
1.1.5 Enzymatic-responsive hydrogel	25
<b>1.2 Surface-assisted self-assembly of LMWG</b>	<b>27</b>
1.2.1 Surface seeding of LMWG self-assembly	28
1.2.2 Surface induced pH responsive self-assembly of LMWG	32
1.2.2.1 Surface-confined acidic catalyst for self-assembly of LMWG	33
1.2.2.2 Electrochemical trigger of pH-responsive self-assembly of peptides	34
1.2.3 Localized enzyme assisted self-assembly of peptides (LEASA)	41
<b>1.3 Polyelectrolyte multilayer films</b>	<b>43</b>
1.3.1 Polyelectrolyte Multilayer assemblies	44
1.3.2 Deposition methods	45
1.3.3 Growth regime and tunable properties of PEM films	46
1.3.4 Coating features and applications	48
<b>References</b>	<b>50</b>

## **Chapter 2: Materials and methods** **59**

<b>2.1 Materials</b> .....	<b>61</b>
2.1.1 Buffer solutions.....	61
2.1.2 Polymers and enzymes.....	61
2.1.3 Preparation and characterization of molecules.....	62
<b>2.2 Methods: Physical-chemical characterizations</b> .....	<b>63</b>
2.2.1 Quartz crystal microbalance with dissipation.....	63
2.2.1.1 Principle of the QCM-D.....	63
2.2.2 Atomic force microscopy.....	65
2.2.2.1 Principle of AFM.....	65
2.2.3 Fourier transform Infrared spectroscopy.....	67
2.2.3.1 Principle of infrared spectroscopy.....	67
2.2.3.2 Fourier transform infrared spectroscopy.....	69
2.2.3.3 FTIR attenuated total reflection.....	70
2.2.4 UV-visible spectroscopy.....	72
2.2.4.1 Principle of enzymatic assay.....	72
2.2.5 Confocal laser scanning microscopy.....	73
<b>References</b> .....	<b>74</b>

## **Chapter 3: Spatiotemporal tuning of peptides nanofibers growth from an enzyme-modified surface** **75**

<b>3.1 Abstract</b> .....	<b>77</b>
<b>3.2 Introduction</b> .....	<b>78</b>
<b>3.3 Results and discussion</b> .....	<b>79</b>
3.3.1 Localized enzymatic assisted self-assembly of (KL) <sub>n</sub> OEt.....	79
3.3.2 Toward the temporal control of the self-assembly and nanofibers growth.....	84
<b>3.4 Conclusion</b> .....	<b>88</b>
<b>3.5 Supporting Information</b> .....	<b>89</b>
3.5.1 Material and methods.....	89
3.5.1.1 List of Chemicals.....	89
3.5.1.2 Synthesis of Lysine-Leucine ethyl ester (KLOEt) and $\alpha$ -chymotrypsin <sup>RHO</sup> .....	90
3.5.1.2 Multilayer film preparation and hydrogel self-assembly.....	92
3.5.1.3 Fluorescence Microscopy.....	93

3.5.1.4 Circular Dichroism (CD).....	93
3.5.1.5 Matrix-Assisted Laser Desorption/Ionization Time-of-Flight (MALDI-TOF).....	93
3.5.1.6 Cryo-Scanning Electron Microscopy (cryo-SEM).....	94
3.5.1.7 Wet Scanning Transmission Electron Microscopy (Wet STEM).....	94
3.5.3 Supporting figures.....	95
<b>References.....</b>	<b>101</b>

## **Chapter 4: Bioactive seed layer for surface sonfined self-assembly of peptides 103**

<b>4.1 Abstract.....</b>	<b>105</b>
<b>4.2 Introduction.....</b>	<b>106</b>
<b>4.3 Results and discussion.....</b>	<b>107</b>
<b>4.4 Conclusion.....</b>	<b>112</b>
<b>4.5 Supporting information.....</b>	<b>113</b>
4.5.1 Materials and methods.....	113
4.5.1.1 List of chemicals.....	113
4.5.1.2 Peptides characterization and preparation of modified PAA-CGGG-Fmoc and PAA-CFF-Fmoc.....	114
4.5.1.3 Preparation of modified PAA: PAA-CFF-Fmoc and PAA-CGGG-Fmoc.....	116
4.5.1.4 Multilayer film preparation and hydrogel self-assembly.....	120
4.5.1.5 Fluorescence spectroscopy.....	120
4.5.2 Preliminary tests of gelation in vials.....	121
4.5.3 Influence of the decrease of ALP density on the hydrogel formation.....	122
4.5.4 Supporting figures.....	123
<b>References.....</b>	<b>127</b>

## **General conclusion and outlooks 129**

## **Annexes 133**

# List of abbreviations

## A

AFM	Atomic force microscopy
ALP	Alkaline phosphatase
AP	Aggregation propensity
ATR	Attenuated total reflection

## B

BSA	Bovine serum albumin
-----	----------------------

## C

Cbz	Carboxybenzyl
CD	Circular dichroism
Chymo	$\alpha$ -Chymotrypsin
Cryo-TEM	Cryo transmission electron microscopy
Cryo-SEM	Cryo scanning electron microscopy

## D

DAP	2,3-diaminophenazine
DIC	Diisopropylcarbodiimide
DMF	Dimethylformamide
DNA	Deoxyribonucleic acid

## E

<i>EA-SA</i>	Enzyme-assisted self-assembly
EG	Oligoethyleneglycol
E-QCM	Electrochemical quartz crystal microbalance
ESEM	Environmental scanning Electron microscope
<i>E.Coli</i>	<i>Escherichia coli</i>

## F

FITC	Fluorescein isothiocyanate
Fmoc	Fluorenylmethoxycarbonyl
FTIR	Fourier transform infrared spectroscopy

## G

GdL            Glucono- $\delta$ -lactone

## H

HA            Hyaluronic acid  
HOBt        hydroxybenzotriazole  
HPR        Horse radish peroxidase

## L

LB            Langmuir Blodgett  
LbL        Layer-by layer  
*LCASA*     Localized catalytic assisted self-assembly  
*LEASA*     Localized enzymatic assisted self-assembly  
LMWG       Low molecular weight gelator

## M

MALDI-TOF Matrix assisted laser desorption/ionization time-of flight  
mTG        Transglutaminase

## N

Nap        Naphtalene  
NMR        Nuclear magnetic resonance

## O

ODP        *o*-diphenylenediamine  
OHD        1-(2-*n*-hexylphenylazo)-2-hydroxy-6-naphtalene sulfonate

## P

<sup>+</sup>PA        Peptide amphiphile  
PAA        Poly(acrylic acid)  
PAH        Poly (allylamine hydrochloride)  
PEG        Poly (ethylene glycol)  
PEI        Poly (ethyleneimine)  
PEM        Polyelectrolyte multilayer  
p-HEMA    Poly (2-hydroxyethyl methacrylate)  
PLL        Poly-(L-lysine)  
*p*-NPP     *para*-Nitrophenyl phosphate disodium  
*p*-NPA     *para*-Nitrophenyl acetate  
*p*-NP      *para*-Nitrophenol  
PVA        Poly(vinyl alcohol)

PSS Poly(styrene sulfonate)  
Pyr Pyrene

## **Q**

QCM-D Quartz crystal microbalance  
QCM-D Quartz crystal microbalance with dissipation monitoring

## **S**

SAH S-adenosyl-homocysteine  
SPR Surface plasmon resonance

## **T**

TA Tannic acid

## **W**

Wet-STEM Wet scanning transmission electron microscopy

# General Introduction

Chemical surface modification is probably one of the most convenient way to confer specific properties to a material. The control of interactions between a surface and its environment can be achieved through a large panel of functionalization methods allowing decoration of the surface with a wide range of molecules and/or (bio)macromolecules. Due to the versatility of this approach, surface science finds applications in different fields such as textile, energy storage, automotive, aerospace, electronics, biomaterials, biosensor design and many others.

The Langmuir-Blodgett (LB) method, arising in the middle of the last century, was one of the first approaches developed and is still commonly used to functionalize planar surfaces through an organic coating. In this process, one layer of amphiphilic molecules (*sine qua non* condition) is formed at a liquid-air interface of a solution and transferred onto a planar substrate by dipping. This operation can be repeated several times. Nowadays, many alternatives to LB are well-established to modify all kinds of substrates: self-assembled monolayer, silanization, plasma polymer grafting or photochemical treatment are all efficient methods widely used, displaying specific features and allowing access to different chemical and physical properties of the modified surface.

In the beginning of the 90<sup>th</sup>, an approach based on the alternated deposition of negatively and positively charged entities on a substrate emerged. Mainly using polyelectrolytes, this new surface modification process is called “Layer-by-Layer” (LbL) and allows the buildup of multilayer films with an accurate control over the film thickness through the number of deposition steps. LbL is an efficient technique to functionalize all kinds of surfaces and to give them different properties depending on the molecules/(bio)macromolecules or inorganic materials adsorbed. Despite all these advantages, the LbL process is considerably time-consuming and tedious when a film thickness of several micrometers is required. This may explain why, at least partially, only few industrial applications based on LbL have emerged so far.

Since 2011, our group has designed several one-pot strategies to form polyelectrolyte-based films on surfaces triggered by the application of an electric stimulus. To do so, the electrochemical generation of a catalyst gradient (metallic ions, protons) was employed to induce the self-construction of oligomers, polymers, small molecules or inorganic nanoparticles at the electrode surface. This responsive approach represents a convenient way of surface functionalization using all the constituents simultaneously in solution and allowing a high control of the bottom-up deposition. Indeed when the electric stimulus is stopped, the film buildup stops so that its thickness can be well controlled at the nanometer scale. In this process, the gradient of catalysts generated from the surface activate the formation of the film (Figure 1). The catalyst formed at the interface was called "*morphogen*" in analogy with biology. Indeed, self-organizations resulting in complex tissue morphologies are driven by gradients of morphogen, specific molecules to which cells respond in a concentration dependent manner.

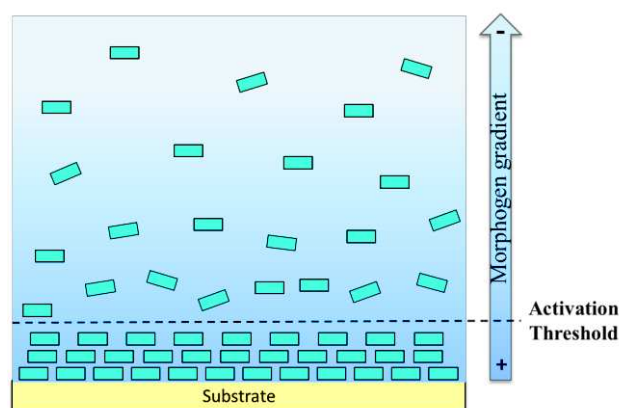


**Figure 1:** Schematic representation of spatial morphogen gradient directing localized self-assembly of the surface coating.

Nature provides many examples of functional and spontaneous localized self-assemblies involved in vital processes such as cell motility, intracellular transport and muscle contraction. Hierarchical assembly of functional structures depends on the capacity to guide the organization of smaller elements into larger or more complex structures. Thus, the key factor to develop such a bottom-up strategy is in the localized control of chemical interactions between molecular building blocks and their local environment. In this approach, peptide derivatives appear to be valuable building-blocks with tunable chemical interactions that can drive formation of nanoarchitectures such as fibers, spheres, tubes or micelles.

The purpose of my Ph.D. was to develop smart surfaces able to modify and to control chemical interactions between peptide sequences exclusively near the surfaces. The strategy was based on the development of enzymatically active surfaces with specific couple of enzyme and peptidic building-block. Functionalized surfaces by active enzymes, obtained by the LbL method, allow to induce a dynamic transformation of specific peptides leading to their surface confined supramolecular self-assembly. The enzymatic transformation of peptide precursors into self-assembled building blocks is obtained near the surface. This spontaneous self-assembly of peptides resulted in entangled 3D network of fibers entrapping water defined as the scaffold of a hydrogel coating.

This manuscript is divided in four chapters (Figure 2). The first chapter briefly reviews the latest strategies to trigger self-assembly of peptide-based hydrogels in solution and near an interface. The second chapter presents the material and methods used. Chapter three describes the concept of *Localized Enzyme-Assisted Self-Assembly (LEASA)* of oligopeptides upon reverse hydrolysis of  $\alpha$ -chymotrypsin allowing the oligomerization of KLOEt precursor peptide. In chapter four, we introduce the new concept of *bioactive seed-layer* using alkaline phosphatase and Fmoc-FFY( $\text{PO}_4^{2-}$ ) precursor peptide that triggers spatiotemporal control of fiber network exclusively at the film/solution interface. A conclusion and some outlooks are ending the manuscript.

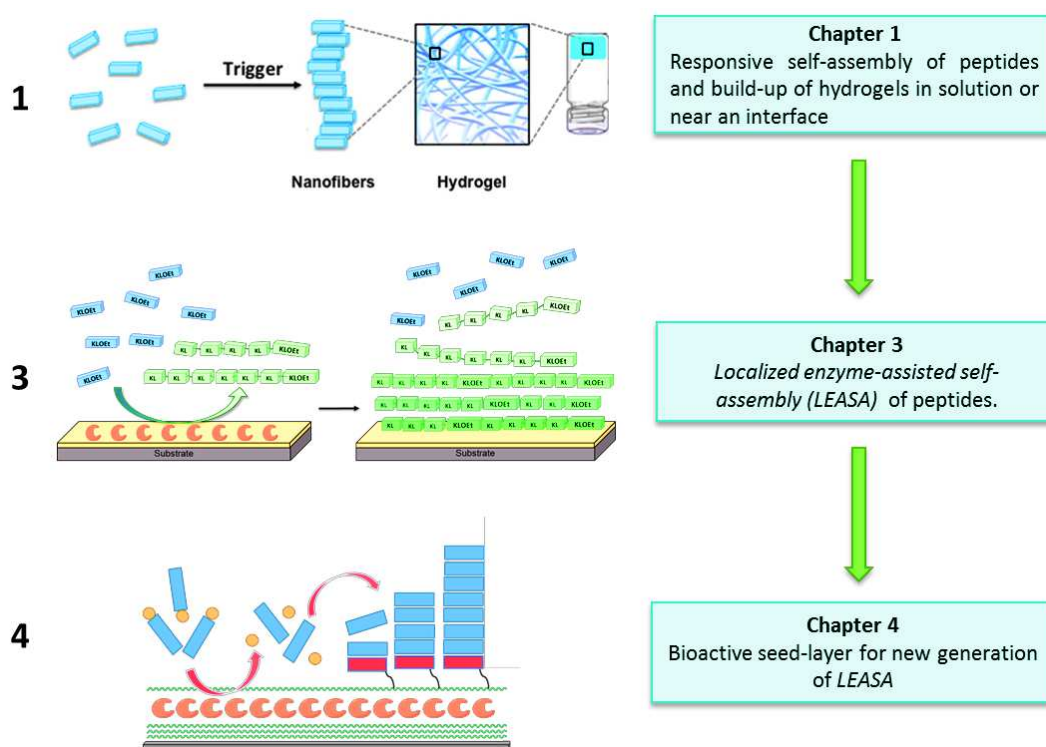
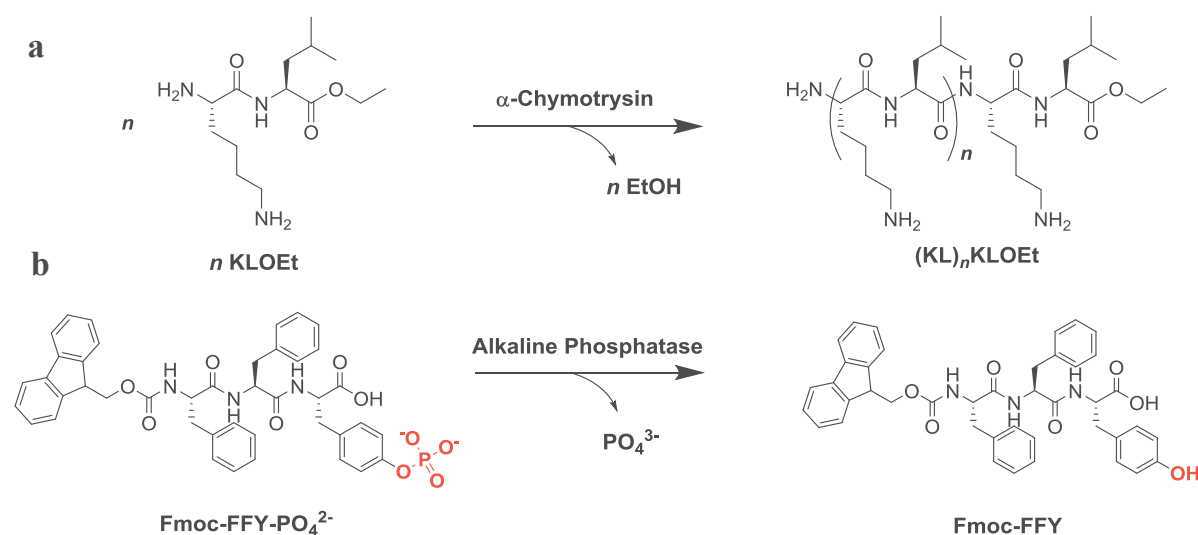


Figure 2: Schematic presentation of different chapters composing my thesis manuscript.

**Chapter one** presents several responsive approaches described in the literature to trigger the self-assembly of peptides and the buildup of hydrogels in solution or near an interface. To understand the process at a molecular scale, we review different structural or environmental factors involved in the process of peptides self-assembly. These parameters are determinant to predict supramolecular interactions of peptide sequences with their neighboring environment and their stimulation. In this context, few examples of surface-confined assisted self-assembly of small molecules are reported triggered by pH, electrochemical or enzymatic stimuli. We will also describe briefly LbL process as functionalization of surface.

The **second chapter** presents the materials and the methods. Several techniques were employed to characterize the functionalization of surface and the self-assembly of peptides and hydrogels materials.



**Scheme 1:** Chemical transformation of peptides (a) KLOEt catalyzed by  $\alpha$ -chymotrypsin and (b) Fmoc-FFY( $\text{PO}_4^{2-}$ ) catalyzed by alkaline phosphatase.

**Chapter three** presents a simple chemical approach based on *localized enzyme-assisted self-assembly (LEASA)* of peptides leading to the growth of fibrillar network hydrogels starting exclusively at the surface. The enzyme  $\alpha$ -chymotrypsin is confined onto the surface through the LbL method to transform KLOEt peptides into oligopeptides  $(\text{KL})_n\text{OEt}$  (Scheme 1.a). The hydrogel buildup results from the local accumulation of  $(\text{KL})_n\text{OEt}$  produced from the confined enzyme layer at the interface. When the critical gelation concentration is reached, the self-assembly of peptide oligomers occurs, leading to a complete control of the nucleation and growth. The purpose of this study was to control the time of initiation of  $(\text{KL})_n\text{OEt}$  self-

assembly by tuning the surface density of the enzyme and the concentration of KLOEt in solution.

**Chapter four** presents the design of a new generation of *LEASA* allowing the control of the hydrogel formation exclusively at and from a surface. Alkaline phosphatase (ALP) was used as catalytically active enzyme inducing the dephosphorylation of Fmoc-FFY( $\text{PO}_4^{2-}$ ) leading to the local production of the hydrogelator Fmoc-FFY (Scheme 1.b). The ability of the surface to initiate and to tune its own coating is based on the use of seeding polyelectrolytes architectures that offers the possibility to design highly organized and enzymatically active nanometer size hydrogels. The use of a *bioactive seed-layer* allows controlling and tuning both the network kinetics and the fiber morphologies.

A **general conclusion** summarizes the PhD. Work. In addition some outlooks are given at the end of the manuscript.



# Chapter 1

## Bibliographic review

---

# Chapter 1

## Bibliographic review

### Summary

<b>1.1</b>	<b>Supramolecular hydrogels of small molecules</b>	<b>10</b>
1.1.1	Classification of gels	10
1.1.2	Low molecular weight gelation process	11
1.1.3	Peptide based hydrogels	12
1.1.3.1	<i>Amino acid building blocks and their classification</i>	13
1.1.3.2	<i>Peptide sequences for the design of efficient hydrogelators</i>	15
1.1.4	Toward the design of responsive hydrogels based on aromatic PA	20
1.1.4.1	<i>Gelation of LMWG triggered by physical stimuli</i>	21
1.1.4.2	<i>Gelation of LMWG triggered by chemical stimuli</i>	21
1.1.5	Enzymatic-responsive hydrogel	25
<b>1.2</b>	<b>Surface-assisted self-assembly of LMWG</b>	<b>27</b>
1.2.1	Surface seeding of LMWG self-assembly	28
1.2.2	Surface induced pH responsive self-assembly of LMWG	32
1.2.2.1	<i>Surface-confined acidic catalyst for self-assembly of LMWG</i>	33
1.2.2.2	<i>Electrochemical trigger of pH-responsive self-assembly of peptides</i>	34
1.2.3	Localized enzyme assisted self-assembly of peptides ( <i>LEASA</i> )	41
<b>1.3</b>	<b>Polyelectrolyte multilayer films</b>	<b>43</b>
1.3.1	Polyelectrolyte Multilayer assemblies	43
1.3.2	Deposition methods	45
1.3.3	Growth regime and tunable properties of PEM films	46
1.3.4	Coating features and applications	48
	<b>References</b>	<b>50</b>

This chapter is a bibliographic review divided into three parts. The first part entitled “Supramolecular hydrogels of small molecules” focuses on the definition and the different mechanisms of gelation. The design of short peptides behaving as efficient hydrogelators with different stimuli used to initiate the gelation process in solution are in particular described. The second part of this chapter I called “Surface-assisted self-assembly of low molecular weight hydrogelators” is dedicated to the description of the different strategies used to initiate the self-assembly exclusively at an interface. The last part describes briefly the LbL process and gives few physico-chemical characteristics.

## 1.1 Supramolecular hydrogels of small molecules

Mechanisms involved in gelation of low-molecular weight gelators and the rules governing these processes are described. We will focus on the advantage to use peptides as gelators and the description of a range of stimuli to obtain gelation in solution.

### 1.1.1 Classification of gels

According to the international union for pure and applied chemistry (IUPAC), gels can be defined as a **non-fluid colloidal network able to retain solvent in their swollen state**. Resulting from the association of gelators and solvent, gels can be classified upon their source, composition, medium or intermolecular junctions that support the three-dimensional (3D) networks (Figure 1.1). The bibliographic study reported in this manuscript will mainly focus on gels and gelators where the water is the solvent, called hydrogels and hydrogelators respectively.

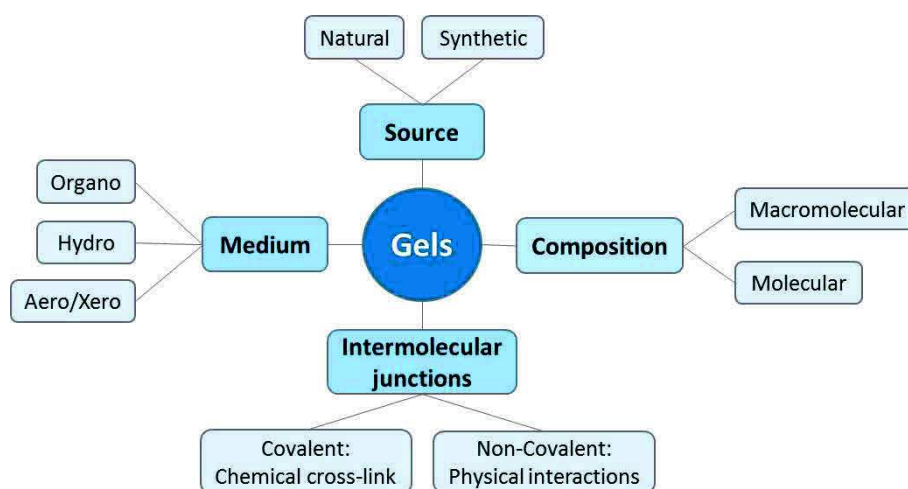


**Figure 1.1.** Classification of gels according to the origin of the gelator involved (natural or synthetic), its nature (molecular or macromolecular), the medium used (organo, hydro or aero/wero gels) and the cross-linking nature between gelators (covalent bonds or non-covalent interaction).<sup>1</sup>

Hydrogels can be formed from macromolecules or small molecules. Most of hydrogels used for medical applications are formed from natural polymers often assembled through physical interactions, chemical covalent cross-linking or both. Well-known examples are polypeptides, such as collagen,<sup>2-3</sup> poly-L-lysine<sup>4</sup> and polysaccharides such as alginic acid,<sup>5</sup> hyaluronic acid<sup>6</sup> or

agarose.<sup>7</sup> “Synthetic” polymers such as poly (2-hydroxyethyl methacrylate) (pHEMA), poly(vinyl alcohol) (PVA) and poly(ethylene glycol) (PEG) are commonly used to form water-swollen crosslinked macromolecular networks.<sup>8</sup> In that case, multimodality and polydispersity of polymers are parameters that can be difficult to control. In addition, the purity of natural polymer depends often from the origin of the product. All this parameters lead to the irreproducibility of the material formed from batch to batch: a problem well known in material science.

Another type of material based on the supramolecular architecture of “small” molecules has recently draw the attention of the scientific community. These architectures result from non-covalent interactions between molecular entities having low molecular weight in comparison with polymers. Their gelation occurs spontaneously in water through the self-assembly of the molecular entities and without any addition of chemical reagents. Compared to natural or synthetic polymers, small molecules can be prepared in large amount with a high degree of purity and without any doubt about their chemical structure. This aspect allows to obtain reproducible gels. Moreover, the knowledge of the chemical structure of the gelating agent allows to better study, understand and tune the properties of the resulting gel. Finally, the non-covalent nature of the internal organization of the hydrogel ensures the possible reversibility of the gelation process, opening the gate to the design of adaptable chemical system.

Thus supramolecular hydrogels appear to have widespread potential applications in different areas: medicine, cosmetic or pharmacology for instance.

### 1.1.2 Low molecular weight gelation process

Around 1900, Brenzinger *et al.* described for the first time the existence of colloidal hydrogels composed by benzoyl-L-cystine.<sup>9-10</sup> By that time, hierarchical self-assembly of a low molecular weight gelator (LMWG) was not understood and these works were forgotten. However one century later, modern physical methods (light and electron microscopy, rheology, calorimetry, X-Ray crystallography) have provide valuable knowledge over fibrous organization from gelators and the relationship between the chemical structure of low molecular weight gelator (LMWG) and the gel properties.<sup>11</sup>

Over the past decades, hydrogelation processes were often described as serendipitous results of failed crystallizations.<sup>12</sup> Indeed, crystallization processes provide high molecular self-

organization that can be realized as follows: a “super-saturated” solution is prepared at high temperature and then slowly cooled down, giving rise to highly organized structures as observed in crystals as shown in Figure 1.2.

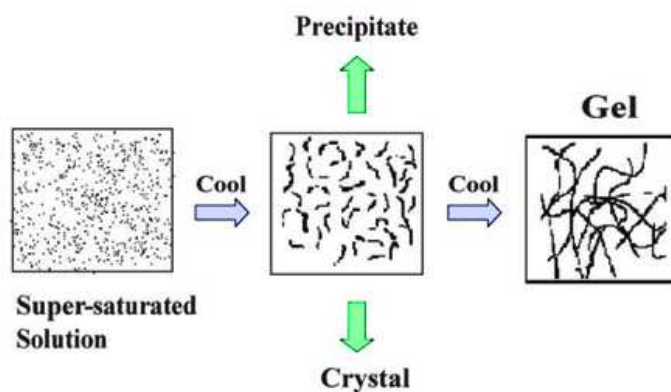


**Figure 1.2.** : Schematic representation of different possible pathways leading to precipitate, crystal or gel from supersaturated solution of molecules.<sup>1</sup>

Yet, such a process often provides precipitates or self-association of LMWG leading to hierarchical structures entrapping water rather than crystals. The self-assembly of small molecules is issued from the right balance between the solvophobic and solvophilic interactions with the medium. If chemical species are too solvophobic, they may precipitate or crystalize. The gelation process is thus based on low solubility of gelator units. Fortuitous gelations of small molecules have enabled the scientific community to understand the relation between structure of gelators and the resulting self-assembly.

### 1.1.3 Peptide based hydrogels

Supramolecular hydrogels derived from a large range of small molecules such as nucleic acid,<sup>13</sup> sugar derivatives,<sup>14</sup> aromatic compounds.<sup>15</sup> Among them, peptide building blocks have advantageous features mainly due to the panel of chemical moieties displayed by the lateral chains of their constituting amino acids. Besides, the polyamide backbone of peptide sequences can be involved in intra- or intermolecular hydrogen bonds inducing organized conformations able to fold in secondary structures (coil, helices,  $\beta$ -sheets) and leading to a large range of nanoscale objects: fibers, tubes, spheres or sheets (Figure 1.3).

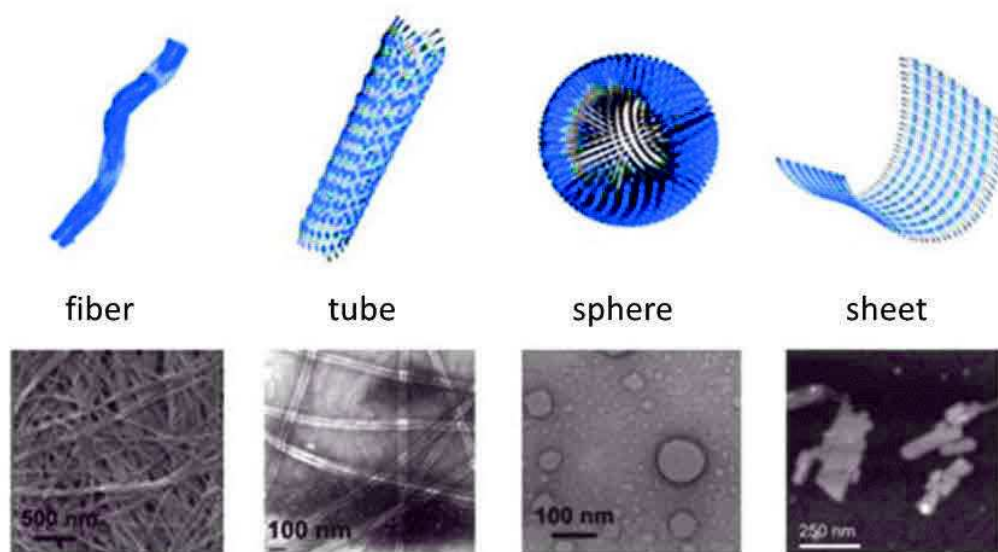


*Figure 1.3.: Examples of supramolecular nanostructures accessible via peptide self-assembly.<sup>16</sup>*

Due to their inherent biological compatibility, peptides are considered as valuable building blocks for production of biomaterials used in regenerative medicine,<sup>17</sup> drug delivery,<sup>18</sup> 3D cell-culture,<sup>19</sup> or enzyme immobilization for biosensing.<sup>20</sup> In order to create such functional materials, properties of peptide-based hydrogels can be tailored through suitable hierarchical assemblies of small molecules. How do peptide sequences guide self-assembly processes and morphological properties of the hydrogels?

### 1.1.3.1 Amino acid building blocks and their classification

To master the rules of peptide based hydrogelators design, it is necessary to know the characteristic properties of the twenty natural amino acids that can constitute peptidic building blocks.

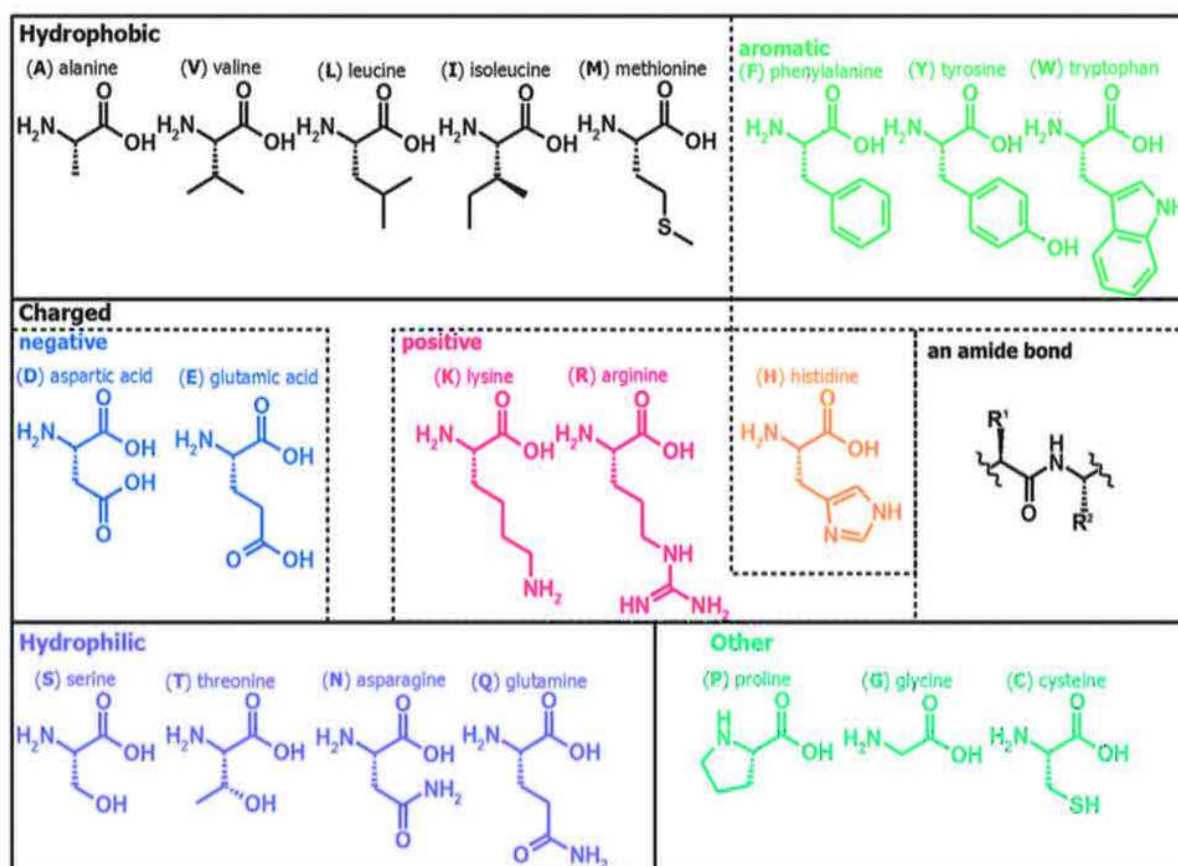


**Figure 1.4.** : Classification of the twenty natural amino acids according to their physico-chemical properties: hydrophobic (aromatic and non-aromatic), charged (positive, negative) and hydrophilic.<sup>21</sup>

All amino acids, except Glycine (G), are chiral molecules with lateral chains displaying a large panel of chemical groups. Due to the nature of these functions, amino acids are classified in three main categories: hydrophobic, hydrophilic and charged amino acids (Figure 1.4). The category of hydrophobic amino acids is subdivided in two groups. The “aliphatic amino acids”, Alanine (A), Valine (V), Leucine (L), Isoleucine (I), Methionine (M), exhibit alkyl moieties as lateral chains forming a hydrophobic environment when incorporated in a peptide sequence. Others amino acids, Phenylalanine (F), Tyrosine (Y), Tryptophan (W) have aromatic residues and are thus also classified into the category of hydrophobic amino acids. These amino acids can be involved in intermolecular  $\pi$ - $\pi$  stacking. Hydrophilic amino acids exhibit hydroxyl groups (Serine (S), Threonine (T)) or amide (Asparagine (N), Glutamine (Q)) moieties as donor/acceptors of hydrogen bonds. The last category of amino acids comprises positively charged Histidine ((H), pKa = 6.5), Lysine ((K), pKa = 10), Arginine ((R), pKa = 12) and negatively charged Aspartic acid (D) and

Glutamic acid (E) with similar  $pK_a = 4$ . These charged amino acids generate either repulsive or attractive electrostatic interactions. With two hydrogen atoms as lateral chain, glycine is not involved in non-covalent interactions but provides flexibility to the peptide. Cysteine (C) with SH moiety, shows great advantages for peptide functionalization with biomolecules or chromophores.

### 1.1.3.2 Peptide sequences for the design of efficient hydrogelators

Peptide sequences involved in self-assembly processes usually contain **amphiphilic properties** with hydrophilic regions enhancing its water solubility and hydrophobic regions enhancing interactions between gelators leading to their organized self-assembly. Sequences with strong hydrophobicity aggregate or precipitate in water whereas very hydrophilic sequences are completely soluble into water and never give rise to hydrogel formation. Thus, a right balance has to be found between hydrophobicity and hydrophilicity in the peptide amphiphile sequence to design peptide-based hydrogelator.

We present non-exhaustive list of three peptide amphiphiles (PA) categories: aliphatic alternating and aromatic peptides amphiphiles are briefly described below.

#### *Aliphatic peptide amphiphiles*

Since the 90's, Stupp's group largely contributed to develop a class of functional PA hydrogelators,<sup>22</sup> linear molecules with a hydrophilic head/hydrophobic tail structure. In fact, the peptide sequence comprises four characteristic regions as shown in Figure 1.5: the role of region 1 is to allow van der Waals interactions, region 2 allows intermolecular hydrogen bonds, region 3 improves the overall solubility of the PA and the region 4 may display a (bio)function.

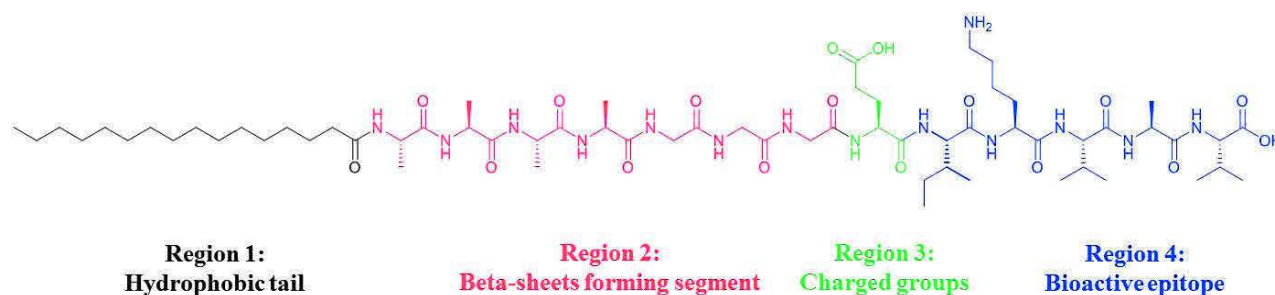


**Figure 1.5.:** Molecular structure of a representative PA with four rationally designed chemical entities<sup>22</sup>

Spherical or cylindrical micelles and lamellar structures are some examples of nano-objects self-assembled in solution.<sup>22</sup> Despite the complexity of such chemical systems that can be created, this kind of PA requires long synthesis from solid support strategy.

### *Alternating peptide amphiphiles*

A second class of PA is composed of peptide with sequences alternating polar (X) and non-polar (Z) amino acids leading to the formation of  $(XZXZ)_n$  sequences (Figure 1.6).

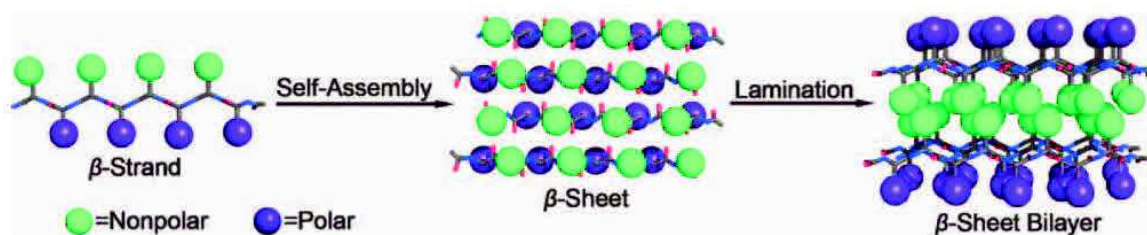


**Figure 1.6:** Peptide self-assembly and arrangement of amino acid side chains in the  $\beta$ -sheet bilayer.<sup>23</sup>

In this class PA, also called amphipathic peptides,<sup>24</sup> self-assemble into cofacial  $\beta$ -sheets fibrils. Formation of these primary structures, is driven by segregation hydrophilic (X) chains from hydrophobic (Z) residues on opposite faces of the sheets. In aqueous medium, sheets laminate to form secondary bilayered architectures. Indeed, hydrophobic residues gather to form internal core exposing hydrophilic residues to the aqueous environment.

Zhang et al were the first to report that self-assembly of amphipathic sequences into  $\beta$ -sheets fibrils could lead to the formation of hydrogels.<sup>25</sup> In such systems, assembly propensity of peptides seems to be very dependent from the alternating sequences, the concentration and environmental factors such as pH.<sup>26</sup>

### *Aromatic peptide amphiphiles*

In parallel to the development of aliphatic and alternating PA, another kind of PA have been reported based on shorter peptide sequence and including aromatic group or aromatic amino acids. In 1995, Vergner<sup>27</sup> has reported a pioneer work about the gelation of a dipeptide sequence leucine - aspartic acid ( $\text{NH}_2\text{-LD-COOH}$ ), protected on the N-terminal position by an aromatic group: the fluorenylmethoxycarbonyl group (Fmoc). Few years later, the interest in aromatic PA grew up, in particular with the intensive investigation led by the group of Xu, highlighting the self-assembly

properties of aromatic PA, such as Fmoc-protected peptides.<sup>28-30</sup> These precursor works have introduced a new class of very efficient aromatic peptide hydrogelators that is actively developed by several research groups all over the world since 2004.

By analogy with the four different regions characterizing the aliphatic PA sequence described above, the amphiphilic property stands on four key segments (Figure 1.7): an aromatic moiety placed at the N-terminal end, a polar linker between the aromatic group and a peptide sequence with a polar C-terminal end.



**Figure 1.7:** Generic structure of an aromatic PA constituted from four segments: an aromatic part, a chemical group used as linker (ester moiety in this case), di-, tri- or tetra-peptides and the hydrophilic C-terminal part.<sup>31</sup>

N-terminal aromatic functions derived from a large range of amine protecting groups and confer hydrophobic properties to peptide sequences. In addition to Fmoc, naphthalene (Nap),<sup>32</sup> pyrene (Pyr)<sup>33</sup> and carboxybenzyl (Cbz)<sup>34</sup> are also commonly used.

On another hand, hydrophilic interactions of aromatic PA can be controlled by the presence of an adequate “linker” junction between the N-terminal aromatic group and the peptide sequence of the building block. This short segment can be essential to the hydrogelation process. Indeed, Ulijn *et al.*<sup>35</sup> have reported the gelation of tyrosine - leucine (NH<sub>2</sub>-YL-COOH) dipeptide functionalized with Fmoc moieties at N-terminal position (FmocNH-YL-COOH) bonded to the dipeptide core through four different linkers : carbonyl, methylcarbonyl, methoxycarbonyl, and ethylcarbonyl. The study reveals that flexible linkers, such as methoxycarbonyl, enhance hydrogelation.

The overall amphiphilic property of the aromatic PA also depends on the amino acids involved in the sequence. It must be noted that aromatic PA have a low number of amino acids, from a single amino acid to rarely more than four. Thus, aromatic PA belongs to the LMWG

category without ambiguity. Gazit et al. were the first to report self-assembling properties of aromatic diphenylalanine (NH<sub>2</sub>-FF-COOH) sequences.<sup>36-37</sup> In this work, rapid evaporation of aqueous medium leads to the formation of nanotubes obtained in dry state. At the same time, the same dipeptide sequence NH<sub>2</sub>-FF-COOH with a Fmoc moiety on the N-terminal position was described as giving a spontaneous hydrogelation driven by  $\pi$ - $\pi$  stacking and hydrogen bonds.<sup>19, 38-39</sup> FmocNH-FF-COOH sequences self-assemble into fibrous structures, scaffold of a hydrogel. Ulijn's group<sup>39</sup> assessed this supramolecular assembly with diverse methods of spectroscopy: Fourier transform infrared spectroscopy (FTIR), circular dichroism (CD) or fluorescence spectroscopy. These characterizations revealed that self-assemblies ordered into anti-parallel  $\beta$ -sheets gathering into large nanoribbons due to  $\pi$ - $\pi$  interactions of fluorenyl moieties.

These investigations over NH<sub>2</sub>-FF-COOH dipeptide sequences permitted to fully understand the gelation process of phenylalanine building blocks. However, experimental investigation over aggregations properties of every possible dipeptide sequence is a meticulous task requiring time and patience. To skirt such tedious investigations, Tuttle and Ulijn developed a simulation protocol to screen all possible dipeptide combinations ( $20^2 = 400$  dipeptides) to predict their aggregation propensity (AP) toward peptide self-assembly (Figure 1.8).<sup>40</sup> Polarity, shape and potential non-covalent interactions of amino acid functionalities were include in parametrization of the computational study to determine aggregation propensity of every dipeptide sequences. This virtual screening of dipeptide aggregation properties provides valuable knowledge to orient the design of dipeptide sequence and to control the self-assembly process.

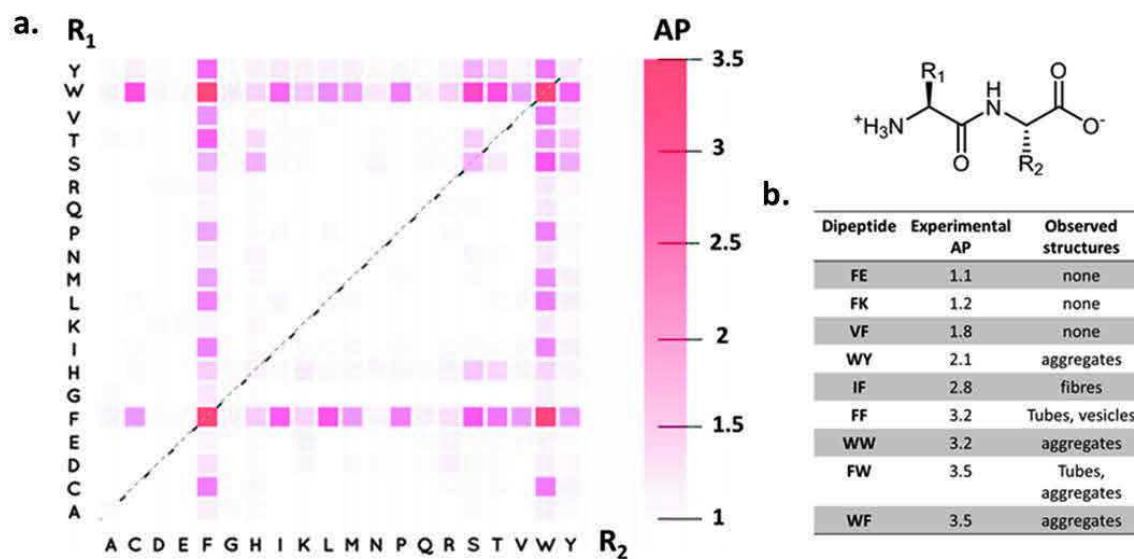


**Figure 1.8:** (a) Two-dimensional grids indicating the aggregation propensity (AP) scores for dipeptides. Horizontal and vertical axes show the amino acids one-letter codes. (b) Table presenting experimental AP scores for selected dipeptide sequences.<sup>40</sup>

The resulting AP scores provided by the computational simulation are classified on a scale from 0 to 3.5 (Figure 1.8.a). On this scale, sequences with  $AP > 2$  have high aggregation propensity. As expected, the grid indicates that sequences containing F and W residues have high degrees of aggregation proving that aromatic PA are likely to self-assemble. This recent predictive method is thus a powerful tool to design gelating peptides. In fact, experimental AP scores quote from literature were compared to computational data and validate the computational model (Figure 1.8.b). Tuttle recently extended this approach to create a new computational library composed of 8000 (tri-) peptide sequences and predicted their AP.<sup>41</sup> Thus, simulation of AP of di- or tri-peptides appears as a valuable method to design effective aromatic PA.

Carboxylic acid (and/or carboxylate) in C-terminal position, is a highly polar group and its role in aromatic PA is crucial to get the right hydrophilic/hydrophobic balance leading to self-assembly. Therefore, the functionalization of the C-terminal end of aromatic PA peptides have a significant impact on the hydrogelator's features and gelation process. A great diversity of molecules can be grafted onto the carboxylic group. Amide group ( $\text{CONH}_2$ )<sup>42</sup> or oligoethyleneglycol (EG) chains,<sup>43</sup> polar and hydrosoluble groups are known to enhance the gelator solubility. On the contrary, alkyl groups<sup>44</sup> leading to alkyl ester groups, such as methyl ( $\text{COOMe}$ ),

ethyl (COOEt) or propyl (COOPr) promote their precipitation in water.<sup>45</sup> Consequently, the functionalization of the C-terminal position enhances or weakens peptides hydrophobic/hydrophilic balance. It is reasonable to think that chemical modifications of this carboxylic group can change aggregation propensity of peptides.

Thus, several research groups have developed strategies to trigger the hydrogelation in solution by changing the hydrophobic/hydrophilic balance of aromatic PA through different stimuli.

#### 1.1.4 Toward the design of responsive hydrogels based on aromatic PA

Compared to aliphatic and amphipatic PA, aromatic PA are small molecules which require only few steps of synthesis. As described above, the chemical structure (mainly peptide sequence) of aromatic PA strongly influences the gelation propensity. In the last decade, research groups have developed different tools to induce the gelation by using an external stimulus (Figure 1.9). Some of them can be qualified as “physical”, such as change of temperature or the application of ultrasounds to enhance intermolecular interactions. The others are “chemical” stimuli such as change of pH or the addition of a chemical reagent in the medium to modify the structure of the aromatic PA in order to adapt its hydrophilicity/hydrophobicity balance.

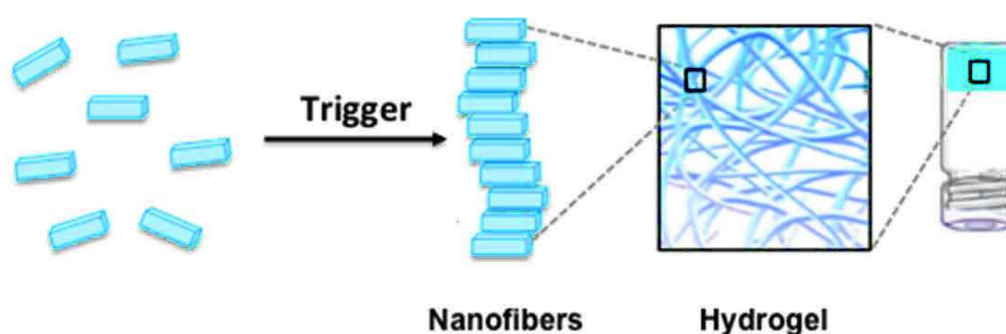


**Figure 1.9:** Schematic representation of the gelation triggers by a “chemical” or a “physical” stimulus. This initiation induces the self-assembly of the LMWG in the whole solution and leads to the formation of a fibrous network self-supporting the hydrogel.<sup>46</sup>

Development of such responsive hydrogels presents a huge interest to control self-assembly of small molecules and tune properties of resulting gels.

#### 1.1.4.1 Gelation of LMWG triggered by physical stimuli

Change of temperature, by heating and cooling cycles, is a common technique giving reversible hydrogelation.<sup>27</sup> At high temperature, intermolecular non-covalent interactions are disrupted to increase solubility of peptides. When the bulk cools down to room temperature, the solubility of peptides decreases with the formation of non-covalent interactions leading to formation of supramolecular organization.

Ultrasounds are able to rearrange aggregates of LMWG and to trigger the gelation process.<sup>47-48</sup> This technique, mainly used in laboratories to solubilize chemical compounds, gives to the system adequate energy to disrupt weak intramolecular interactions and to arrange weak intermolecular interactions. According to Ratcliff et al.,<sup>49</sup> ultrasounds triggering gelation processes are involved into the reshaping of supramolecular assemblies.

To induce physical sol-gel transitions, temperature and ultrasounds are able to disrupt hydrophobic and hydrophilic interactions between peptides and to push the system to reach a new thermodynamic minimum.<sup>50</sup>

#### 1.1.4.2 Gelation of LMWG triggered by chemical stimuli

Supramolecular self-assembly of LMWG can also be initiated through a chemical transformation in solution of a “precursor” peptide into a hydrogelator to decrease its global hydrophilicity. Among the chemist’s tool kit, the pH change is probably the simplest way to do that. The consequence of a pH change on the precursor peptide containing-solution can result in an increase or a decrease of the ionization degree of the peptide or by the hydrolysis of one pH-sensitive part of the precursor peptide yielding to the hydrogelator.

As described previously in this chapter, some amino acids (aspartic acid, glutamic acid, lysine, arginine and histidine) have ionizable groups according to the pH value. Thus, the overall charge of the hydrogelator peptide having such amino acids in its sequence can be tune with the pH and so the hydrophilicity/hydrophobicity balance as well. Another chemical group of aromatic PA is also sensitive to pH: the C-terminal carboxylic acid group (C<sub>t</sub>OOH). Decrease of the pH below the pK<sub>a</sub> of the C<sub>t</sub>OOH group (~4.5) decreases the solubility of the considered peptide and enhances the formation of intra or intermolecular hydrogen bonds between hydrogelators and their environment. In 2009, Tang *et al.* reported the mechanism explaining the pH-responsive self-

assembly of FmocNH-FF-COOH (F: phenylalanine) used as model of aromatic PA (Figure 1.10).<sup>51</sup> The authors have shown that this pH-responsive self-assembly leads to dramatic pKa shifts of  $\approx 6.4$  and  $\approx 2.2$  pH units above the theoretical pKa ( $\approx 3.5$ ) of FmocNH-FF-COOH.

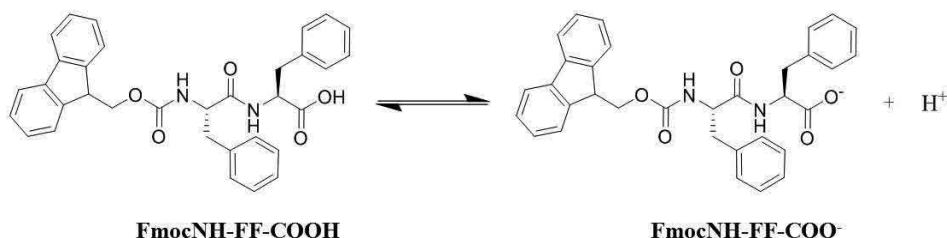


**Figure 1.10:** Acid-base equilibrium of the dipeptides FmocNH-FF-COOH in solution. At pH < 4.5 (pKa COOH/COO<sup>-</sup>), the neutral acid form is predominant and at pH > 4.5 its basic carboxylate form is predominant.<sup>51</sup>

To investigate experimental pKa shifts during the self-assembly of FmocNH-FF-COOH, Tang et al monitored the pH of FmocNH-FF-COOH samples as a function of added HCl<sub>(aq)</sub>. FmocNH-FF-COOH was dissolved in aqueous solution at pH = 10.5 and HCl<sub>(aq)</sub> was progressively added to the bulk. Following HCl addition, two apparent pKas were measured (Figure 1.11). The first one observed at pH = 10.2-9.5 promoted the self-assembly of peptides in  $\beta$ -sheets giving translucent hydrogels. The second pKa, pKa<sub>2</sub>, appears at pH = 6.2-5.2 where the bulk is a turbid viscous fluid containing large fibers. Below pH = 5.2, morphological study revealed appearance of large nanoribbons that precipitate in solution. At this stage, the degree of ionization is very low and consistent with aggregation of FmocNH-FF-COOH. In parallel, the degree of ionization decreases from 1 to 0.24.

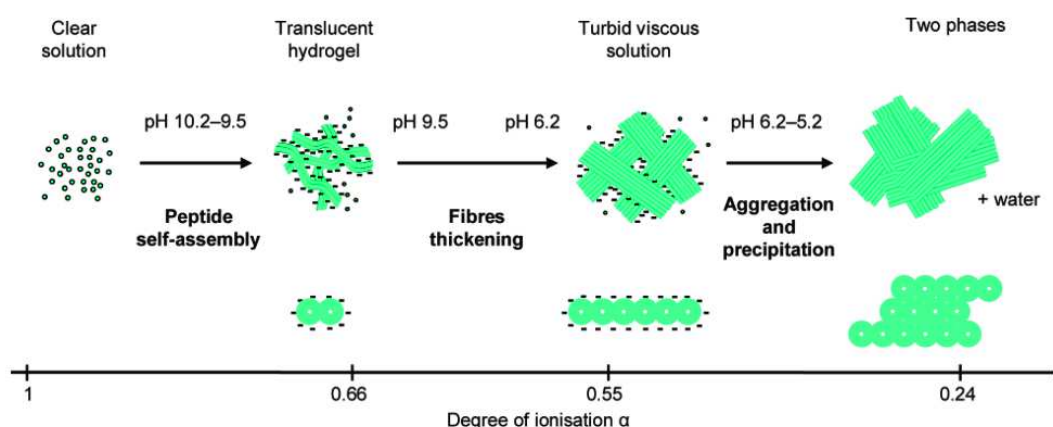


**Figure 1.11:** Self-assembly mechanism of FmocNH-FF-COOH from high to low pH above critical gelation concentration as function of the degree of ionization of peptides.<sup>51</sup>



Recently, a similar method was developed to trigger the self-assembly of NapNH-VG-COOH leading to the formation of an hydrogels. Protons were generated in-situ via the hydrolysis of anhydride derivatives into corresponding acids (Figure 1.12.b).<sup>55</sup> In this approach, the rate of proton release in solution affects self-assembly of NapNH-VG-COOH and the morphology of fibers formed.

Self-assembly of peptides can also be generated under basic conditions. Xu and coworkers<sup>56</sup> reported a gelation process based on the ester hydrolysis of the precursor peptide **1** represented in Figure 1.13. This aromatic PA is composed of a naphthalene ring on N-terminal position and a single amino acid, *i.e.* phenylalanine. The C-terminal position has been modified with the 4-(2-aminoethoxy)-4-oxobutanoic acid moiety containing an ester group and a carboxylic group to ensure the hydrophilicity of peptide **1**. When a dilute solution of sodium hydroxide is added to the compound **1** in solution, the pH increases and the ester group is hydrolyzed to form the peptide **2**. Less soluble peptide **2** self-assembles into fibers.

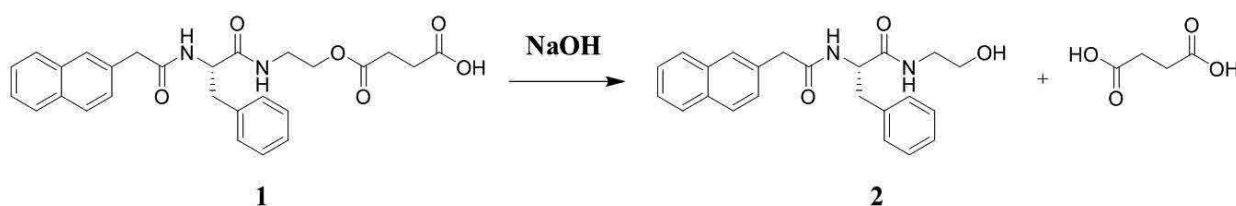


**Figure 1.13:** Chemical transformation of the aromatic PA **1** when the pH increase due to the addition of diluted solution of sodium hydroxide. The ester group of **1** is hydrolyzed providing hydrogelator **2**.<sup>56</sup>

Despite the efficiency of these strategies, it must be noted that the addition of acid or base can lead to side-reactions on the peptide sequence and to hydrogel that may be not stable during a long period at extreme pH. Furthermore, despite the alternative using chemicals able to release protons overtime, the kinetic of gel formation is slow to better control the final pH, this way requires time to get the gel. For all these reasons, a more convenient stimulus has been investigated in the last decade, ensuring a highly specific chemical transformation of the precursor peptide, with very low loading in the reaction medium and a very fast triggering of the gelation: this is the addition of an enzyme.

### 1.1.5 Enzymatic-responsive hydrogel

The enzymatic control over peptide self-assembly is an attractive approach for the development of responsive hydrogels in particular for biomedical applications.<sup>57-59</sup> In this strategy, a selective enzymatic transformation of precursor PA generates a hydrogelator with suitable amphiphilic features enhancing their self-assembly propensity. From a practical point of view, the enzyme is added into the solution of precursor peptide and then the gelation occurs spontaneously in the following few seconds or minutes.

In 2004, Xu and colleagues were the first to report the enzyme-assisted self-assembly (EASA) to get hydrogelation.<sup>29, 60</sup> In this pioneer work, alkaline phosphatase (ALP) catalyzes the dephosphorylation of a non-assembling aromatic PA precursor, FmocNH-Y( $\text{PO}_4^{2-}$ )-COOH, affording FmocNH-Y-COOH as amphiphilic self-assembling molecules (Figure 1.14). In solution, electrostatic repulsions from anionic phosphate groups inhibit the gelation process. Consequently, upon removal of the hydrophilic phosphate by ALP, FmocNH-Y-COOH peptides self-assemble through intermolecular hydrogen bonding and  $\pi$ - $\pi$  stacking.

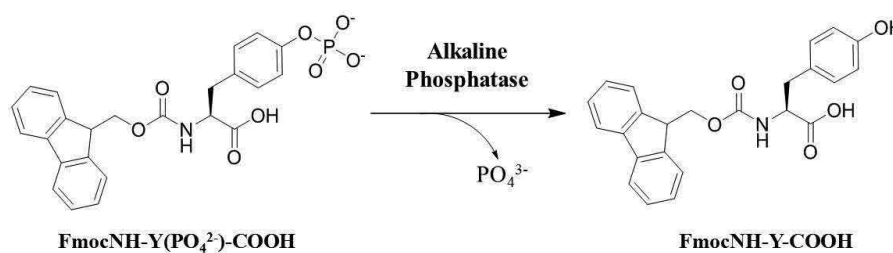


**Figure 1.14:** Aromatic PA precursor FmocNH-Y( $\text{PO}_4^{2-}$ )-COOH undergoes the enzymatic hydrolysis from alkaline phosphatase of the phosphate group on tyrosine residue, leading to the hydrogelator FmocNH-Y-COOH.

Actually, two distinct strategies are described to modulate the hydrophilic/hydrophobic of peptide sequences.<sup>61</sup> The enzyme can either cleave a covalent bond to remove meaningful chemical function from a non-assembling peptide precursor, as described by Xu *et al.* (Figure 1.14), or form a covalent bond between two peptides for instance. The first strategy is largely more used than the second one. In both cases, the enzymatic modification of the precursor peptide core triggers supramolecular self-assembly of the generated hydrogelators.<sup>62</sup> Figure 1.15.a-c presents a non-exhaustive list of examples illustrating the enzymatic conversions setting out self-assembly of peptides. In addition to ALP used by Xu *et al.*, esterase,<sup>56, 63</sup>  $\beta$ -lactamase<sup>64</sup> and subtilisin<sup>65</sup> catalyze

the cleavage of covalent bonds to regulate amphiphilic properties of aromatic peptides. Esterase catalyzes the hydrolysis of an ester group to trigger the self-assembly of NapNH-FF-COOH aromatic PA.<sup>57</sup>  $\beta$ -lactamase, known to catalyze the hydrolysis of  $\beta$ -lactam antibiotics, has also been used to reveal the self-assembling property of an aromatic PA. Ulijn's group reported the removal of a hydrophobic feature from a non-assembling precursor (FmocNH-LLL-COOMe) resulting from the action of subtilisin.<sup>66</sup> In that case, the hydrolysis of methyl ester increases the solubility of the peptide sequence (FmocNH-LLL-COOH) which triggers its self-assembly.

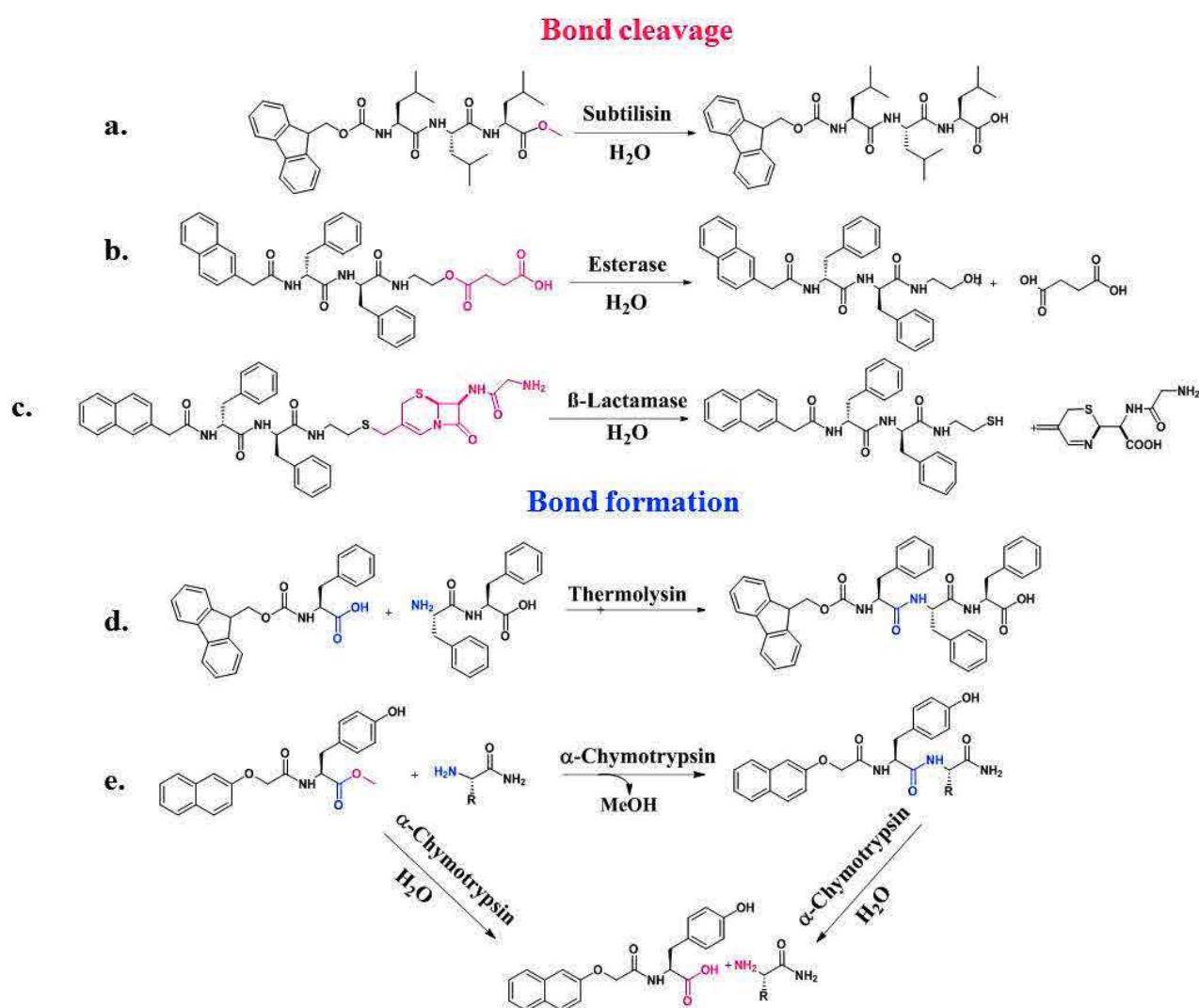


*Figure 1.15: Examples of enzyme-catalyzed reactions used in enzymatic responsive materials.*

Remarkable work was recently reported using proteases to form covalent bonds between short peptides to initiate gelation. In fact, **under appropriate conditions** proteases can perform

their reverse hydrolytic reaction favoring formation of a peptidic bond (amide group) between two non-assembling peptides to form one effective hydrogelator.<sup>67</sup> For instance, thermolysin from *Bacillus Thermoproteolyticus Rokko*, was selected by Toledano *et al.* to catalyze the “ligation” between FmocNH-F-COOH and the H<sub>2</sub>N-FF-COOH dipeptide. In that case, the product resulting from a peptide bond condensation, *i.e.* FmocNH-F-CO-NHCO-FF-COOH, self-assembled to form a network entrapping water (Figure 1.15.d).

More recently,  $\alpha$ -chymotrypsin was used to control dynamic assembly and disassembly of hydrogelator *in situ* (Figure 1.15.e).  $\alpha$ -Chymotrypsin well known to hydrolyze peptide bonds, shows capacity to catalyze transacylation<sup>68</sup> between peptide methyl/ethyl ester and hydrophobic amino acids. In 2013, Ulijn and coll. reported the condensation of Nap-Y-OMe with hydrophobic amino acids (X= F-CONH<sub>2</sub>, Y-CONH<sub>2</sub> or L-CONH<sub>2</sub>) to afford NapNH-FX-CONH<sub>2</sub> molecules that self-assemble into unidirectional nanofibers.<sup>69</sup> After 96h in the presence of  $\alpha$ -chymotrypsin, the enzymatic hydrolysis of peptide bonds led to the formation of non-interacting NapNH-Y-OH and NH<sub>2</sub>-X-COOH and fibers disassembled.

## 1.2 Surface-assisted self-assembly of LMWG

Since the middle of the last century, the functionalization of surfaces has emerged as a convenient method to control interactions between a material and its surrounding environment. Many effective approaches have been developed providing new properties to the substrate such as biocompatibility, flame retardancy, anticorrosive, self-cleaning, scratch-resistant, anti-reflective and so on. Currently, the recent boom of nanoarchitectonic systems paves the way to design chemical systems on surfaces responsive to several stimuli from the surrounding medium. This new research field is already considered as a hot topic by the scientific community since it opens up the possibility to design original “smart” functionalities to materials. However, such kind of systems require a precise and controlled design of nanostructures on a surface. To address this challenge, surface were considered as valuable support to control and pattern bottom-up assemblies of LMWG over space and time. This spatiotemporal control will allow tuning of resulting nanostructures.

This second part of the Chapter one reviews the state-of-the-art strategies developed toward the design of surface-assisted self-assembly of LMWG. The purpose is restricted to LMWG leading to gelation in water through a self-assembly process that occurs exclusively from a planar surface. This means that the self-assembly of biomacromolecules, block copolymers or inorganic species used as gelators are not take into account as well as all studies concerning particles assemblies through surface modification, self-assemblies occurring at liquid-liquid or liquid gas interfaces, and photolithographic investigations. All publications reported herein have been published in the last two decades and, in particular, more intensively over the 2013-2016 years which is the period of time of my PhD. Therefore, the following bibliographic review is constituted of few articles but is exhaustive according to the limitation scope defined just above.

### **1.2.1 Surface seeding of LMWG self-assembly**

One easy way to induce the self-assembly of LMWG exclusively from a surface and not in solution is to change the surface hydrophilicity/hydrophobicity balance of the surface. Very recently, the influence of surface properties of substrates on physical and mechanical aspects of a supramolecular hydrogel has been reported.<sup>70</sup> In this work, the initiation of the self-assembly of C<sub>14</sub>-cytidine (Figure 1.16.a) was studied on two kinds of glass surfaces exhibiting either hydrophilic groups, *i.e.* hydroxyl groups (OH-surface), or hydrophobic phenyl moieties (Ph-surface) (Figure 1.16.b). For both samples modified through silanization procedures, the surface-assisted self-assembly of C<sub>14</sub>-cytidine formed a fibrous networks leading to a hydrogel.

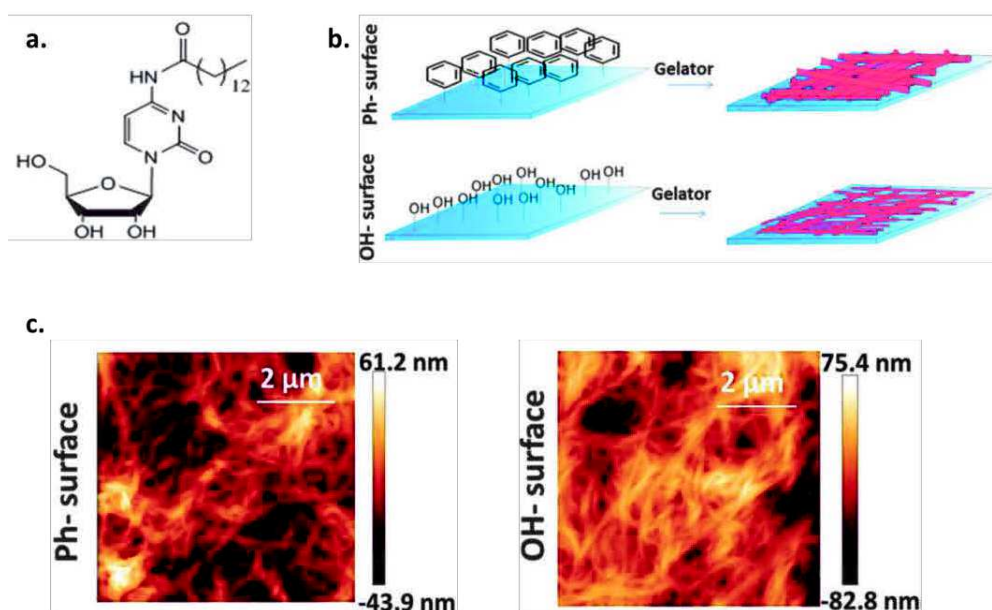


**Figure 1.16:** (a) Chemical structure of the hydrogelator  $C_{14}$ -cytidine; (b) Schematic representation of the two glass surfaces studied exhibiting either a hydrophobic or a hydrophilic property and used as substrates for hydrogel formation; (c) When both substrates are brought in contact with  $C_{14}$ -cytidine solution, distinct fibrillary network are induced in each case.<sup>70</sup>

However, analysis of each hydrogels by atomic force microscopy (AFM) revealed different physical and mechanical properties (Figure 1.16.c). Fibers self-assembled on Ph-surface present larger diameters (61.7 nm) than gel assembled on OH-surface (47 nm). Moreover, measurement of Young's modulus *via* AFM nano-indentations indicates that the gel grown on hydrophobic surface are stiffer than gels grown on hydrophilic. These results showed that physical properties of surfaces affect the process of gelators self-assembly leading to morphologically and mechanically distinct materials.

Another approach, developed by Bieser *et al.* in 2005, was based on a system composed of an anionic hydrogelator in the presence of a cationic surface. The hydrogelator studied was an aromatic amphiphile dye, *i.e.* 1-(2-*n*-hexylphenylazo)-2-hydroxy-6-naphtalene sulfonate (OHD) and the substrate was a glass surface modified with aminopropyltriethoxysilane (Figure 1.17.a). At acidic pH, the surface is positively charged due to the presence of ammonium group ( $-\text{NH}_3^+$ ) while OHD is negatively charged, whatever the pH because of the sulfonate group ( $\text{pK}_a < 0$ ). When the so-modified glass substrate is brought in contact with a highly diluted OHD solution, in fact 50

times below the minimal gelation concentration in solution, the dye is capable of gelling exclusively on the positively charged surface. The environmental scanning electron microscope (ESEM) image of the resulting surface-confined hydrogel shows a broccoli-like structure (Figure 1.17.b.).

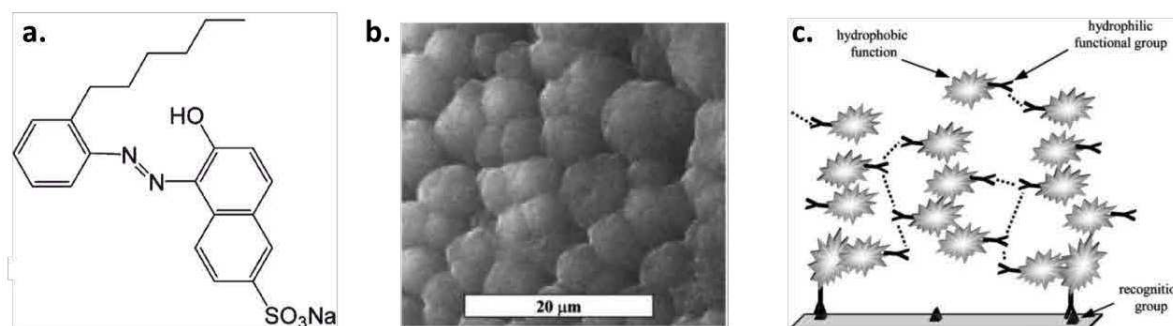


**Figure 1.17:** (a) Chemical structure of the aromatic amphiphilic dye, 1-(2-n-hexylphenylazo)-2-hydroxy-6-naphthalene sulfonate (OHD); (b) Broccoli-like structure of the OHD hydrogel formed on modified-glass surface observed by ESEM (c) Model proposed by the authors to explain the localized gelation on surface through electrostatic attraction of hydrogelator onto a surface.

The authors suggest that the gelation is due to a high local concentration of gelators at the interface, due to the electrostatic interaction between OHD and the surface, sufficient to get the gelation (Figure 1.17.c). This work has demonstrated for the first time that it is possible to obtain a localized gelation with LMWG solution under its critical gelation concentration. The surface plays the role of nucleation agent.

To get a more specific self-assembly of the LMWG from a surface, the gelator can also be used it-self to modify the substrate. This seeding surface strategy has been introduced in 2011 by using an aromatic PA as hydrogelator.<sup>71</sup> The peptide FmocNH-FF-COOH was grafted covalently on a silica wafer surface through silanization to seed the self-assembly of this dipeptide present in solution. Thus, immersion of seeded surface into aqueous solution of FmocNH-FF-COOH results in the formation of nanorods displaying  $\beta$ -sheets antiparallel structures. The self-assembly process was driven by  $\pi$ - $\pi$  interactions of the Fmoc and phenylalanine aromatic moieties attached to the surface (Figure 1.18.a).

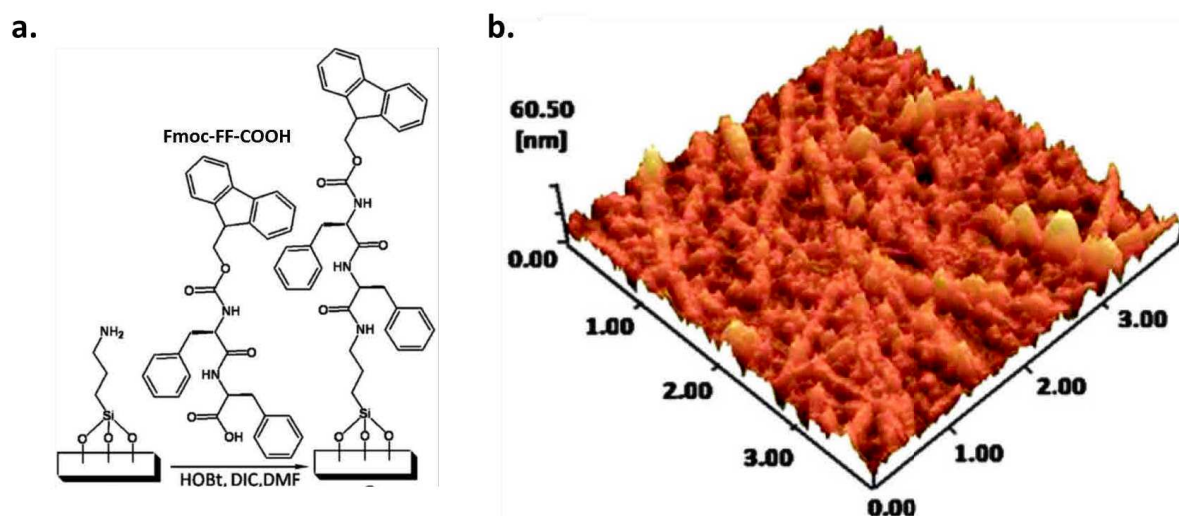


**Figure 1.18:** (a) Chemical modification of a silica wafer through silazination with aminopropyltriethoxysilane, followed by the coupling of the aromatic PA FmocNH-FF-COOH in the presence of a carbodiimide reagent (HOBt=hydroxybenzotriazole, DMF=dimethylformamide, DIC=diisopropylcarbodiimide); (b) Three-dimensional AFM image ( $4\mu\text{m}\times 4\mu\text{m}$ ) of FmocNH-FF modified silica wafer after self-assembly in aqueous solution of FmocNH-FF-COOH (2 mg/mL) and a rinsing step with aqueous acidic solutions.

Increasing concentration of FmocNH-FF-COOH generated a higher density of nanorods structures growing from the seeding surface. In comparison, immersion of an unmodified silica wafer into FmocNH-FF-COOH solution led to the physical adsorption of nanofibers that are originally formed in solution. Thus, hydrophobic interaction drives the recognition between FmocNH-FF-COOH building blocks and FmocNH-FF-COOH sequences immobilized on the surface and control the local self-assembling of peptides. The formation of nanorods structures observed exclusively on the surface (and not in solution) is explained by a local concentration threshold reached at the interface thanks to the presence of the immobilized FmocNH-FF-COOH moieties (Figure 1.18.b). It must be noted that prior to this study, several works carried out at the dry state have demonstrated that diphenylalanine forms nanotubes when an organic solution of this peptide is evaporated onto a substrate.<sup>72,73</sup>

In 2012, an application of surface-induced hydrogelation was reported in the biomedical research field using an aromatic PA. Tripeptide NapNH-FFG-COOH is selectively recognized by unknown receptors distributed all around human platelet (Figure 1.19). This interaction between the peptide and the whole platelet membrane creates a high local concentration of the hydrogelator

peptide, leading to the growth of nanofibers specifically from the cell. This organization was observed by cryo-TEM (Figure 1.19.b).<sup>74</sup>

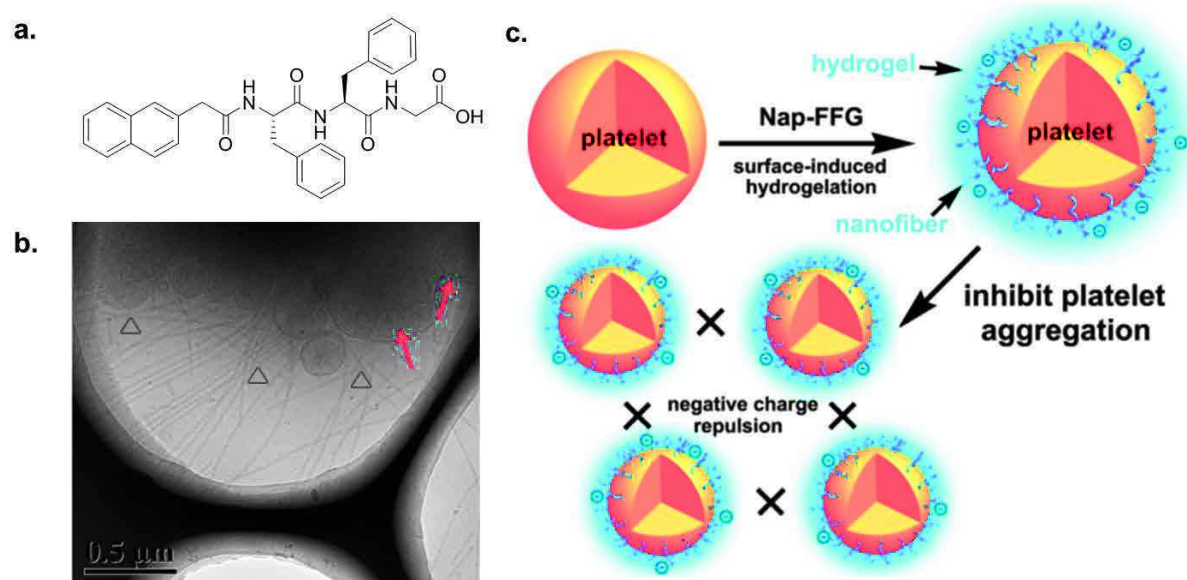


**Figure 1.19:** (a) Chemical structure of the aromatic PA NapNH-FFG-COOH; (b) Cryo-TEM images of platelets in presence of  $0.2 \text{ mg.mL}^{-1}$  of NapNH-FFG-COOH. Red arrows point out organelles of platelets and triangles point out nanofibers; (c) A possible mechanism of surface-induced hydrogelation of NapNH-FFG-COOH to inhibit platelet aggregation by negative charge repulsion.<sup>74</sup>

As proposed by the authors, this surface-induced self-assembly of NapNH-FFG-COOH leads to the formation of a thin hydrogel layer all around the cell. A protection against any aggregation with others platelets is obtained probably due to the negative charges bear by the hydrogelator peptides (ionized carboxylate group in C-terminal position).

This work provides a novel strategy to inhibit thrombus formation and may counterpart infection diseases through selective surface-induced gelation around different kinds of pathogens such as bacteria and virus.

## 1.2.2 Surface induced pH responsive self-assembly of LMWG

Herein, we present that control over such dynamic organization of LMWG could be resolved through a directed generation of chemical reactants in space and time. Because the pH is an external parameter allowing initiation of gelation processes, protons were chosen as valuable compound to pattern spatiotemporal self-assembly of LMWG at interfaces. Generation of a proton

gradient rising from the surface was implemented by two different methods: (i) surface functionalization with acidic functions to catalyze formation of the gelator and (ii) electrochemical stimulus to generate protons from an electrode. In this last approach, the spatiotemporal pattern of the self-assembly is controlled through the fine adjustment of the electrical signals applied to the system and the choice of the electrode.

### 1.2.2.1 Surface-confined acidic catalyst for self-assembly of LMWG

As described in the first part of the Chapter 1, in the mechanism of pH-responsive hydrogelation, the supramolecular self-assembly of LMWG is allowed by the protonation of non-gelating species, disturbing their hydrophilic/hydrophobic balance, and leading to self-assembling hydrogelators.

In 2014, van Esch and coworkers<sup>75</sup> adopted another strategy where protons do not displace an acid/base equilibrium but rather catalyze the *in situ* formation of hydrogelators. Confinement of acidic catalysts on the surface was realized in several steps mainly based on soft-lithographic methods. Alkenethiols were deposited on a glass surface and covalently grafted by microcontact printing. Then, thiols moieties were oxidized in contact with hydrogen peroxide solution to form sulfonic acid catalysts. In this way, the decrease of the pH near the surface catalyzed the triple condensation of the trihydrazine **1** with three aldehydes compounds **2** to afford a trihydrazone-based hydrogelator **3** (Figure 1.20.a). The resulting LMWG is not stable in solution because of the reversible feature of the hydrazone bond. However, if the concentration of **3** reaches a critical threshold near the surface, hydrogelators self-assemble spontaneously into fibers *via*  $\pi$ - $\pi$  stacking and hydrogen bond interactions (Figure 1.20.b). Thus, the catalytic rate of hydrazone bond formation is the key parameter to control the rate of the self-assembly but also to modulate the morphology and mechanical properties of the fibrous network.

**Figure 1.20:** (a) Catalytic formation of trihydrazone based hydrogelator **3** from the soluble building blocks **1** and **2** leading to nanofibers growth to trap the surrounding water to form a hydrogel; (b) Schematic representation of **3** self-assembly oriented by catalytic activity of the surface; (c) Confocal microscopy image of patterns, composed of self-assembled fibers of **3**, which reflect the stamped catalytic pattern. White line: 10  $\mu$ m width with 15  $\mu$ m spacing.<sup>75</sup>

Patterned glass slides (lines, circles, squares, etc) with the acidic catalyst were brought into contact with a solution containing the precursors **1** and **2**. To follow the self-assembly of **3** by confocal fluorescence microscopy, a fluorescent probe carrying an aldehyde group was added to the mixture of **1** and **2**. The hydrogel pattern closely follows the catalyst pattern underneath (Figure 1.20.c) and indicates that the surface-confined sulfonate groups induced fiber formation.

#### **1.2.2.2 Electrochemical trigger of pH-responsive self-assembly of peptides**

In 2010, Cameron and collaborators developed a convenient method to direct the self-assembly of an aromatic PA, FmocNH-LG-COOH, into an ultrathin hydrogel membrane on an electrode (Figure 1.21.a).<sup>76</sup> In this approach, the self-assembly of dipeptides hydrogelator was triggered in response to a decrease of pH generated from the electrode surface. To do that, an electrochemical oxidation of hydroquinone into 1,4-benzoquinone was realized, releasing two protons per hydroquinone oxidized (Figure 1.21.b.). At neutral pH, the precursor peptide deprotonated is highly soluble in water. Once protonated, its limit of solubility is almost reached, inducing the self-assembly process. Thus, the control over the gradient of protons rising from the surface presents a great potential to pattern specifically the self-assembly of FmocNH-LG-COOH in space and in time as well: indeed, without the application of the right oxidative potential, no self-assembly occurs.

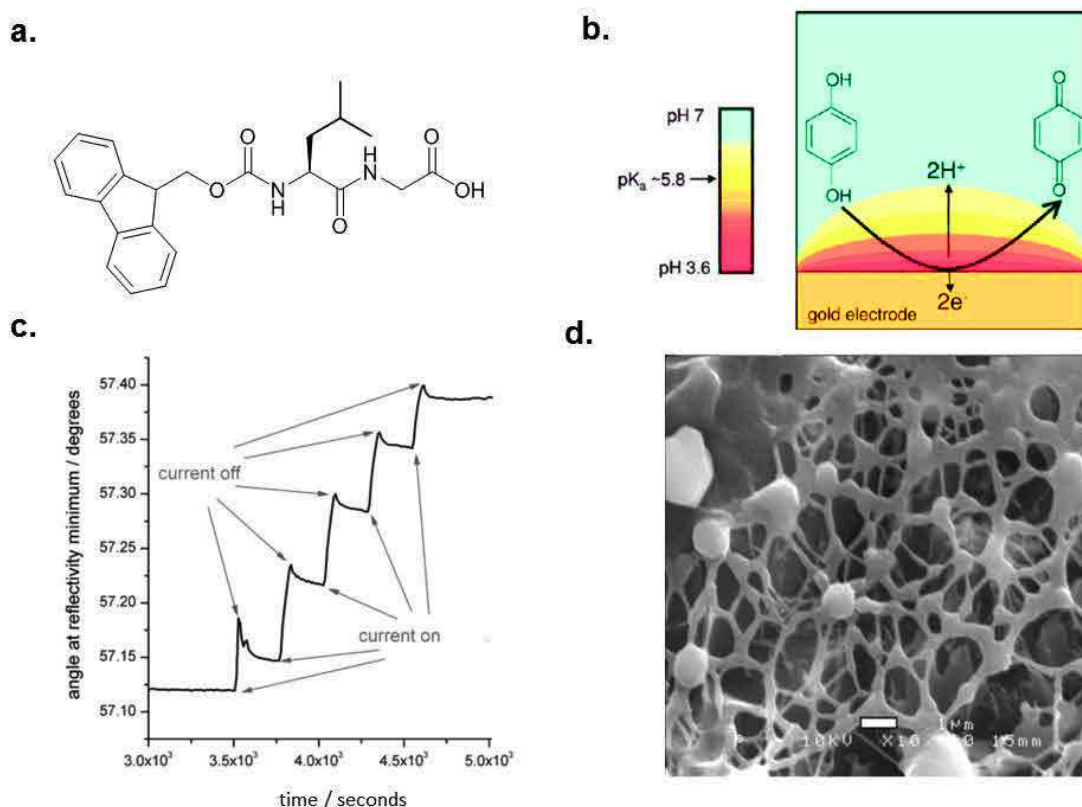


**Figure 1.21:** (a) Chemical structure of the aromatic PA, FmocNH-LG-COOH; (b) Electrochemical oxidation of 1,4-hydroquinone in 1,4-benzoquinone, releasing two protons per molecule of hydroquinone from the electrode surface, generating a gradient of protons going from the bottom to the top; (c) SPR experiment showing the stepwise growth of the dipeptide hydrogel with each 60 s current pulse; (d) Cryo-SEM image of the top surface of an electrochemically grown gel film. The scale bar is 1  $\mu m$ .<sup>76</sup>

The adjustment of the current intensity allows a precise control of the growth of a fibrous network, entrapping water at the interface. In fact, when a current of  $20 \mu A \cdot cm^{-2}$  is applied for 60 s, the formation of a stable transparent gel was obtained and followed *in situ* by surface plasmon resonance (SPR), TEM and cryo-SEM microscopy (Figures 1.21.c-d). SPR was coupled with an electrochemical device to characterize the real-time evolution of thin films thickness ( $\leq 200$  nm) as function of the electrical signal applied. The control over duration and voltages of electrical inputs affects the pH near the surface and thus impacts the FmocNH-LG-COOH self-assembly, in particular the resulting thickness and the density of gel, observed by confocal microscopy (using a fluorescent dye during the gel buildup),

The authors successfully patterned the self-assembly of FmocNH-LG-COOH through localized electrical signals on microelectrodes. By controlling the process of hydrogelation, fabrication of precise functional materials is foreseen.

When 80-100 nm of hydrogel is reached and the electrochemical stimulus is stopped, slow growth of a thicker gel (48 hours) was reported by Cameron in 2013.<sup>77</sup> The first electro-stimulated gel on the surface plays the role of a seeding layer for a second gelation that occurs without any stimulus (Figure 1.21a). From a practical point of view, when a neutral solution (pH 7) of non-assembling peptides Fmoc-LG-COOH is brought in contact with the seeding layer, a millimetric hydrogel constituted of large and long fibers is formed (Figure 1.22.b).

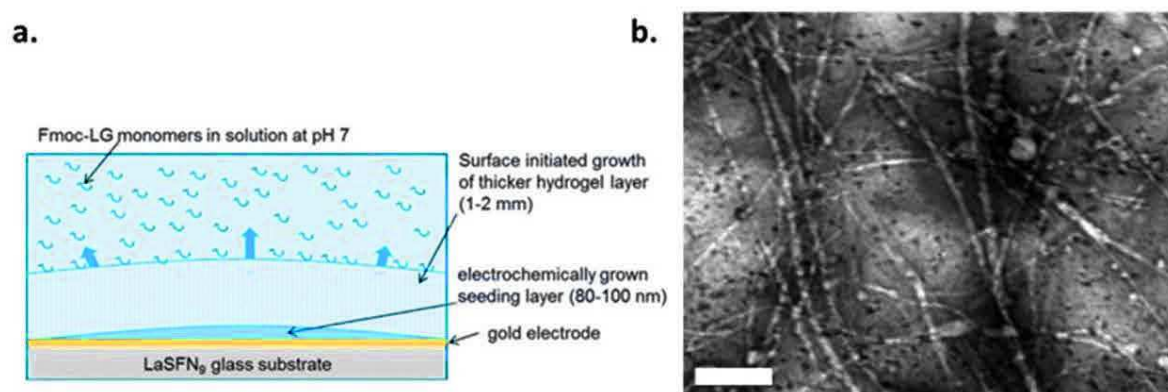


**Figure 1.22:** (a) Schematic representation of the surface initiated growth of a FmocNH-LG-COOH based film; (b) TEM image of the seeding layer grown electrochemically onto the TEM grid (Scale bar: 20 nm).<sup>77</sup>

To explain this second self-assembly process of peptides FmocNH-LG-COOH, Cameron and collaborators claimed that residual protons trapped into the first seeding thin gel lowered the pH at the interface of the two gels and shifted the pK<sub>a</sub> of FmocNH-LG-COOH. Thus, the self-assembling process could nucleate from a small number of peptide-based spheres aggregates localized on the top of the seeding layer. It must be noted that Horse Radish Peroxidase (HRP) could also be successfully embedded into the second hydrogel layer affording a catalytic function to the hydrogel. The HRP activity was probed by UV-visible spectrophotometry monitoring the conversion of *o*-phenylenediamine (ODP) in orange 2,3-diaminophenazine (DAP). This result highlights the possibility offers by this strategy to design biosensors.

To sum up the contribution of Cameron and coworkers in this field, a gradient of protons generated at the interface of an electrode induces the gelation of aromatic PA. This protons-containing hydrogel can play the role of seeding layer through the slow release of protons, triggering the self-assembly of a second layer of peptide-based hydrogel.

The self-assembly of another hydrogelator initiated locally by electrochemical oxidation of hydroquinone was recently investigated using patterned electrodes.<sup>78</sup> By using the N-protected phenylalanine amino acid with Fmoc group, FmocNH-F-COOH (Figure 1.23.a), the group of Payne has extended the electrochemical control over the LMWG self-assembly by studying the reversible assembly/disassembly of hydrogelators. In this approach, the self-assembly of FmocNH-F-COOH was locally initiated through an electrochemical production of protons and monitored with electrochemical quartz crystal microbalance (E-QCM). As demonstrated by Cameron, the proton gradient created at the interface directed the self-assembly.

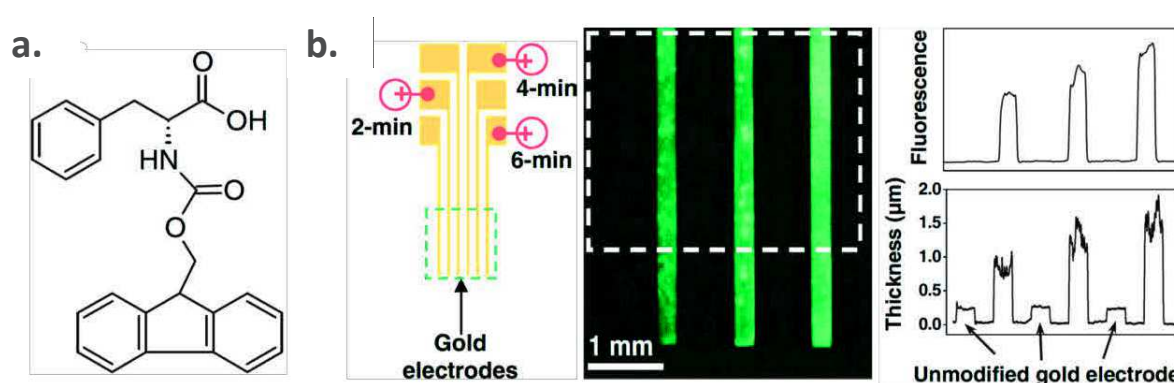


**Figure 1.23:** (a) Chemical structure of the FmocNH-F-COOH; (b) Spatial-selectivity of FmocNH-F-COOH electrodeposition. Chip study with patterned gold electrodes (250  $\mu\text{m}$  wide gold lines patterned onto silicon wafer) demonstrates spatial selectivity of electrodeposition of 10mM FmocNH-F-COOH (0.005 M fluorescein-labeled dextran was included for visualization).<sup>78</sup>

The spatially directed self-assembly of FmocNH-F-COOH was implemented by using a gold-electrode made of independent indentations. Each electrode indentation was partially immersed in a solution of Fmoc-F-COOH (10mM) with fluorescein labeled dextran and submitted to an anodic current (1 A.m<sup>-2</sup>) for 2, 4 and 6 min. Thus, the protected amino acid FmocNH-F-COOH is involved in the nanofibers constituting the gel backbone becomes soluble again in water. Characterization of surfaces by fluorescence microscopy and profilometry have revealed that the self-assembly of FmocNH-F-COOH can be selectively controlled in space (normal and lateral direction) and in time by localized application of the electrical signals and its duration, respectively (Figure 1.23.b). A reversible assembly/disassembly of the hydrogel was obtained on an electrode chip. The gel disassembled in response to a cathodic current that increases the pH at proximity of the electrode surface. When simultaneous cathodic and anodic currents are addressed to adjacent

electrodes, spatially-specific assembly and disassembly of FmocNH-F-COOH were observed on the same chip. This spatial and temporal control over the proton gradient is the key process to pattern reversibly assembly and disassembly of aromatic N-protected amino acid.

In 2014, Adams and coworkers have applied this surface-generated protons to electrochemically triggered spatially and temporally resolved multi-component gels.<sup>79</sup> By using different aromatic PA present simultaneously in solution and a gradient of protons produced from an electrode through the oxidation of hydroquinone, the authors have demonstrated the possibility to control the chemical constitution of a gels

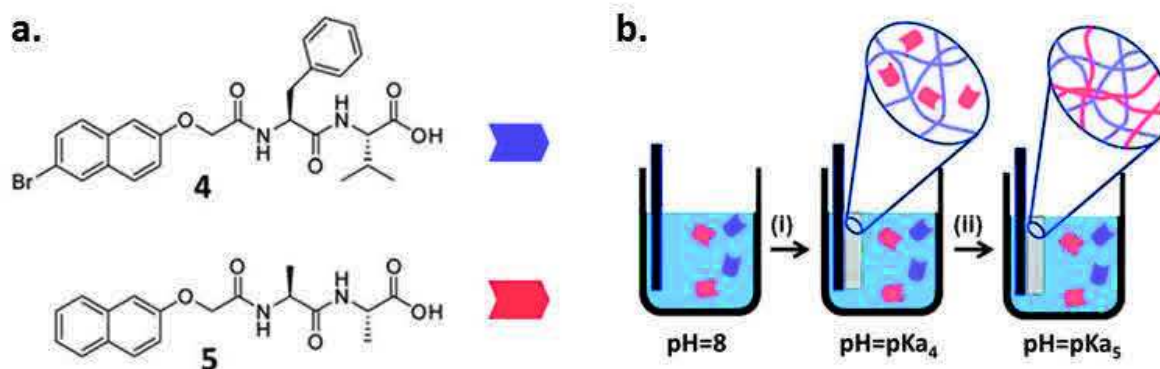


**Figure 1.24:** (a) Schematic representation of dipeptide based LMWG 4 and 5; (b) Schematic representation showing sequential assembly of two LMWG 4 and 5 in multicomponent system.<sup>79</sup>

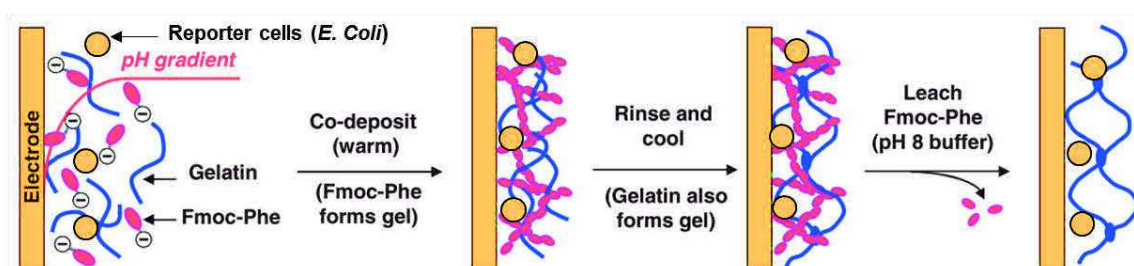
Indeed, different aromatic PA exhibit a variability of their pKa: this means that the sensitivity to the pH differs from one peptide to another. Therefore, playing with the electrochemical parameters allowing the oxidation of hydroquinone, it is possible to tune the production of protons and thus the self-assembly propensity of different peptides. Aromatic dipeptides 4 and 5 were selected as building blocks to design multi-component hydrogels (Figure 1.24.a.). Due to their distinct pKa values (pKa<sub>4</sub>=6.6 and pKa<sub>5</sub>=5.0), 4 and 5 show independent propensity to self-assemble in the vicinity of the electrode/surface. Surface gelation of 4 was obtained by the intensity application of 5 to 10  $\mu\text{A}$ , meanwhile 5 do not provide any gel on the electrode: in this conditions, 5 is not an effective hydrogelator. However, when a current of 20 to 100  $\mu\text{A}$  is applied, a mixture solution of 4 and 5 provides two different volume of hydrogel. At 50  $\mu\text{A}$  (during 1000 seconds), hydrogel 4 have a higher volume (30.5 mm<sup>3</sup>) than 5 (6.7 mm<sup>3</sup>). These

preliminary investigations showed the important influence of the apparent pKa of LMWGs on the ability to form a gel.

Thus, in the same bulk, the self-assembly of **4** and **5** was controlled upon number of protons generated from the surface by NMR. Fine adjustment of the pH near the electrode surface permitted to reach pKa<sub>4</sub> in the first place. LMWG **4** self-assembled to form 3D network of fibers entrapping both water and the second non self-assembling LWMG **5** (Figure 1.24.b). Then, a continuous decrease of pH initiate the self-assembly of LMWG **5** to finally form an interpenetrated multi-component hydrogel. Chemical composition of gels can be controlled temporally and spatially through fine adjustment of electrical inputs that tuned the self-assembly assembling property of both LMWGs **4** and **5**. This patterning of the gel composition appears an effective tool to generate specific region of functionality in space and over time. In this context, sequential growth of interpenetrated LMWG hydrogel presents a great potential for many applications.

Surface-assisted self-assembly relied on electrodeposition of the pH-responsive hydrogelator, FmocNH-F-COOH (Figure 1.23.a) based on a pH gradient was used to prepare an efficient biosensor based on the encapsulation of bacteria.<sup>20</sup> The aim of this study was to develop a multi-component matrix able to detect the presence of S-adenosyl-homocysteine (SAH) in the surrounding solution, used as a model substrate. The fabrication of this sensitive matrix was achieved in two steps (Figure 1.25): First, self-assembly of FmocNH-F-COOH was trigger through the application of an anodic current generating localized proton gradient. This gelation is realized with a warm solution containing the hydrogelator of course, but also gelatin and cells (*E. Coli*) leading to their entrapment into the self-assembled structure. When the system is cool down, an interpenetrated network is formed, due to the assembly of gelatin chains. This hybrid network is viable for *E. Coli*.

### 1. Electrochemical self-assembly



### 2. Enzymatic covalent crosslink

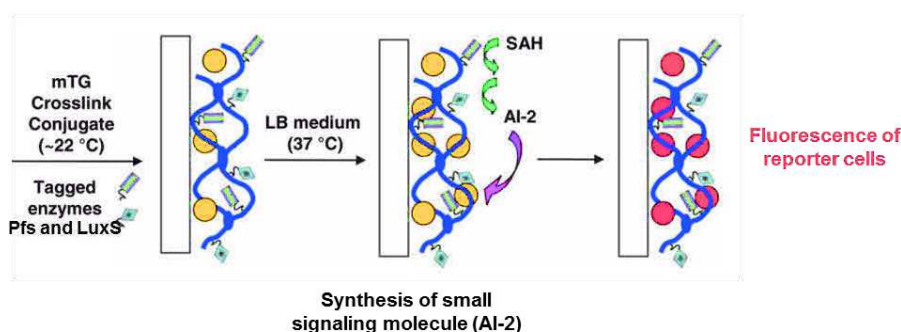


**Figure 1.25:** Experimental pathway for the co-deposition of gelatin and Fmoc-F-COOH. Thus, multifunctional gelatin based matrix is capable of in situ synthesis and detection of a bacterial quorum sensing signaling molecules.<sup>20</sup>

Then, the peptide-based scaffold was dissolved thanks to a simple addition of a basic buffer (pH =8) providing a gelatin matrix embedded with cells. By using transglutaminase (mTG), the covalent immobilization of two conjugated enzymes (Pfs and Luxs) was done, as well as the cross-linking of the gelatin architecture. In this way, SAH is transformed through a cascade of enzymatic reactions (based on Pfs and Luxs), leading to the signaling molecule AI-2. This compound is recognized by *E. coli*, engineered to express a fluorescent protein (DsRed) upon exposure to AI-2.

In summary, the association of electrochemical triggered co-deposition and enzymatic crosslinking assisted the development of multifunctional materials. In this concept, spatiotemporal control of Fmoc-F-COOH self-assembly is fundamental for the fabrication of the main scaffold functionalized by different biological components. Electrochemical control over surface-induced self-assembly contributes to create functional gels.

### 1.2.3 Localized enzyme assisted self-assembly of peptides (LEASA)

As described in the first part of this Chapter 1, since 2004, enzyme catalysis emerged as a valuable stimulus to spontaneously and selectively transform non-assembling precursors into efficient LMWG.

In 2009, Ulijn and coworkers were the first to immobilize covalently an enzyme, *i.e.* thermolysin, in order to study the local self-assembly of a mixture composed of FmocNH-L-COOH and the diamino acids NH-LL-COOH (Figure 1.26a).<sup>80</sup> Thermolysin is able to both catalyze the coupling reaction between FmocNH-L-COOH and several diamino acids NH-LL-COOH, and also the hydrolysis of amide bonds, leading to a statistic distribution of oligopeptides FmocNH-L<sub>n</sub>-COOH. These aromatic PA can thus self-assemble to form fibers.

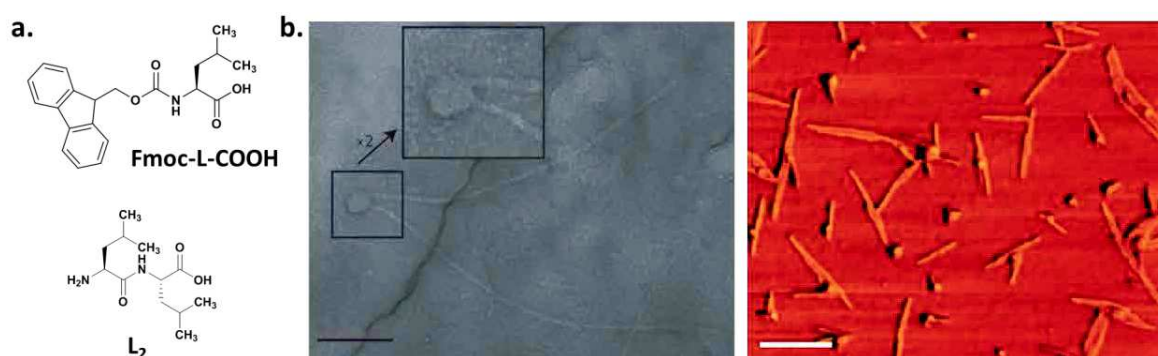


**Figure 1.26:** (a) Chemical structures of FmocNH-F-COOH and L<sub>2</sub>; (b) (left) TEM image observed with fiber propagation, demonstrating confined fiber growth from spherical structures (scale bar 100 nm); (right) The same process as visualized by AFM phase imaging (scale bar 250 nm).<sup>80</sup>

The enzyme was grafted on glass wafer through a silanization method displaying free epoxyde groups. When a thermolysin solution is brought in contact with this so-modified surface, the ring-opening reaction of oxiranes by the amino groups all along the enzyme ensures the covalent attachment. Then, in the presence of both FmocNH-L-COOH and the diamino acids NH-LL-COOH, oligopeptides FmocNH-L<sub>n</sub>-COOH were produced from the surface. At the early stages of the self-assembly process, the nucleation have been visualized both by TEM and AFM (Figure 1.26.b).

This recent pioneer work has shown that the confinement of enzymes onto a surface can be a fine strategy to locally nucleate and growth of LMWG-fibers at the interface.

In 2014, the group of Xu has applied this approach to the pericellular enzymatic assisted self-assembly of D-peptides.<sup>81</sup> This project is based on the fact that mammalian cancer cells secrete alkaline phosphatase. This enzyme is both released in the surrounding environment of cancer cells, but exposed on the external side of the cell membrane.

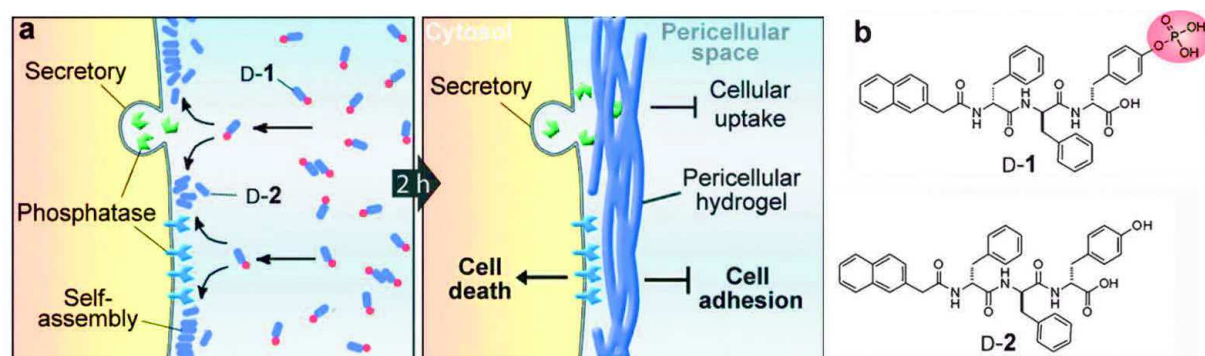


**Figure 1.27:** (a) Enzymatic-catalyzed formation of pericellular hydrogels to induce cell death; (b) Molecular structures of the precursor Nap-FFY- $PO_4^{2-}$  (D-1) and the hydrogelator Nap-FFY (D-2).<sup>81</sup>

When mammalian cancer cells are brought in contact with a solution of the aromatic PA, NapNH-FFY( $PO_4^{2-}$ )-COOH (D-1 in Figure 1.26.b), alkaline phosphatase locally confined on cells membranes initiates the self-assembly of NapNH-FFY (D-2) by removing the phosphate group from the D-1 peptide sequence. As a result, NapNH-FFY-COOH hydrogelator self-assembled into fibers to form a thin hydrogel layer all around cancer cells. Consequently, the growth of this pericellular hydrogel blocked cellular mass exchanges, refrained cell migration and cell adhesion to finally induce apoptosis.

Enzyme responsive self-assembly is an attractive approach to trigger hydrogelation process. Enzymatic catalysis are highly selective able to transform continuously precursor molecule into LMWG. This autonomous control over the rate of LMWG formation confined to the surface contributes to development of smart surface able to direct organization of matter in space and time.

This second part of the Chapter one reviewed recent researches on surface assisted self-assembly of small molecules in aqueous medium. Among all strategies reported, aromatic AP or

protected single amino acids are the most useful for surface-assisted self-assembly process. This mini-review highlighted three main strategies implemented for this purpose. First, surfaces grafted with chemical entities were used in order to create new environment of interactions for small building-blocks at proximity of the surface. In a second strategy, pH responsive hydrogelations from a surface have been intensively developed for *in situ* formation of self-assembling building blocks. The decrease of pH is confined at the vicinity of the surface by electrical signal or soft lithography of specific moieties. Finally in a third strategy, natural enzymes were used as highly selective and efficient stimuli able to catalyze the formation of self-assembling building blocks. This last approach was published in pioneer and single paper in 2009 and was applied to biological system very recently, in 2014. During the three years of my PhD, my research work was based on this third strategy in order to design sophisticated surface displaying both catalytic properties and the ability to initiate the self-assembly of LMWG in spatiotemporal controlled way. A special attention was also paid on the identification of parameters leading to this goal.

### 1.3 Polyelectrolyte multilayer films

The control of the interactions between a material and its environment can be achieved by functionalization of its surface. Different techniques of surface functionalization have been developed usually dependent on the nature of both the material and the deposited molecules or macromolecules. In this thesis, we used the layer-by layer (LbL) deposition of polyanions and polycations leading to what is called “polyelectrolyte multilayer (PEM)” to functionalize the surfaces. Introduced in 1991 by Prof Gero Decher.<sup>82</sup> The LbL technique presents many advantages as the fact that it can be applied to almost all kinds of substrates whatever their chemical nature and topography, the fact that the surface properties of the film can be tuned and different types of molecules/macromolecules can be deposited. In the following section, we will summarize the different properties of PEM.

#### 1.3.1 Polyelectrolyte Multilayer assemblies

Polyelectrolyte multilayers (PEM) are obtained by the LbL deposition method that consists in the alternated deposition of negatively (polyanions) and positively (polycations) charged polymer chains on the surface of a material (Figure 1.28). The substrate, usually negatively

charged, is immersed into a polycation solution for a short period of time (5 to 20 min). The positively charged chains are adsorbed on the surface through electrostatic interactions. After a rinsing step, to eliminate excess of adhering polymer chains, the surface becomes positively charged due to the overcompensation of charges.

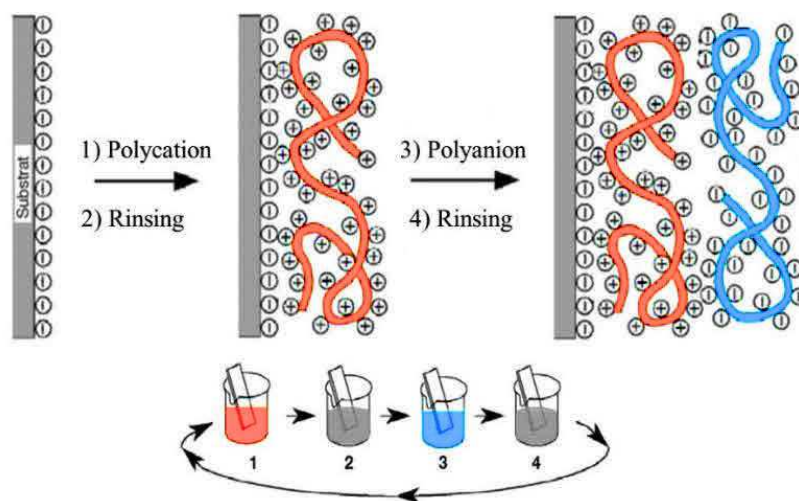


**Figure 1.28:** Schematic representation of polyelectrolyte multilayer (PEM) film buildup by dipping process.<sup>82</sup>

Thus, this surface can be used to adsorb a layer of polyanion by the same process. Here again, at the end of the polyanion deposition step, after rinsing, a charge overcompensation is observed, the surface becomes negatively charged. The LbL deposition can be repeated until the desired film thickness is reached. The layer-by-layer assembly is a method of choice to functionalize a large variety of materials. In this thesis, the LbL method was used to functionalize different kinds of flat surfaces such as glass slides,<sup>82</sup> silicon wafers,<sup>83</sup> quartz crystal<sup>84</sup> or polydimethylsiloxane (PDMS) sheet.<sup>85</sup>

### 1.3.2 Deposition methods

Different experimental methods were developed to build-up PEM films. The **dip-coating** deposition was the first method introduced by Gero Decher at the beginning of the 1990's (Figure 1.29.a). This process relies on the alternated immersion of the substrate into polycation and polyanion solutions. Each deposition step of charged macromolecules is followed by a rinsing step with either buffer or pure water.<sup>86</sup>

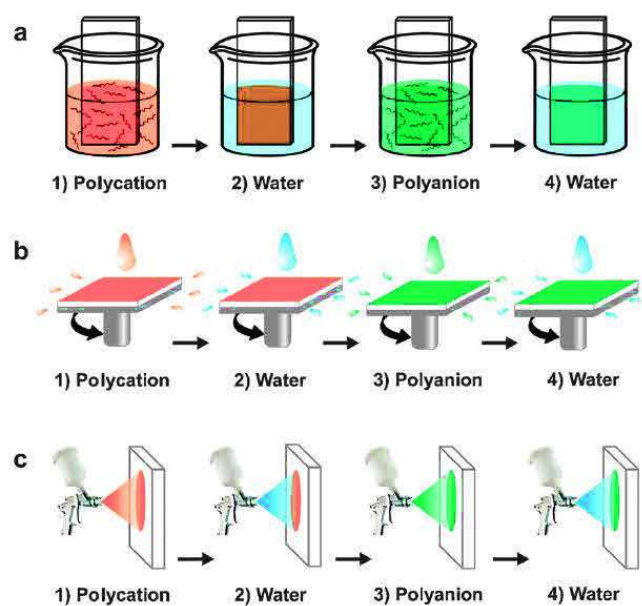


**Figure 1.29** Schematic representation of PEM films buildup processes (a) dipping LbL assembly, (b) spin-assisted LbL assembly, (c) spray-assisted LbL assembly. The growth of the film is based on the repetition of the cycles (steps 1 to 4).<sup>87</sup>

**Spin-coating**<sup>88</sup> is another process that can be used to build-up PEM. It was first used in the 2000's to reduce the time of deposition of polyelectrolytes (Figure 1.29.b).

The LbL buildup is assisted by a device allowing homogenous repartition of macromolecules adsorbed on a planar surface. A small amount of a polyelectrolyte solution is deposited on a rotating substrate at high speed. The centrifugal force generated by high speed rotation pulls out the polymer solution to create a homogenous deposition of polyelectrolytes on the substrate. This technique presents two advantages: charged polymer chains can be deposited in less than 1 min and no rinsing

step is required between each polyanion and polycation adsorption step. However, a planar surface with a reasonable size of the substrate is required.

The **spraying method** introduced by Schlenoff et al.<sup>89</sup> in 2000 consists in scattering droplets of polyelectrolyte solutions on a surface held vertically, allowing the drainage of the excess solution (Figure 1.29.c). This technique allows obtaining uniform coating on large substrates in a short period of time.

### 1.3.3 Growth regime and tunable properties of PEM films

PEM films can have two types of growth regimes: the film thickness can increase either linearly or exponentially with the number of deposition steps as represented in Figure 1.30.

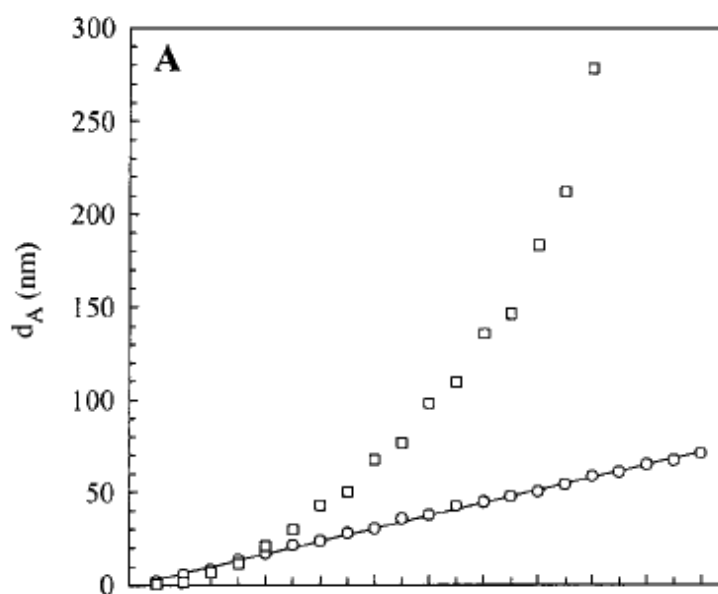


**Figure 1.30:** Evolution of the thickness of a (○) PEI-(PSS/PAH)<sub>i</sub> linear film and a (□) PEI-(PGA/PLL)<sub>i</sub> exponential film as a function of the number of deposited *i* layer pairs.<sup>90</sup>

In the case of linearly growing films, the adsorbed polyelectrolytes interact only with the top of the film which results in a stratified architecture. Poly(allyl amine)/Poly(styrene sulfonate) (PAH/PSS) is one of the most prominent example of linearly growing films.<sup>82</sup>

In the case of exponentially growing films, the thickness and mass increase at each "bilayer" deposition step, are proportional to the already deposited mass of the film. The exponential growth can be explained by the diffusion of at least one of the polyelectrolytes in and out of the entire film during each deposition step.<sup>91</sup> Polypeptides and polysaccharides films have generally an exponential growth. That is for example the case of the poly(L-lysine)/hyaluronic acid (PLL/HA)<sup>91</sup> or PLL/poly(L-glutamic acid) (PLL/PGA) systems.<sup>92</sup> Such films are highly hydrated and can often play the role of a reservoir for active compounds such as enzymes.

Different physical-chemical parameters can influence the buildup of PEM films, especially their growth mode, thickness, and roughness. The ionic strength of polyelectrolyte solutions has a strong influence on the film growth. PEM films are thicker at a high ionic strength compared to low ionic strength.<sup>93</sup> At high salt concentration, polyelectrolyte chains adopt a "loopy" conformation due to the screening of charges by salt. At low salt concentration, the charges on a polyelectrolyte repel each other giving a "flat" or rigid-rod like conformation to the polymer chain (Figure 1.31). The adsorbed layer of polyelectrolyte is thus thicker at high ionic strength compared to low ionic strength.

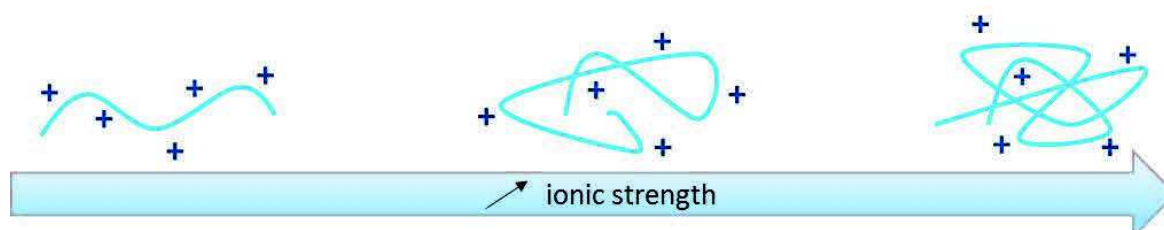


**Figure 1.31:** Conformation changes of a polycationic polymer with the ionic strength

The pH of weak polyelectrolyte solutions is described as a significant parameter affecting their degree of ionization.<sup>94</sup> A variation of pH induces a change in the number of charges on the polyelectrolytes. As in the case of ionic strength, pH affects the chain conformation of weak polyelectrolytes. As a consequence, thickness and roughness of PEM films can easily be tuned by varying the pH.<sup>95</sup>

Electrostatic interactions were historically employed as the main driving forces for LbL assemblies. Over the years, weaker interactions were also investigated. Among them, hydrogen

bonding<sup>96</sup> (5 to 30 kcal.mol<sup>-1</sup>) shows interesting properties as driving force for adsorption of macromolecules onto a substrate. In 1997, Rubner *et al.*<sup>97</sup> developed hydrogen-bonding multilayer coatings by alternated deposition of polyaniline and poly(vinylpyrrolidone), poly(vinyl alcohol), poly(acrylamide), or poly(ethylene oxide). This new type of systems showed a real sensitivity to environmental parameters such as pH. In fact, modification of pH can directly influence nonionic polymer's capacity to form hydrogen bonds.<sup>98</sup> Polyphenols were reported in literature as good candidates for LbL assembly based on H-bonds. Among them, tannic acid (TA) is a natural water-soluble polyacid described as a good H-donors with compounds containing carbonyl groups. TA was associated with charged or neutral polymers<sup>99</sup> but it was also complexed with diverse macromolecules such as proteins.<sup>100</sup>

### 1.3.4 Coating features and applications

Due to the versatility of the LbL method, PEM films have been developed for a large range of applications in fields as different as biologically active membranes,<sup>101</sup> drug release<sup>102-103</sup> or biologically active coatings.<sup>104-106</sup> Indeed, LbL coatings can be functionalized by different biological molecules such as proteins,<sup>107</sup> polypeptides,<sup>92</sup> DNA,<sup>108</sup> capsules,<sup>109</sup> or cells<sup>110</sup> (Figure 1.32). To remain active, proteins have to keep their conformation. Analysis by Fourier transform infrared spectroscopy showed that the secondary structure of proteins are preserved when inserted in PEM films.<sup>111</sup>

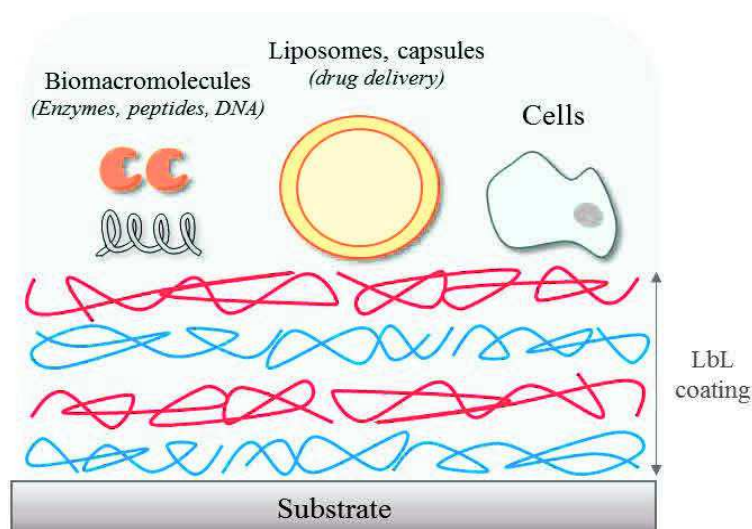


**Figure 1.32:** Schematic representation of layer-by-layer coating hosting biological species.

Moreover, it has been shown that enzymes such as glucose isomerase, glucoamylase, glucose oxidase and peroxidase,<sup>101</sup> embedded in PEM films, retain their enzymatic activity. Proteins (or enzymes) can be adsorbed or embedded in PEM films to obtain specific properties such as anti-inflammatory property,<sup>105</sup> enzymatic transformation of starch into glucose<sup>101</sup> or differentiation and proliferation of osteoblastic precursor cell.<sup>112</sup>

In this thesis work, LbL coating method was used to create enzymatically active films to initiate hydrogel growth.

---

## References

1. Sangeetha, N. M.; Maitra, U. Supramolecular gels: Functions and uses. *Chemical Society Reviews* **2005**, *34* (10), 821.
2. Tuttolomondo, M. V.; Galdoporpora, J. M.; Trichet, L.; Voisin, H.; Coradin, T.; Desimone, M. F. Dye-collagen interactions. Mechanism, kinetic and thermodynamic analysis. *RSC Advances* **2015**, *5* (71), 57395.
3. Eglin, D.; Maalheem, S.; Livage, J.; Coradin, T. In vitro apatite forming ability of type I collagen hydrogels containing bioactive glass and silica sol-gel particles. *Journal of Materials Science: Materials in Medicine* **2006**, *17* (2), 161.
4. Chen, L.; An, H. Z.; Doyle, P. S. Synthesis of Nonspherical Microcapsules through Controlled Polyelectrolyte Coating of Hydrogel Templates. *Langmuir* **2015**, *31* (33), 9228.
5. Augst, A. D.; Kong, H. J.; Mooney, D. J. Alginate Hydrogels as Biomaterials. *Macromolecular Bioscience* **2006**, *6* (8), 623.
6. Ranga, A.; Lutolf, M. P.; Hilborn, J.; Ossipov, D. A. Hyaluronic Acid Hydrogels Formed in Situ by Transglutaminase-Catalyzed Reaction. *Biomacromolecules* **2016**, *17* (5), 1553.
7. Priya, M.; Kumar, R.; Sivashanmugam, A.; Nair, S.; Jayakumar, R. Injectable Amorphous Chitin-Agarose Composite Hydrogels for Biomedical Applications. *Journal of Functional Biomaterials* **2015**, *6* (3), 849.
8. Buwalda, S. J.; Boere, K. W. M.; Dijkstra, P. J.; Feijen, J.; Vermonden, T.; Hennink, W. E. Hydrogels in a historical perspective: From simple networks to smart materials. *Journal of Controlled Release* **2014**, *190*, 254.
9. Brenzinger, Z. *Physiol. Chem.* **1892**, *16*, 537.
10. Gortner, R. A. H., W. F. An Interesting Colloid Gel. *Journal of the American Chemical Society* **1921**, *43*, 2199.
11. Menger, F. M.; Caran, K. L. Anatomy of a Gel. Amino Acid Derivatives That Rigidify Water at Submillimolar Concentrations. *Journal of the American Chemical Society* **2000**, *122* (47), 11679.
12. Houton, K. A.; Morris, K. L.; Chen, L.; Schmidtman, M.; Jones, J. T. A.; Serpell, L. C.; Lloyd, G. O.; Adams, D. J. On Crystal versus Fiber Formation in Dipeptide Hydrogelator Systems. *Langmuir* **2012**, *28* (25), 9797.
13. Li, X.; Kuang, Y.; Lin, H.-C.; Gao, Y.; Shi, J.; Xu, B. Supramolecular Nanofibers and Hydrogels of Nucleopeptides. *Angewandte Chemie International Edition* **2011**, *50* (40), 9365.

14. Chen, Q.; Lv, Y.; Zhang, D.; Zhang, G.; Liu, C.; Zhu, D. Cysteine and pH-Responsive Hydrogel Based on a Saccharide Derivative with an Aldehyde Group. *Langmuir* **2010**, *26* (5), 3165.
15. Hsu, L.-H.; Hsu, S.-M.; Wu, F.-Y.; Liu, Y.-H.; Nelli, S. R.; Yeh, M.-Y.; Lin, H.-C. Nanofibrous hydrogels self-assembled from naphthalene diimide (NDI)/amino acid conjugates. *RSC Advances* **2015**, *5* (26), 20410.
16. Zelzer, M.; Ulijn, R. V. Next-generation peptide nanomaterials: molecular networks, interfaces and supramolecular functionality. *Chemical Society Reviews* **2010**, *39* (9), 3351.
17. Ravichandran, R.; Griffith, M.; Phopase, J. Applications of self-assembling peptide scaffolds in regenerative medicine: the way to the clinic. *Journal of Materials Chemistry B* **2014**, *2* (48), 8466.
18. Bhuniya, S.; Seo, Y. J.; Kim, B. H. (S)-(+)-Ibuprofen-based hydrogelators: an approach toward anti-inflammatory drug delivery. *Tetrahedron Letters* **2006**, *47* (40), 7153.
19. Jayawarna, V.; Ali, M.; Jowitt, T. A.; Miller, A. F.; Saiani, A.; Gough, J. E.; Ulijn, R. V. Nanostructured Hydrogels for Three-Dimensional Cell Culture Through Self-Assembly of Fluorenylmethoxycarbonyl–Dipeptides. *Adv Mater* **2006**, *18* (5), 611.
20. Liu, Y.; Terrell, J. L.; Tsao, C. Y.; Wu, H. C.; Javvaji, V.; Kim, E.; Cheng, Y.; Wang, Y. F.; Ulijn, R. V.; Raghavan, S. R.; Rubloff, G. W.; Bentley, W. E.; Payne, G. F. Biofabricating Multifunctional Soft Matter with Enzymes and Stimuli-Responsive Materials. *Advanced Functional Materials* **2012**, *22* (14), 3004.
21. Ulijn, R. V.; Smith, A. M. Designing peptide based nanomaterials. *Chemical Society Reviews* **2008**, *37* (4), 664.
22. Cui, H.; Webber, M. J.; Stupp, S. I. Self-assembly of peptide amphiphiles: From molecules to nanostructures to biomaterials. *Peptide Science* **2010**, *94* (1), 1.
23. Bowerman, C. J.; Nilsson, B. L. Review self-assembly of amphipathic  $\beta$ -sheet peptides: Insights and applications. *Peptide Science* **2012**, *98* (3), 169.
24. Swanekamp, R. J.; DiMaio, J. T. M.; Bowerman, C. J.; Nilsson, B. L. Coassembly of Enantiomeric Amphipathic Peptides into Amyloid-Inspired Rippled  $\beta$ -Sheet Fibrils. *Journal of the American Chemical Society* **2012**, *134* (12), 5556.
25. Zhang, S.; Holmes, T.; Lockshin, C.; Rich, A. Spontaneous assembly of a self-complementary oligopeptide to form a stable macroscopic membrane. *Proceedings of the National Academy of Sciences* **1993**, *90* (8), 3334.
26. Lee, N. R.; Bowerman, C. J.; Nilsson, B. L. Effects of Varied Sequence Pattern on the Self-Assembly of Amphipathic Peptides. *Biomacromolecules* **2013**, *14* (9), 3267.

27. Vegners, R.; Shestakova, I.; Kalvinsh, I.; Ezzell, R. M.; Janmey, P. A. Use of a gel-forming dipeptide derivative as a carrier for antigen presentation. *Journal of Peptide Science* **1995**, *1* (6), 371.
28. Zhang, Y.; Gu, H.; Yang, Z.; Xu, B. Supramolecular Hydrogels Respond to Ligand–Receptor Interaction. *Journal of the American Chemical Society* **2003**, *125* (45), 13680.
29. Yang, Z.; Gu, H.; Fu, D.; Gao, P.; Lam, J. K.; Xu, B. Enzymatic Formation of Supramolecular Hydrogels. *Adv Mater* **2004**, *16* (16), 1440.
30. Yang, Z.; Gu, H.; Zhang, Y.; Wang, L.; Xu, B. Small molecule hydrogels based on a class of antiinflammatory agents. *Chemical Communications* **2004**, (2), 208.
31. Fleming, S.; Ulijn, R. V. Design of nanostructures based on aromatic peptide amphiphiles. *Chemical Society Reviews* **2014**, *43* (23), 8150.
32. Wang, H.; Yang, C.; Tan, M.; Wang, L.; Kong, D.; Yang, Z. A structure-gelation ability study in a short peptide-based 'Super Hydrogelator' system. *Soft Matter* **2011**, *7* (8), 3897.
33. Zhang, Y.; Yang, Z.; Yuan, F.; Gu, H.; Gao, P.; Xu, B. Molecular Recognition Remolds the Self-Assembly of Hydrogelators and Increases the Elasticity of the Hydrogel by 106-Fold. *Journal of the American Chemical Society* **2004**, *126* (46), 15028.
34. Ryan, D. M.; Anderson, S. B.; Senguen, F. T.; Youngman, R. E.; Nilsson, B. L. Self-assembly and hydrogelation promoted by F5-phenylalanine. *Soft Matter* **2010**, *6* (3), 475.
35. Fleming, S.; Debnath, S.; Frederix, P. W. J. M.; Tuttle, T.; Ulijn, R. V. Aromatic peptide amphiphiles: significance of the Fmoc moiety. *Chemical Communications* **2013**, *49* (90), 10587.
36. Reches, M.; Gazit, E. Casting Metal Nanowires Within Discrete Self-Assembled Peptide Nanotubes. *Science* **2003**, *300* (5619), 625.
37. Reches, M.; Gazit, E. Formation of Closed-Cage Nanostructures by Self-Assembly of Aromatic Dipeptides. *Nano Letters* **2004**, *4* (4), 581.
38. Reches, M.; Gazit, E. Self-assembly of peptide nanotubes and amyloid-like structures by charged-termini-capped diphenylalanine peptide analogues. *Israel Journal of Chemistry* **2005**, *45* (3), 363.
39. Smith, A. M.; Williams, R. J.; Tang, C.; Coppo, P.; Collins, R. F.; Turner, M. L.; Saiani, A.; Ulijn, R. V. Fmoc-Diphenylalanine Self Assembles to a Hydrogel via a Novel Architecture Based on  $\pi$ - $\pi$  Interlocked  $\beta$ -Sheets. *Adv Mater* **2008**, *20* (1), 37.
40. Frederix, P. W. J. M.; Ulijn, R. V.; Hunt, N. T.; Tuttle, T. Virtual Screening for Dipeptide Aggregation: Toward Predictive Tools for Peptide Self-Assembly. *The Journal of Physical Chemistry Letters* **2011**, *2* (19), 2380.

- 
41. FrederixPim, W. J. M.; Scott, G. G.; Abul-Haija, Y. M.; Kalafatovic, D.; Pappas, C. G.; Javid, N.; Hunt, N. T.; Ulijn, R. V.; Tuttle, T. Exploring the sequence space for (tri-)peptide self-assembly to design and discover new hydrogels. *Nat Chem* **2015**, *7* (1), 30.
42. Nalluri, S. K. M.; Ulijn, R. V. Discovery of energy transfer nanostructures using gelation-driven dynamic combinatorial libraries. *Chemical Science* **2013**, *4* (9), 3699.
43. Kar, T.; Mandal, S. K.; Das, P. K. Organogel–Hydrogel Transformation by Simple Removal or Inclusion of N-Boc-Protection. *Chemistry – A European Journal* **2011**, *17* (52), 14952.
44. Tena-Solsona, M.; Miravet, J. F.; Escuder, B. Tetrapeptidic Molecular Hydrogels: Self-assembly and Co-aggregation with Amyloid Fragment A $\beta$ 1-40. *Chemistry – A European Journal* **2014**, *20* (4), 1023.
45. Ryan, D. M.; Doran, T. M.; Anderson, S. B.; Nilsson, B. L. Effect of C-Terminal Modification on the Self-Assembly and Hydrogelation of Fluorinated Fmoc-Phe Derivatives. *Langmuir* **2011**, *27* (7), 4029.
46. Johnson, E. K.; Adams, D. J.; Cameron, P. J. Peptide based low molecular weight gelators. *Journal of Materials Chemistry* **2011**, *21* (7), 2024.
47. Pappas, C. G.; Mutasa, T.; Frederix, P. W. J. M.; Fleming, S.; Bai, S.; Debnath, S.; Kelly, S. M.; Gachagan, A.; Ulijn, R. V. Transient supramolecular reconfiguration of peptide nanostructures using ultrasound. *Materials Horizons* **2015**, *2* (2), 198.
48. Yu, X.; Liu, Q.; Wu, J.; Zhang, M.; Cao, X.; Zhang, S.; Wang, Q.; Chen, L.; Yi, T. Sonication-Triggered Instantaneous Gel-to-Gel Transformation. *Chemistry – A European Journal* **2010**, *16* (30), 9099.
49. Bardelang, D.; Camerel, F.; Margeson, J. C.; Leek, D. M.; Schmutz, M.; Zaman, M. B.; Yu, K.; Soldatov, D. V.; Ziessel, R.; Ratcliffe, C. I.; Ripmeester, J. A. Unusual Sculpting of Dipeptide Particles by Ultrasound Induces Gelation. *Journal of the American Chemical Society* **2008**, *130* (11), 3313.
50. Ramos Sasselli, I.; Halling, P. J.; Ulijn, R. V.; Tuttle, T. Supramolecular Fibers in Gels Can Be at Thermodynamic Equilibrium: A Simple Packing Model Reveals Preferential Fibril Formation versus Crystallization. *ACS Nano* **2016**, *10* (2), 2661.
51. Tang, C.; Smith, A. M.; Collins, R. F.; Ulijn, R. V.; Saiani, A. Fmoc-Diphenylalanine Self-Assembly Mechanism Induces Apparent pKa Shifts. *Langmuir* **2009**, *25* (16), 9447.
52. Xie, Y.; Wang, X.; Huang, R.; Qi, W.; Wang, Y.; Su, R.; He, Z. Electrostatic and Aromatic Interaction-Directed Supramolecular Self-Assembly of a Designed Fmoc-Tripeptide into Helical Nanoribbons. *Langmuir* **2015**, *31* (9), 2885.

- 
53. Urry, D. W.; Gowda, D. C.; Peng, S.; Parker, T. M.; Jing, N.; Harris, R. D. Nanometric design of extraordinary hydrophobic-induced pKa shifts for aspartic acid: Relevance to protein mechanisms. *Biopolymers* **1994**, *34* (7), 889.
54. Adams, D. J.; Butler, M. F.; Frith, W. J.; Kirkland, M.; Mullen, L.; Sanderson, P. A new method for maintaining homogeneity during liquid-hydrogel transitions using low molecular weight hydrogelators. *Soft Matter* **2009**, *5* (9), 1856.
55. Draper, E. R.; Mears, L. L. E.; Castilla, A. M.; King, S. M.; McDonald, T. O.; Akhtar, R.; Adams, D. J. Using the hydrolysis of anhydrides to control gel properties and homogeneity in pH-triggered gelation. *RSC Advances* **2015**, *5* (115), 95369.
56. Zhao, F.; Gao, Y.; Shi, J.; Browdy, H. M.; Xu, B. Novel Anisotropic Supramolecular Hydrogel with High Stability over a Wide pH Range. *Langmuir* **2011**, *27* (4), 1510.
57. Yang, Z. X., Keming; Guo, Zufeng; Guo, Zhihong; Xu, Bing. Intracellular enzymatic formation of nanofibers results in hydrogelation and regulated cell death. *Adv Mater* **2007**, *19*, 3152.
58. Zhao, F.; Ma, M. L.; Xu, B. Molecular hydrogels of therapeutic agents. *Chemical Society Reviews* **2009**, *38* (4), 883.
59. Szkolar, L.; Guilbaud, J. B.; Miller, A. F.; Gough, J. E.; Saiani, A. Enzymatically triggered peptide hydrogels for 3D cell encapsulation and culture. *Journal of Peptide Science* **2014**, *20* (7), 578.
60. Yang, Z.; Xu, B. A simple visual assay based on small molecule hydrogels for detecting inhibitors of enzymes. *Chem. Commun. (Cambridge, U. K.)* **2004**, (21), 2424.
61. Yang, Z.; Xu, B. Using Enzymes to Control Molecular Hydrogelation. *Adv Mater* **2006**, *18* (22), 3043.
62. Yang, Z.; Liang, G.; Xu, B. Enzymatic Hydrogelation of Small Molecules. *Accounts of Chemical Research* **2008**, *41* (2), 315.
63. Zhou, J.; Du, X.; Li, J.; Yamagata, N.; Xu, B. Taurine Boosts Cellular Uptake of Small d-Peptides for Enzyme-Instructed Intracellular Molecular Self-Assembly. *Journal of the American Chemical Society* **2015**.
64. Yang, Z.; Ho, P.-L.; Liang, G.; Chow, K. H.; Wang, Q.; Cao, Y.; Guo, Z.; Xu, B. Using  $\beta$ -Lactamase to Trigger Supramolecular Hydrogelation. *Journal of the American Chemical Society* **2007**, *129* (2), 266.
65. Xu, H.; Das, A. K.; Horie, M.; Shaik, M. S.; Smith, A. M.; Luo, Y.; Lu, X.; Collins, R.; Liem, S. Y.; Song, A.; Popelier, P. L. A.; Turner, M. L.; Xiao, P.; Kinloch, I. A.; Ulijn, R. V. An investigation of the conductivity of peptide nanotube networks prepared by enzyme-triggered self-assembly. *Nanoscale* **2010**, *2* (6), 960.

- 
66. Das, A. K.; Collins, R.; Ulijn, R. V. Exploiting Enzymatic (Reversed) Hydrolysis in Directed Self-Assembly of Peptide Nanostructures. *Small* **2008**, *4* (2), 279.
67. Toledano, S.; Williams, R. J.; Jayawarna, V.; Ulijn, R. V. Enzyme-triggered self-assembly of peptide hydrogels via reversed hydrolysis. *Journal of the American Chemical Society* **2006**, *128* (4), 1070.
68. Qin, X.; Xie, W. C.; Tian, S.; Cai, J. L.; Yuan, H.; Yu, Z.; Butterfoss, G. L.; Khuong, A. C.; Gross, R. A. Enzyme-triggered hydrogelation via self-assembly of alternating peptides. *Chemical Communications* **2013**, *49* (42), 4839.
69. Debnath, S.; Roy, S.; Ulijn, R. V. Peptide Nanofibers with Dynamic Instability through Nonequilibrium Biocatalytic Assembly. *Journal of the American Chemical Society* **2013**, *135* (45), 16789.
70. Angelerou, M. G. F.; Sabri, A.; Creasey, R.; Angelerou, P.; Marlow, M.; Zelzer, M. Surface-directed modulation of supramolecular gel properties. *Chemical Communications* **2016**, *52* (23), 4298.
71. Liu, Y.; Xu, X.-D.; Chen, J.-X.; Cheng, H.; Zhang, X.-Z.; Zhuo, R.-X. Surface self-assembly of N-fluorenyl-9-methoxycarbonyl diphenylalanine on silica wafer. *Colloids and Surfaces B: Biointerfaces* **2011**, *87* (1), 192.
72. Reches, M.; Gazit, E. Controlled patterning of aligned self-assembled peptide nanotubes. *Nat Nano* **2006**, *1* (3), 195.
73. Demirel, G.; Buyukserin, F. Surface-Induced Self-Assembly of Dipeptides onto Nanotextured Surfaces. *Langmuir* **2011**, *27* (20), 12533.
74. Zheng, W.; Gao, J.; Song, L.; Chen, C.; Guan, D.; Wang, Z.; Li, Z.; Kong, D.; Yang, Z. Surface-Induced Hydrogelation Inhibits Platelet Aggregation. *Journal of the American Chemical Society* **2013**, *135* (1), 266.
75. Olive, A. G. L.; Abdullah, N. H.; Ziemecka, I.; Mendes, E.; Eelkema, R.; van Esch, J. H. Spatial and Directional Control over Self-Assembly Using Catalytic Micropatterned Surfaces. *Angewandte Chemie International Edition* **2014**, *53* (16), 4132.
76. Johnson, E. K.; Adams, D. J.; Cameron, P. J. Directed Self-Assembly of Dipeptides to Form Ultrathin Hydrogel Membranes. *Journal of the American Chemical Society* **2010**, *132* (14), 5130.
77. Johnson, E. K.; Chen, L.; Kubiak, P. S.; McDonald, S. F.; Adams, D. J.; Cameron, P. J. Surface nucleated growth of dipeptide fibres. *Chemical Communications* **2013**, *49* (77), 8698.
78. Liu, Y.; Kim, E.; Ulijn, R. V.; Bentley, W. E.; Payne, G. F. Reversible Electroaddressing of Self-assembling Amino-Acid Conjugates. *Advanced Functional Materials* **2011**, *21* (9), 1575.

79. Raeburn, J.; Alston, B.; Kroeger, J.; McDonald, T. O.; Howse, J. R.; Cameron, P. J.; Adams, D. J. Electrochemically-triggered spatially and temporally resolved multi-component gels. *Materials Horizons* **2014**, *1* (2), 241.
80. Williams, R. J.; Smith, A. M.; Collins, R.; Hodson, N.; Das, A. K.; Ulijn, R. V. Enzyme-assisted self-assembly under thermodynamic control. *Nat Nano* **2009**, *4* (1), 19.
81. Kuang, Y.; Shi, J.; Li, J.; Yuan, D.; Alberti, K. A.; Xu, Q.; Xu, B. Pericellular Hydrogel/Nanonets Inhibit Cancer Cells. *Angewandte Chemie International Edition* **2014**, *53* (31), 8104.
82. Decher, G. Fuzzy nanoassemblies: Toward layered polymeric multicomposites. *Science* **1997**, *277* (5330), 1232.
83. Dubas, S. T.; Schlenoff, J. B. Polyelectrolyte Multilayers Containing a Weak Polyacid: Construction and Deconstruction. *Macromolecules* **2001**, *34* (11), 3736.
84. Lvov, Y.; Ariga, K.; Onda, M.; Ichinose, I.; Kunitake, T. Alternate Assembly of Ordered Multilayers of SiO<sub>2</sub> and Other Nanoparticles and Polyions. *Langmuir* **1997**, *13* (23), 6195.
85. Mertz, D.; Vogt, C.; Hemmerlé, J.; Mutterer, J.; Ball, V.; Voegel, J.-C.; Schaaf, P.; Lavallo, P. Mechanotransductive surfaces for reversible biocatalysis activation. *Nature Materials* **2009**, *8* (9), 731.
86. Decher, G.; Hong, J. D.; Schmitt, J. Buildup of ultrathin multilayer films by a self-assembly process: III. Consecutively alternating adsorption of anionic and cationic polyelectrolytes on charged surfaces. *Thin Solid Films* **1992**, *210* (1-2), 831.
87. Li, Y.; Wang, X.; Sun, J. Q. Layer-by-layer assembly for rapid fabrication of thick polymeric films. *Chem. Soc. Rev.* **2012**, *41* (18), 5998.
88. Lee, S.-S.; Hong, J.-D.; Kim, C. H.; Kim, K.; Koo, J. P.; Lee, K.-B. Layer-by-Layer Deposited Multilayer Assemblies of Ionene-Type Polyelectrolytes Based on the Spin-Coating Method. *Macromolecules* **2001**, *34* (16), 5358.
89. Schlenoff, J. B.; Dubas, S. T.; Farhat, T. Sprayed polyelectrolyte multilayers. *Langmuir* **2000**, *16* (26), 9968.
90. Lavallo, P.; Gergely, C.; Cuisinier, F. J. G.; Decher, G.; Schaaf, P.; Voegel, J.-C.; Picart, C. Comparison of the structure of polyelectrolyte multilayer films exhibiting a linear and an exponential growth regime: An in situ atomic force microscopy study. *Macromolecules* **2002**, *35* ((11)), 4458
91. Picart, C.; Lavallo, P.; Hubert, P.; Cuisinier, F. J. G.; Decher, G.; Schaaf, P.; Voegel, J.-C. Buildup mechanism for poly(L-lysine)/hyaluronic acid films onto a solid surface. *Langmuir* **2001**, *17* (23), 7414.

92. Boulmedais, F.; Ball, V.; Schwinté, P.; Frisch, B.; Schaaf, P.; Voegel, J.-C. Buildup of Exponentially Growing Multilayer Polypeptide Films with Internal Secondary Structure. *Langmuir* **2003**, *19* (2), 440.
93. Decher, G.; Schmitt, J. Fine-tuning of the film thickness of ultrathin multilayer films composed of consecutively alternating layers of anionic and cationic polyelectrolytes. *Progress in Colloid & Polymer Science* **1992**, *89*, 160.
94. Shiratori, S. S.; Rubner, M. F. pH-dependent thickness behavior of sequentially adsorbed layers of weak polyelectrolytes. *Macromolecules* **2000**, *33* (11), 4213.
95. Silva, J. M.; Caridade, S. G.; Costa, R. R.; Alves, N. M.; Groth, T.; Picart, C.; Reis, R. L.; Mano, J. F. pH Responsiveness of Multilayered Films and Membranes Made of Polysaccharides. *Langmuir* **2015**, *31* (41), 11318.
96. Arunan, E.; Desiraju Gautam, R.; Klein Roger, A.; Sadlej, J.; Scheiner, S.; Alkorta, I.; Clary David, C.; Crabtree Robert, H.; Dannenberg Joseph, J.; Hobza, P.; Kjaergaard Henrik, G.; Legon Anthony, C.; Mennucci, B.; Nesbitt David, J. Definition of the hydrogen bond (IUPAC Recommendations 2011). In *Pure and Applied Chemistry*, 2011; Vol. 83, p 1637.
97. Stockton, W. B.; Rubner, M. F. Molecular-level processing of conjugated polymers .4. Layer-by-layer manipulation of polyaniline via hydrogen-bonding interactions. *Macromolecules* **1997**, *30* (9), 2717.
98. Wang, L.; Wang, Z.; Zhang, X.; Shen, J.; Chi, L.; Fuchs, H. A new approach for the fabrication of an alternating multilayer film of poly(4-vinylpyridine) and poly(acrylic acid) based on hydrogen bonding. *Macromolecular Rapid Communications* **1997**, *18* (6), 509.
99. Erel-Unal, I.; Sukhishvili, S. A. Hydrogen-Bonded Multilayers of a Neutral Polymer and a Polyphenol. *Macromolecules* **2008**, *41* (11), 3962.
100. Lomova, M. V.; Brichkina, A. I.; Kiryukhin, M. V.; Vasina, E. N.; Pavlov, A. M.; Gorin, D. A.; Sukhorukov, G. B.; Antipina, M. N. Multilayer Capsules of Bovine Serum Albumin and Tannic Acid for Controlled Release by Enzymatic Degradation. *ACS Applied Materials & Interfaces* **2015**, *7* (22), 11732.
101. Onda, M.; Lvov, Y.; Ariga, K.; Kunitake, T. Sequential reaction and product separation on molecular films of glucoamylase and glucose oxidase assembled on an ultrafilter. *J Ferment Bioeng* **1996**, *82* (5), 502.
102. Izumrudov, V. A.; Kharlampieva, E.; Sukhishvili, S. A. Multilayers of a Globular Protein and a Weak Polyacid: Role of Polyacid Ionization in Growth and Decomposition in Salt Solutions. *Biomacromolecules* **2005**, *6* (3), 1782.
103. Vazquez, E.; Dewitt, D. M.; Hammond, P. T.; Lynn, D. M. Construction of hydrolytically-degradable thin films via layer- by-layer deposition of degradable polyelectrolytes. *Journal of the American Chemical Society* **2002**, *124* (47), 13992.

- 
104. Chluba, J.; Voegel, J.-C.; Decher, G.; Erbacher, P.; Schaaf, P.; Ogier, J. Peptide hormone covalently bound to polyelectrolytes and embedded into multilayer architectures conserving full biological activity. *Biomacromolecules* **2001**, *2* (3), 800.
105. Jessel, N.; Atalar, F.; Lavalle, P.; Mutterer, J.; Decher, G.; Schaaf, P.; Voegel, J.-C.; Ogier, J. Bioactive coatings based on a polyelectrolyte multilayer architecture functionalized by embedded proteins. *Adv Mater* **2003**, *15* (9), 692.
106. Thierry, B.; Kujawa, P.; Tkaczyk, C.; Winnik, F. M.; Bilodeau, L.; Tabrizian, M. Delivery platform for hydrophobic drugs: Prodrug approach combined with self-assembled multilayers. *Journal of the American Chemical Society* **2005**, *127* (6), 1626.
107. Lojou, É.; Bianco, P. Adsorption of acid proteins onto auto-assembled polyelectrolyte or basic protein films – application to electrocatalytic reactions controlled by hydrogenase. *J. Electroanal. Chem.* **2004**, *573* (1), 159.
108. Decher, G.; Lehr, B.; Lowack, K.; Lvov, Y.; Schmitt, J. New nanocomposite films for biosensors: layer-by-layer adsorbed films of polyelectrolytes, proteins or DNA. *Biosensors and Bioelectronics* **1994**, *9* (9), 677.
109. Peyratout, C. S.; Dähne, L. Tailor-Made Polyelectrolyte Microcapsules: From Multilayers to Smart Containers. *Angewandte Chemie International Edition* **2004**, *43* (29), 3762.
110. Soumetz, F. C.; Pastorino, L.; Ruggiero, C. Human osteoblast-like cells response to nanofunctionalized surfaces for tissue engineering. *Journal of Biomedical Materials Research Part B: Applied Biomaterials* **2008**, *84B* (1), 249.
111. Schwinté, P.; Voegel, J.-C.; Picart, C.; Haikel, Y.; Schaaf, P.; Szalontai, B. Stabilizing Effects of Various Polyelectrolyte Multilayer Films on the Structure of Adsorbed/Embedded Fibrinogen Molecules: An ATR-FTIR Study. *Journal of Physical Chemistry B* **2001**, *105*, 11906.
112. Crouzier, T.; Fourel, L.; Boudou, T.; Albigès-Rizo, C.; Picart, C. Presentation of BMP-2 from a Soft Biopolymeric Film Unveils its Activity on Cell Adhesion and Migration. *Adv Mater* **2011**, *23* (12), H111.

# Chapter 2

## Materials and methods

---

---

# Chapter 2

## Materials and methods

---

### Summary

<b>2.1</b>	<b>Materials.....</b>	<b>61</b>
2.1.1	Buffer solutions.....	61
2.1.2	Polymers and enzymes.....	61
2.1.3	Preparation and characterization of molecules.....	62
<b>2.2</b>	<b>Methods: Physical-chemical characterizations .....</b>	<b>63</b>
2.2.1	Quartz crystal microbalance with dissipation .....	63
2.2.1.1	<i>Principle of the QCM-D.....</i>	<i>63</i>
2.2.2	Atomic force microscopy.....	65
2.2.2.1	<i>Principle of AFM.....</i>	<i>65</i>
2.2.3	Fourier transform Infrared spectroscopy.....	67
2.2.3.1	<i>Principle of infrared spectroscopy.....</i>	<i>67</i>
2.2.3.2	<i>Fourier transform infrared spectroscopy.....</i>	<i>69</i>
2.2.3.3	<i>FTIR attenuated total reflection.....</i>	<i>70</i>
2.2.4	UV-visible spectroscopy.....	72
2.2.4.1	<i>Principle of enzymatic assay.....</i>	<i>72</i>
2.2.5	Confocal laser scanning microscopy.....	73
	<b>References.....</b>	<b>74</b>

## 2.1 Materials

### 2.1.1 Buffer solutions

All buffer and aqueous solutions were prepared in Milli-Q ultrapure water (Milli-Q Plus system, Millipore, Billerica, MA) that has a resistivity of 18.2  $\Omega$ . pH of buffer solutions was monitored with pH/mV meter (HANNA instruments) and adjusted by dropwise addition of  $\text{HCl}_{(\text{aq})}$  (0.1M) and/or  $\text{NaOH}_{(\text{aq})}$  (0.1M).

Buffer	Formula	Supplier	Mw (g.mol <sup>-1</sup> )	Concentration (mol.L <sup>-1</sup> )
Borax, pH=9.5	$\text{Na}_2\text{B}_4\text{O}_7$	Fluka	201.22	25 mM
Sodium Acetate, pH=6	$\text{C}_2\text{H}_3\text{NaO}_2$	Sigma Aldrich	32.03	10mM
Sodium Phosphate, pH=8.7	$\text{NaH}_2\text{PO}_4 \cdot \text{H}_2\text{O}$	Sigma Aldrich	138.0	186 mM
	$\text{Na}_2\text{HPO}_4 \cdot 7\text{H}_2\text{O}$	Sigma Aldrich	268.1	
TRIS, pH = 8	$\text{C}_4\text{H}_{11}\text{CO}_3$	Sigma Aldrich	121.13	25 mM

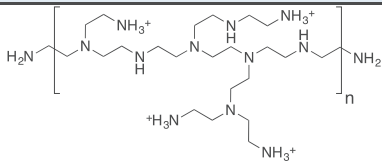
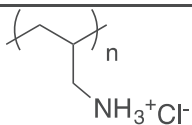
**Table 2.1:** Buffer solution used for the buildup of precursor layer and enzymatic responsive hydrogelations.

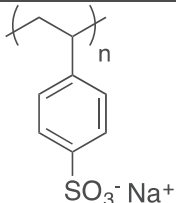
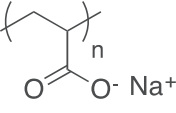
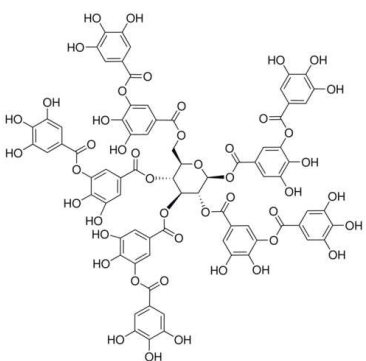
All buffer solutions were stored at 4°C for one week, except odium phosphate buffer, only kept for two days at 4°C.

### 2.1.2 Polymers and enzymes

#### *Polyelectrolytes and tannic acid*

All commercial polyelectrolytes and tannic acid are presented in the table below.

Polymers	Nature	Structure	Suppliers	Mw (g.mol <sup>-1</sup> )
Poly(ethylenimine) (PEI)	Polycation		Sigma Aldrich	750 000 (50% wt. in water )
Poly(allylamine hydrochloride) (PAH)	Polycation		Sigma Aldrich	15 000

Polymers	Nature	Structure	Suppliers	Mw (g.mol <sup>-1</sup> )
Poly (styrene sulfonate) (PSS)	Polyanion		Sigma Aldrich	70 000
Poly(acrylic acid) (PAA)	Polyanion		Sigma Aldrich	100 000
Tannic Acid (TA)	Polyphenol		Alfa Aesar	1701.23

**Table 2.2:** Polyelectrolytes and polyphenol used for the buildup of enzymatic films.

### Enzymes

$\alpha$ -Chymotrypsin type II from Bovine Pancreas (25 kDa, 65 U.mg<sup>-1</sup>, Sigma Aldrich) and Albumin, bovine serum  $\geq 99$ , essentially globulin free (BSA, 66 kDa, Sigma Aldrich) were dissolved in Sodium Acetate buffer (pH=6) with concentrations of 0.2 mg.mL<sup>-1</sup> and 1. mg.mL<sup>-1</sup> respectively. Solutions of  $\alpha$ -Chymotrypsin and BSA have identical molar concentrations. Therefore, a proportional volume ratio of both solutions was prepared to obtain a mixture solution at a fixed molar ratio in  $\alpha$ -Chymotrypsin and BSA.

Alkaline Phosphatase from bovine intestinal mucosa (ALP, 160 kDa, 54 U.mg<sup>-1</sup>, Sigma Aldrich) was dissolved in Borax buffer (pH=9.5) at 1 mg.mL<sup>-1</sup>.

Esterase from porcine liver (162 kDa, 20 U.mg<sup>-1</sup>, Sigma Aldrich) was dissolved in Tris buffer (pH = 8) at 3 mg.mL<sup>-1</sup>.

### 2.1.3 Preparation and characterization of molecules

Protocols are described in the chapters three and four.

## 2.2 Methods: Physical-chemical characterizations

### 2.2.1 Quartz crystal microbalance with dissipation

Quartz crystal microbalance (QCM-D) with dissipation is an acoustic device used to monitor *in-situ* mass deposition of molecules or macromolecules. This sensitive technique is suitable to follow real-time buildup of enzymatic films and hydrogels assembly.

#### 2.2.1.1 Principle of the QCM-D

The fundamental principle of quartz crystal microbalance was developed by G. Sauerbrey in 1959.<sup>1</sup> This technique relies on piezoelectric properties of quartz, deformed when an electrical potential is applied to it.

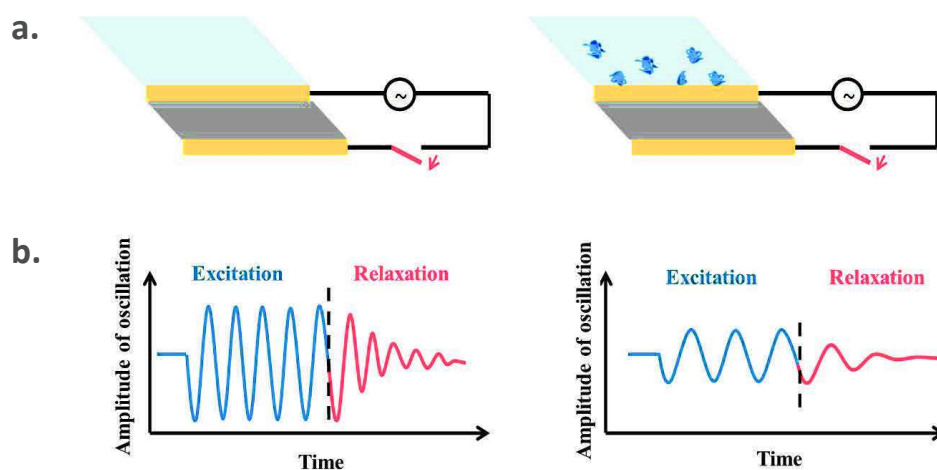


**Figure 2.7:** (a) Schematic representation of a coated gold QCM-D crystal and its driving circuit during the adsorption of molecules (b) The crystal oscillates at its fundamental frequency and its harmonics: the blue curve corresponds to the oscillation signal during the excitation phase and the red curve corresponds to the signal during relaxation phase. A shift of the frequency is obtained when molecules are adsorbed on the surface of the QCM crystal.

The QCM device uses a quartz crystal coated on both sides with gold electrodes (Figure 2.7.a). The application of an electrical potential between the two electrodes induces a shear movement of the quartz crystal. By fixing the lower side of the crystal on a stationary support, the upper side undergoes a horizontal translational movement resulting in mechanical oscillations at its fundamental frequency and its harmonics (Figure 2.7.b). The system behaves as a harmonic oscillator that can be characterized by its resonance frequency  $f_r$  (Hz) :

$$f_r = \frac{1}{2\pi} \sqrt{\frac{k}{M}} \quad (1.1)$$

$M$  is the oscillator mass

$k$  the spring constant ( $\text{N.m}^{-1}$ ).

When a mass  $m$  ( $\text{ng.cm}^{-2}$ ) is deposited on the surface of the crystal ( $m \ll M$ ), the total mass of the resonator changes and a new resonance frequency  $f$  is associated:

$$f = \frac{1}{2\pi} \sqrt{\frac{k}{M+m}} \approx f_r \left(1 - \frac{m}{2M}\right) \quad (1.2)$$

The resonance frequency shift  $\Delta f$  induced by the mass deposition  $m$  on the crystal can be written as following:

$$\Delta f = f - f_r = -\frac{m f_r}{2M} = -\frac{m}{C} \quad (1.3)$$

$C$ , called the Sauerbrey constant, is a constant ( $17.7 \text{ ng.cm}^{-2}.\text{Hz}^{-1}$ ) that depends only on the thickness and on the inherent properties of the quartz crystal.  $C$  is defined as:

$$C = \frac{2M}{f_r} \quad (1.4)$$

By measuring the resonance frequency shift of the system during an experiment, QCM gives access to the deposited mass per surface unit on the crystal as a function of time. It is also possible to determine the frequencies of all odd harmonics of the fundamental resonance frequency and to follow their shifts during an experiment. The Sauerbrey equation can be written as following:

$$m = -C \frac{\Delta f_v}{v} \quad (1.5)$$

Where  $v$  is the overtone number.

In order to evaluate the viscoelastic properties of the material deposited on the crystal, the QCM-D device measures the dissipation factor ( $D$ ).  $D$  is experimentally determined by exciting the quartz crystal at its fundamental frequency and measuring the relaxation time of the system as the resonator energy is dissipated in the crystal, in the deposited material and in the liquid in contact with the crystal. This relaxation time is inversely proportional to the damping constant of the system and allows the determination of the dissipation factor  $D$ . This parameter is defined by the proportion of dissipated energy at each oscillation with respect to the total stored energy as following:

$$D = \frac{E_{dissipated}}{2\pi E_{stocked}} \quad (1.6)$$

If the deposited material is stiff, the relaxation time is short and the dissipation value is small. On the contrary, a soft and viscous material will display a longer relaxation time with high values of dissipation.

### **Experimental Setup**

The QCM-D experiments were performed on a Q-Sense E1 or E4 apparatus (Q-Sense AB, Göteborg, Sweden) by monitoring the resonance frequencies of gold coated crystals, as well as the dissipation factors at four frequencies the fundamental frequency: at 5 MHz ( $\nu = 1$ ) and the 3rd, 5th, and 7th harmonics ( $\nu = 3, 5$  and  $7$ ) at 15, 25, and 35 MHz). The apparatus is equipped with one measurement cell (volume of about 100  $\mu\text{L}$ ). The cell, set at 22°C, allows the “in” and “out” fluxes of the solutions in contact with the crystal surface. Commercial quartz crystals display calibrated dimensions with 1.4 cm of diameter and 0.3 mm of thickness. Before each experiment, the quartz crystal was clean under UV-Ozone for 10-15 minutes. Placed into the cell, the crystal is exposed to the experimental buffer and left to stabilize for around 30 min. The multilayer films were built *in situ* by the layer-by-layer method on the crystal surface. Each deposited layer was obtained exposing the substrate to 600  $\mu\text{L}$  of solution for 5 min alternated 600  $\mu\text{L}$  of buffer for 5 min as a rinsing step. At the end of the experiment, the crystal is cleaned *in situ* with a 2% Hellmanex solution for 10 min, then with a 0.1 M HCl solution for 10 min and finally with a 0.1 M NaOH solution for 10 min. the crystal is then rinsed with water and dried under compressed air.

### **2.2.2 Atomic force microscopy**

Atomic force microscopy (AFM) is a technique developed by Binnig, Quate and Gueber in the early 80's. In our case, this imaging technique is appropriate to evaluate the topography of the surface with sub-nanometer vertical resolution. <sup>2</sup>

#### **2.2.2.1 Principle of AFM**

AFM is based on the measurement of interatomic forces (Van der Waals forces, electrostatic forces) between a tip scanning a sample. This tip is fixed at the extremity of a lever arm calibrated with a fixed spring force also called cantilever. Interactions between the cantilever and the surface induce deformation of the lever. This deflection can be quantified by

the reflection of a laser source detected by a photodiode. Consequently, variation of the tips highness proportionally modifies the electrical tension detected by the photodetector. The sample placed on a piezoelectric ceramic can move in the three directions (x, y and z). Three-dimension topography of samples can then be obtained (Figure 2.8).

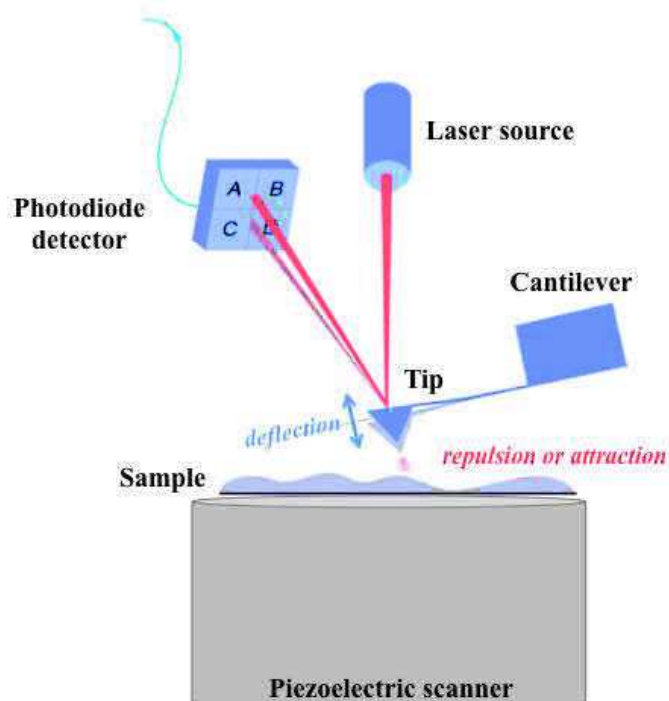


**Figure 2.8:** Schematic representation of atomic force microscopy (AFM) The sample is fixed on a piezoelectric base. Cantilever tip is approach close to the surface. Attractive and repulsive interactions between tip and the sample surface induce the deflection of the cantilever. Movements of a laser source reflected on top of the tip are detected by a photodiode detector.<sup>3</sup>

AFM images were performed in dry state. Two main scanning modes were used to analyze the samples: the **contact mode** and the **tapping mode**.

In contact mode, the tip is constantly interacting with the surface. This mode, commonly used can sometimes deform fragile samples and alter the quality of the images. In tapping mode, the tip oscillates at a fundamental frequency near the surface. In this case, attractive and repulsive forces induced by weak interactions (Van der Waals) modify the oscillation frequency of the cantilever. Since the oscillation frequency is maintained constant, the cantilever has to move away from the sample surface through a control loop. This mode is more adapted to fragile sample due to softer interactions applied to the surface.

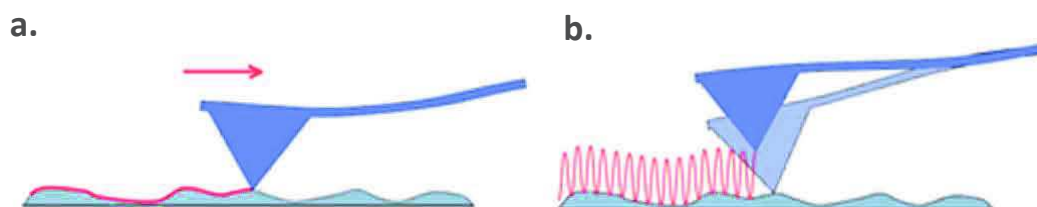


**Figure 2.3** : Schematic representation of AFM scanning modes a) contact mode b) tapping mode.<sup>4</sup>

### **Experimental setup**

Atomic force microscopy (AFM) images were obtained using a BioScope Catalyst (Bruker corp., Santa Barbara, CA, USA). AFM images were recorded in contact mode by using silicon tips mounted on nitride levers. All samples were observed in dry state with triangular cantilevers having a spring constant of 0.4 N/m and a nominal tip radius of 2 nm. AFM images ( $1\mu\text{m} \times 1\mu\text{m}$ ) were treated with the ScanAsyst software (Bruker corp., Santa Barbara, CA, USA).

### **2.2.3 Fourier transform Infrared spectroscopy**

Infrared spectroscopy is a suitable method to identify and to collect information about chemical compound. In the context of this thesis, the device allowed us to monitor *in-situ* supramolecular self-assembly of peptides.

#### **2.2.3.1 Principle of infrared spectroscopy**

Infrared spectroscopy technique is based on the measurements of energetic transitions between fundamental states and excited states of vibrational levels. These transitions are observable after absorption or emission of energetic quanta. The total energy of a molecule is described as the sum of four contributions (Figure 2.9): the electron energy ( $E_e$ ), the vibrational energy ( $E_v$ ), the rotational energy ( $E_r$ ) and translational energy ( $E_t$ ):

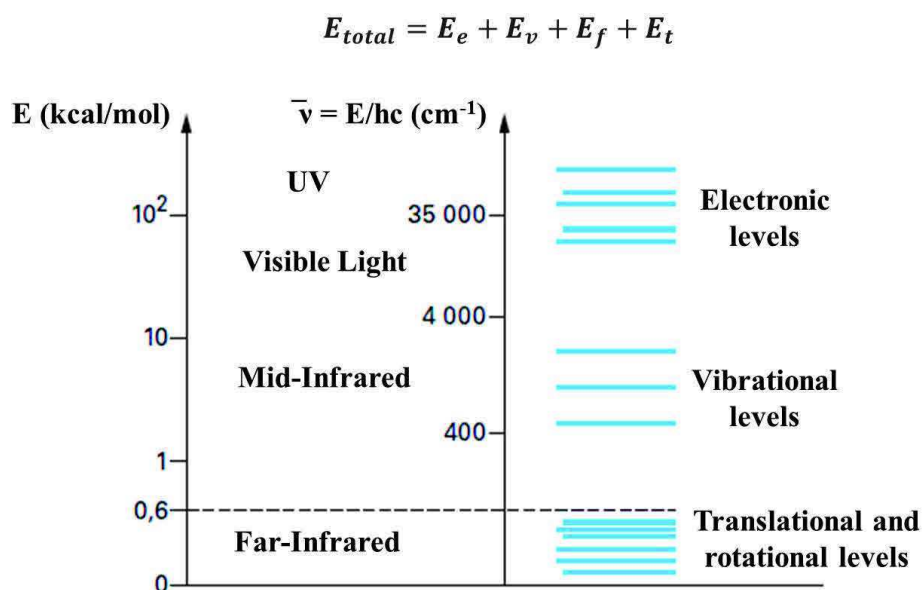


**Figure 2.9:** Respective values of electronic, vibrational, rotational and translational contributions to total energy of one molecule.<sup>5</sup>

Radiations of a molecule in the mid infrared (400-4000  $\text{cm}^{-1}$ ) have an effect on the vibrational energy  $E_v$ . The variation of the vibrational energy is given by the equation of Bohr:

$$\Delta E = E_2 - E_1 = hf = hcv \quad (1.7)$$

With  $E_1$  the initial energy,  $E_2$  the final energy,  $h$  Planck's constant,  $c$  celerity of light,  $f$  the vibration frequency ( $\text{s}^{-1}$ ) and  $\nu$  the wavenumber ( $\text{cm}^{-1}$ ). Due to the proportional relation between the frequency  $f$  and the wavenumber  $\nu$ , we will describe infrared radiations with  $\nu$  ( $\text{cm}^{-1}$ ).

At a bond scale, absorption and emission in the mid-infrared is transduced in different kinds of vibration mode (Figure 2.10). Polyatomic molecules composed of  $N$  atoms present  $3N-6$  normal modes of vibrations and  $3N-5$  modes if the molecule is linear. Each vibration mode presents a characteristic frequency.

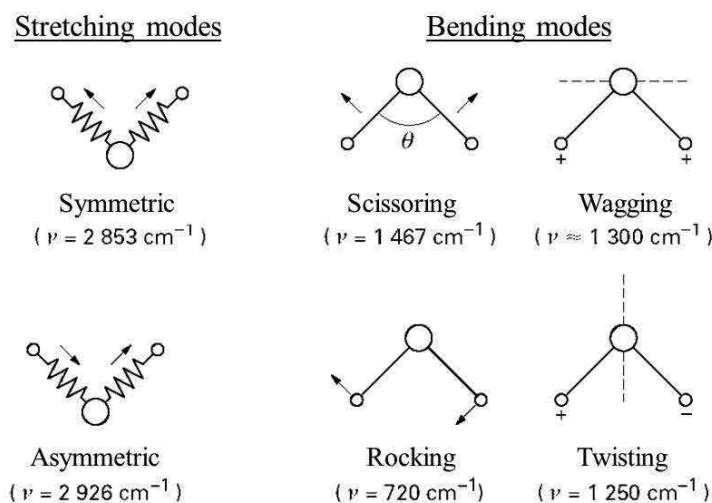


**Figure 2.10:** Representation of vibration modes localized on  $-\text{CH}_2-$ .<sup>5</sup>

The infrared spectra of one chemical compound can give valuable information's about its composition, conformation and environment. Infrared spectroscopy can characterize chemical functions regardless molecule's crude formula. For instance, methylene group ( $-\text{CH}_2$ ) shows a characteristic band at  $2850\text{ cm}^{-1}$  specific to methylene symmetric stretching mode of vibration. However, interactions of molecules with their environment affects this characterization. Non covalent interactions as hydrogen bonds change vibrations of covalent bonds. Consequently, alteration of vibration transitions due to intra or extra molecular interactions might shift the chemical characteristic band in infrared spectroscopy is thus a convenient method to determine supramolecular assembly of molecules and secondary structures of macromolecules as proteins.

### 2.2.3.2 Fourier transform infrared spectroscopy

This infrared device requires the used of Michaelson interferometer (Figure 2.11). Michaelson interferometer is made of two perpendicular mirrors, one fixed ( $M_f$ ), the other mobile ( $M_m$ ) and one semi-reflective blade (S). The beam emitted by an infrared (IR) source is passing through the semi-reflective blade (S) made of KBr coated with germanium and positioned at  $45^\circ$ . When the laser reaches S after it reflection, half of it is reflected by the fixed mirror, whereas the other half is reflected by the mobile mirror. The IR beam reaches back again the semi-reflective blade to be gathered in one and cross the chemical sample with absorbing properties related to its structure.

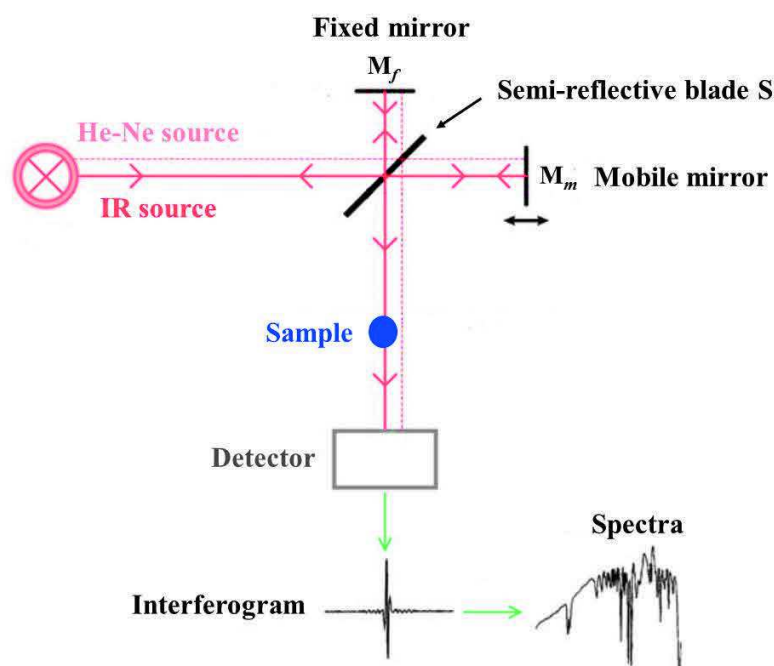


**Figure 2.11:** Schematic representation of a Michelson interferometer used in infrared spectroscopy.

If both mirrors  $M_m$  and  $M_f$  are equidistant from the semi-reflective blade both beams follow the same optical trajectory and are emitted in phase. Modification of the  $M_m$  position increases the optical trajectory of one of the beams. As a result, the two beams will have a phase difference. The intensity of the combined optical signals with tunable phase is called the interferogram. Finally, the interferogram is analyzed by the detector and converted with Fourier transformation to give the infrared spectra corresponding to the sample.

### 2.2.3.3 FTIR attenuated total reflection

FTIR attenuated total reflection method (ATR) was used to monitor *in situ* adsorption of polyelectrolytes, enzymes and peptide supramolecular self-assembly. As we mentioned previously, FTIR technique allows to characterize intermolecular interactions and to determine secondary structures of protein or peptides. This technique in ATR mode is suitable to follow *in situ* the assembly of peptides.

#### Principle of ATR

The principle of ATR was described by Harrick<sup>6</sup> and its applications in the biological field by Fringeli and Gunthard.<sup>7</sup> In our study, we use a trapezoid crystal made of ZnSe (Fig. 2.12).

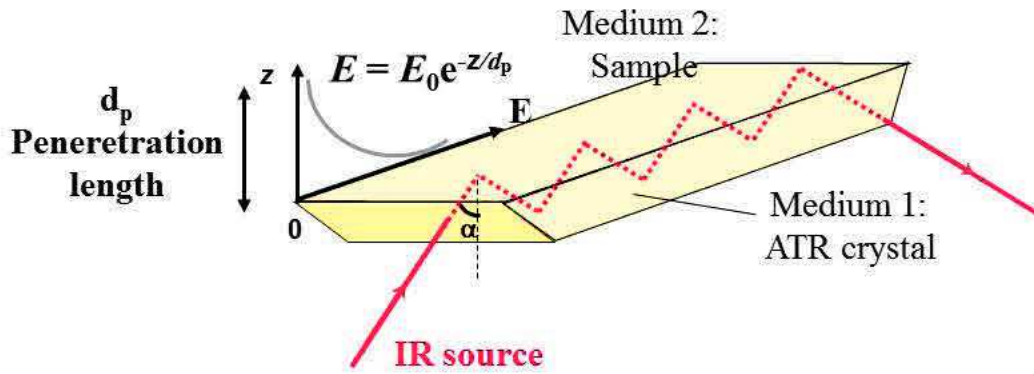


**Figure 2.12:** Schematic representation of the infrared source crossing a ZnSe trapezoidal crystal. The incident IR beam usually penetrates into the crystal with a critical angle  $\alpha = 45^\circ$ , and strikes the interface between the crystal (medium 1) and the sample (medium 2). It creates an evanescent wave in medium 2 above the crystal of ATR. The beam is thus reflected several times before to reach a detector at the other side of the crystal.

The IR beam coming out from the Michaelson interferometer is guided toward one face of a trapezoidal crystal of ZnSe (Figure 2.12). The infrared incident source then arrives at the interface between the ATR crystal (medium 1) and the aqueous solution above the crystal (medium 2). In this case if the  $\alpha$  angle of the incident beam is more important than the critical angle  $\alpha_c$ , the IR source is totally reflected within the crystal. The critical angle is defined by:

$$\alpha_c = \sin^{-1} \left( \frac{n_2}{n_1} \right) \quad (1.8)$$

With  $n_1$  the refractive index of ATR crystal (medium 1) and  $n_2$  the refractive index of the sample (medium 2). By taking into account value of the refractive index of ZnSe  $n_1=2.42$  (at  $1550 \text{ cm}^{-1}$ ) and protein solutions  $n_2=2.5$  (at  $1550 \text{ cm}^{-1}$ ) is possible to set the critical angle value at  $38.8^\circ$ . Using the ZnSe crystal (GRASEBY-SPECAC, England) with a size of  $72 \times 10 \times 6 \text{ mm}^3$ , the incident angle is of  $45^\circ$  and 6 reflections are occurring at the interface of medium 1 and medium 2.

For each reflection, an evanescent wave spreads in medium 2. The intensity  $E$  of this wave decreases exponentially with the increase of the distance  $z$  from the crystal (considering  $z = 0$  as the surface of ZnSe crystal). Intensity  $E$  can be calculated with:

$$E = E_0 e^{-z/d_p} \quad (1.10)$$

With  $E_0$  corresponding to the intensity at the crystal surface ( $z = 0$ ) and  $d_p$  the wavelength penetration depth that can be determined with:

$$d_p = \frac{\lambda}{2\pi n_1 \sqrt{\sin^2 \theta - \left(\frac{n_2}{n_1}\right)^2}} \quad (1.11)$$

With  $\lambda$  the wavelength of incident light. As example the penetration depth for the adsorption of protein solutions onto the ZnSe crystal is  $d_p=1.26 \mu\text{m}$  at  $1550 \text{ cm}^{-1}$ .

### **Experimental setup**

The Fourier Transform Infrared (FTIR) experiments were performed on a Vertex 70 spectrometer (Bruker, Germany) using DTGS detector. The spectra relative to the multilayers were determined in the Attenuated Total Reflection (ATR) mode using a  $45^\circ$  trapezoidal ZnSe (internal reflection element) crystal (6 reflections, dimensions  $72 \times 10 \times 6 \text{ mm}^3$ ) in ATR cell (GRASEBY-SPECAC, England). Reference (bare ZnSe crystal) and sample spectra were taken by collecting 128 interferograms between  $800$  and  $4000 \text{ cm}^{-1}$  at  $2 \text{ cm}^{-1}$  resolution, using Blackman-Harris three-term apodization and the standard Bruker OPUS/IR software (version 5.0). Multilayer films were assembled on ZnSe crystal by dipping method as described above for QCM-D experiments. All the sample spectra, as for the reference, were recorded with the ZnSe crystal in contact with the buffer. All polymers, peptides and enzymes solutions were prepared as previously in  $\text{D}_2\text{O}$  buffers to avoid the signal of water in the amide I band region of peptides.

## **2.2.4 UV-visible spectroscopy**

### **2.2.4.1 Principle of enzymatic assay**

According to IUPAC, enzymatic assay can be define as a set of operations having the object to determine an enzymatic activity. This study permit to record the quantity of substrate (in mole) convert in product by enzymes and per minute. From these investigation results settlement of enzymatic unit (U), also describe as the amount of enzymes that catalyze transformation of  $1 \mu\text{mol}$  of substrate per minute. The enzymatic assay were performed on Alkaline Phosphatase (ALP) able to convert para-Nitrophenyl Phosphate (p-NPP) into yellow *p*-Nitrophenol (*p*-NP) showing absorbance at  $\lambda = 405 \text{ nm}$  (Figure 2.13)

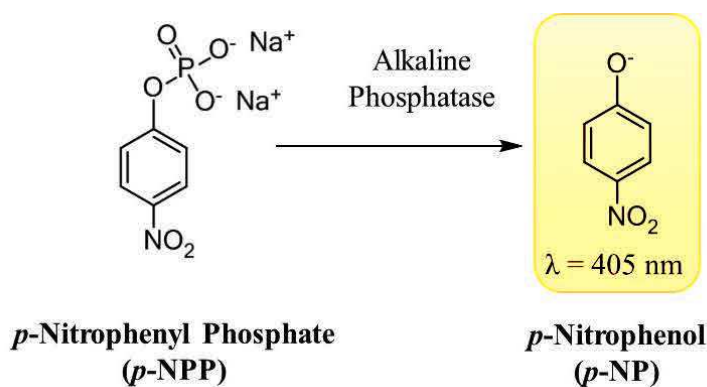


**Figure 2.13:** Enzymatic hydrolysis of *p*-Nitrophenyl Phosphate (*p*-NPP) by alkaline phosphatase and *p*-Nitrophenyl Acetate (*p*-NPA) by esterase.

Kinetic of *p*-NP formation was followed by microplate reader device coupled with UV-Visible spectrometer. Consequently concentration of *p*-NP released in the bulk can be calculated with the Beer-Lambert law:

$$A = \epsilon l C \quad (1.12)$$

With  $A$  the absorbance,  $\epsilon$  the molar attenuation coefficient ( $\text{L}\cdot\text{mol}^{-1}\cdot\text{cm}^{-1}$ ),  $l$  length of the optical path (cm) and  $C$  concentration of the chemical compound ( $\text{mol}\cdot\text{L}^{-1}$ ). Kinetic parameters of the enzymatic catalysis can thus be deduced with this method.

### Experimental setup

Microplate reader UV spectroscopy (FLX-Xenius®, SAFAS, Monaco) was used to monitor the enzymatic activity of the coatings. The enzyme based coatings were built on glass substrates and put in 24-well plate for UV measurements. The Alkaline Phosphatase (ALP) based coating was put in contact with of *p*-NPP solution (1 mL, 1 mM in Borax buffer). Concentration and volume ensure a large excess of substrates for the enzymatic reaction. *p*-NPP, colorless ALP substrate, is transformed in *p*-NP, a yellow product which absorbance is monitored at  $\lambda = 405 \text{ nm}$  a yellow absorbance.

### 2.2.5 Confocal laser scanning microscopy

Confocal laser scanning microscopy images were captured with Zeiss LSM 710 microscope using a x 63 oil objective (Achromplan, N.A. = 1.4). Fluorescein Isothiocyanate (FITC) fluorescence was detected after excitation by argon laser with a cut-off dichroic mirror of 488 nm and emission band-pass filter 493-556 nm (green emission). Rhodamine fluorescence was detected after excitation by argon laser with a cut-off dichroic mirror of 542-582 nm and emission band-pass filter 604-644 nm (red emission). Virtual vertical sections

can be visualized, hence allowing approximate determination of the hydrogel thickness. Images were purchased with ZEN 2011 software and analyzed by Image J (<http://rsb.info.nih.gov/ij/>). Multilayered films were prepared onto 12-mm glass slides by dipping and placed in a special confocal support allowing fluorescence capture in liquid state.

## References

1. Sauerbrey, G. Verwendung von Schwingquartzen zur Wägung dünner Schichten und zur Mikrowägung. *Z. Phys.* **1959**, *155*, 206.
2. The NanoWizard AFM Handbook. **2005**.
3. <http://www.sciencesetavenir.fr/fondamental/materiaux/20150116.OBS0113/en-images-un-nano-monde-haut-en-couleurs.html>.
4. Sittinger, M.; Lukanoff, B.; Burmester, G. R.; Dautzenberg, H. Encapsulation of artificial tissues in polyelectrolyte complexes: preliminary studies. *Biomaterials* **1996**, *17* (10), 1049.
5. Dalibart, M.; Servant, L. Spectroscopie dans l'infrarouge. In *Techniques de l'Ingénieur*: Paris, P2845,, 2000, pp 1.
6. Harricks, N. J. Internal Reflection Spectroscopy. . *Wiley-Interscience*. **1967**.
7. Fringeli, U. P. G., H. H. IR Membrane Spectroscopy. *Berlin: Springer*. **1981**.

Chapter 3:  
Spatiotemporal Tuning of Peptides  
Nanofibers Growth from an Enzyme-  
Modified Surface

---

---

## Chapter 3:

# Spatiotemporal Tuning of Peptides Nanofibers Growth from an Enzyme-Modified Surface

---

### Summary

<b>3.1 Abstract</b> .....	<b>77</b>
<b>3.2 Introduction</b> .....	<b>78</b>
<b>3.3 Results and discussion</b> .....	<b>79</b>
3.3.1 Localized enzymatic assisted self-assembly of (KL) <sub>n</sub> OE <sub>t</sub> .....	79
3.3.2 Toward the temporal control of the self-assembly and nanofibers growth.....	84
<b>3.4 Conclusion</b> .....	<b>88</b>
<b>3.5 Supporting Information</b> .....	<b>89</b>
3.5.1 Material and methods .....	89
3.5.1.1 List of Chemicals .....	89
3.5.1.2 Synthesis of Lysine-Leucine ethyl ester (KLOEt) and $\alpha$ -chymotrypsin <sup>RHO</sup> .....	90
3.5.1.2 Multilayer film preparation and hydrogel self-assembly.....	92
3.5.1.3 Fluorescence Microscopy.....	93
3.5.1.4 Circular Dichroism (CD) .....	93
3.5.1.5 Matrix-Assisted Laser Desorption/Ionization Time-of-Flight (MALDI-TOF).....	93
3.5.1.6 Cryo-Scanning Electron Microscopy (cryo-SEM).....	94
3.5.1.7 Wet Scanning Transmission Electron Microscopy (Wet STEM).....	94
3.5.3 Supporting figures .....	95
<b>References</b> .....	<b>101</b>

### **3.1 Abstract**

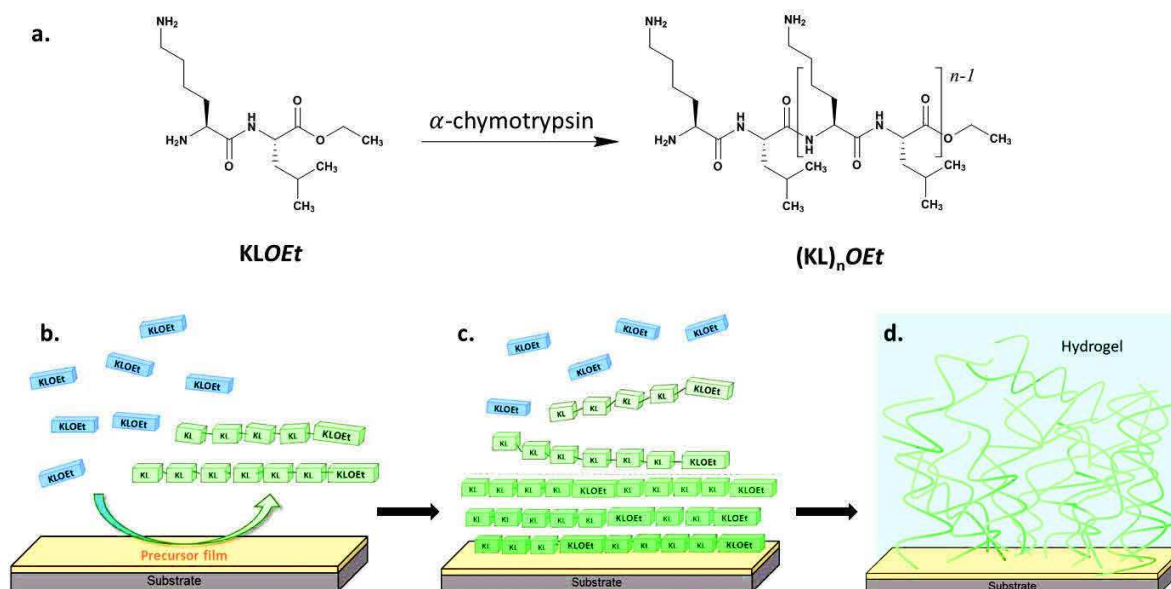
Localized self-assembly allowing both spatial and temporal control over the assembly process is essential in many biological systems. Herein, we present a simple chemical system based on *localized enzyme-assisted self-assembly* (LEASA) of peptides leading to the growth of fibrillar network hydrogels starting exclusively from a  $\alpha$ -chymotrypsin precursor film adsorbed on a surface. When such a film is brought in contact with a KLOEt solution, a micrometer-scaled hydrogel builds up. The formation of this gel results from the local accumulation of  $(KL)_nOEt$  oligopeptides ( $4 \leq n \leq 7$ ) produced from the confined enzyme layer at the interface. When the critical concentration of oligopeptides is reached, they self-assemble into  $\beta$ -sheets that form fibers ( $\emptyset \sim 15$  nm) resulting in a fibrillar gel localized at the interface. One significant feature of this approach is the initiation of the gelation that can be tuned in time (lag time) by controlling not only the concentration of KLOEt solution but also the surface density of  $\alpha$ -chymotrypsin. The enzymatic precursor film can thus self-instruct the resulting gel by influencing its buildup kinetic and its final mass.

## 3.2 Introduction

Biological processes such as cell migration or division are the result of a large number of reactions of fine spatial and temporal tuning.<sup>1-2</sup> Among them, spatially confined enzymatically controlled self-assembly processes play a major role. Reproducing such processes in synthetic systems represents a real challenge that constitutes an essential step towards the design of artificial life mimics. This problem can be addressed by the use of catalytically assisted self-assembly where the catalyst is generated at or fixed on a surface. In this approach, non-interacting species are brought in contact with the surface, undergo a reaction triggered by the presence of a catalyst at or near the surface which leads to their self-assembly. The catalyst can simply be a proton<sup>3</sup> or another ion<sup>4</sup> present at the interface either statically or generated dynamically by electrochemical<sup>5-6</sup> means for example. Adsorbed enzymes can also be used to generate self-assembling species.<sup>7-8</sup> This can be called *localized enzyme assisted self-assembly* (LEASA). Enzyme assisted self-assembly has been introduced in 2004 by the group of Xu<sup>9</sup> and widely extended by Ulijn and coworkers<sup>10-11</sup> to initiate gel formation in the bulk. These groups used peptides with attached aromatic moieties that were initially protected with phosphate groups and then enzymatically deprotected, transforming into self-assembling hydrogelators. The self-assembly resulted from a decrease of solubility of the peptides, bearing aromatic moieties, in water after their deprotection. When such a reaction is triggered by enzymes adsorbed at an interface, a concentration gradient of hydrogelators is obtained near the surface, leading to a localized self-assembly and resulting in the formation of a hydrogel film near the interface.<sup>7-8</sup> However, inducing locally the formation of peptide nanofibrillar networks is not sufficient to allow the development of complex cell-like assemblies in artificial life. One also needs to be able to control the self-assembly process both temporally and in amplitude. Amplitude control can be achieved by adsorbing a seed layer on the surface. The seed-layer, playing the role of nucleation agent, favors the gel formation at the interface for concentrations in assembling species much smaller than required in the bulk to form a gel.<sup>12</sup>

Herein, we present another way to control LEASA using oligomerization of lysine-leucine-ethyl ester dipeptides ((KL)*OEt*) catalyzed by  $\alpha$ -chymotrypsin. Gross and coworkers described the EASA of K*LOEt* in solution.<sup>13</sup> (KL)<sub>n</sub>*OEt* oligomers form physically entangled nanofibrillar networks through intermolecular backbone hydrogen bonding. Up to now, it has never been shown that this system, where its self-assembly relies on hydrogen bonds between oligomers, is also

suitable for LEASA. We designed an enzymatic,  $\alpha$ -chymotrypsin, precursor film using the layer-by-layer process. Both an amplitude control and a temporal control of the self-assembly was implemented by tuning  $\alpha$ -chymotrypsin surface density of the precursor film and KLOEt peptide concentration. The film buildup strategy is represented schematically in scheme 3.1.



**Scheme 3.1:** (a) Enzymatic transformation of the lysine-leucine ethyl ester dipeptides KLOEt into alternating  $(KL)_nOEt$  oligomers by  $\alpha$ -chymotrypsin. (b) Schematic representation of the LEASA concept applied to the self-assembly of oligopeptides formed in contact with an enzymatic ( $\alpha$ -chymotrypsin) precursor film: (c) the accumulation of generated oligopeptides allows to reach locally the critical concentration of gelation (d) leading to the gelation exclusively from the surface.

## 3.3 Results and discussion

### 3.3.1 Localized enzymatic assisted self-assembly of $(KL)_nOEt$

$\alpha$ -Chymotrypsin, categorized as a protease, generally catalyze hydrolysis of peptide bonds. However in appropriate conditions,  $\alpha$ -chymotrypsin is able to catalyze reverse hydrolysis via trans acylation of peptide sequences wearing C-terminal ethyl ester. This remarkable activity leads to the formation of new peptide bonds elongating the substrate sequence. The enzymatic substrate KLOEt dipeptide ethyl ester has been prepared at the multigram scale in three steps from KL with an overall yield of 92% (Paragraph 3.5.1.2 in Supporting Information, SI). We first checked that KLOEt in solution (at  $80 \text{ mg.mL}^{-1}$  in phosphate buffer pH 8.7) in the presence of  $\alpha$ -chymotrypsin ( $10 \text{ mg.mL}^{-1}$ ) formed a gel as reported by Gross et al.<sup>13</sup> We thus investigated an enzymatic

precursor film based on  $\alpha$ -chymotrypsin, adsorbed on a surface, with *KLOEt* as its substrate in order to develop LEASA (Scheme 3.1). For this purpose, we used quartz crystal microbalance with dissipation (QCM-D), a technique that allows following adsorption processes on a quartz crystal in aqueous solution with a nanogram sensitivity. To anchor strongly  $\alpha$ -chymotrypsin on the surface, we first deposited on the quartz crystal a layer of poly(ethylene imine) (PEI), known to deposit on almost any kind of surfaces in a reproducible manner. Because  $\alpha$ -chymotrypsin (isoelectric point of 8.7) is globally slightly positively charged at physiological pH 7.4, it cannot be directly adsorbed onto the PEI layer through electrostatic interactions.<sup>14</sup> Therefore, a layer of tannic acid (TA) was deposited on PEI to absorb  $\alpha$ -chymotrypsin, obtained thanks to hydrogen bonds with TA.<sup>15</sup> The buildup of the enzymatic precursor film, PEI/TA/ $\alpha$ -chymotrypsin, is shown in Figure 3.1.a. According to Sauerbrey equation<sup>16</sup> and assuming a film density of  $1 \text{ g/cm}^{-3}$ , the film thickness is estimated at 35 nm. The contact of the enzymatic precursor film with a *KLOEt* solution ( $1 \text{ mg.mL}^{-1}$ ) led to a huge increase of the fundamental frequency shift as well as an important increase of the corresponding dissipation. After 40 min of contact, both the frequency shift and the dissipation reach a plateau at 1300 Hz and  $395 \times 10^{-6}$ , respectively (Figure 3.1.c). These values indicate an important mass deposition of a highly viscoelastic film, as expected for a gel. During the buildup process, peptides are able to diffuse through the gel in formation to reach the enzymatic precursor film and then to be oligomerized by  $\alpha$ -chymotrypsin. The existence of a plateau overtime can be explained either by a limited diffusion of *KLOEt* from the solution to the enzymatic precursor film through the formed hydrogel or by the limit of detection of QCM-D for thick coating. When using bovine serum albumin (BSA) instead of  $\alpha$ -chymotrypsin, *i.e.* bringing a *KLOEt* solution ( $1 \text{ mg.mL}^{-1}$ ) in contact with the PEI/TA/BSA precursor film, the fundamental frequency shift and dissipation were unchanged. This proves that the strong frequency shift and dissipation increase obtained with the enzymatic precursor film, PEI/TA/ $\alpha$ -chymotrypsin, are due to the presence of  $\alpha$ -chymotrypsin on the surface (Figure 3.1.c).

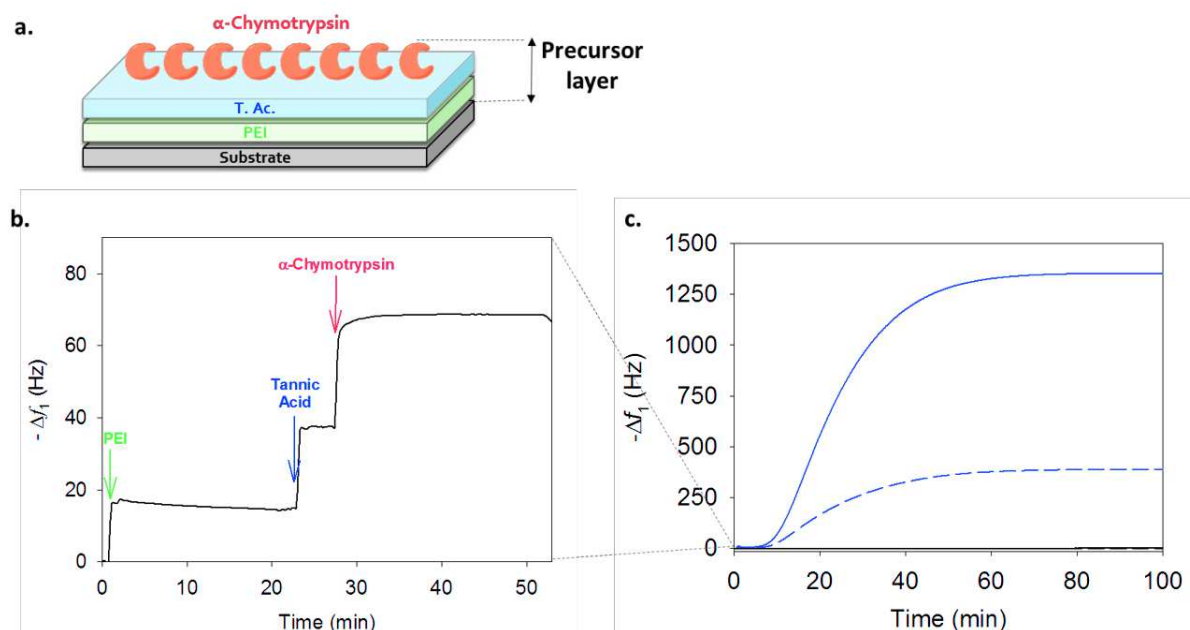


**Figure 3.1:** (a) Schematic representation of the enzymatic precursor multilayer film, PEI/TA/ $\alpha$ -chymotrypsin adsorbed onto the surface. Evolution of the fundamental frequency shift, measured by QCM-D, as a function of time (b) during the buildup of PEI/TA/ $\alpha$ -chymotrypsin followed by (c) the contact of KLOEt solution (blue curve) with the dissipation signal (blue dotted curve). The black curve is the signal obtained when PEI/TA/BS is used as a precursor film. KLOEt solution was prepared at  $1 \text{ mg.mL}^{-1}$  in a Tris buffer at pH 8.5.

To get information on its composition, MALDI-TOF analysis was performed on the gel obtained after 12 h of contact of KLOEt with PEI/TA/ $\alpha$ -chymotrypsin. The sample was collected directly on the surface with a pipette to be dried (see paragraph 3.5.1.6 in SI for experimental detail). A distribution of  $(\text{KL})_n\text{OEt}$  oligomers with  $n$  ranging from 2 to 7, centered around  $(\text{KL})_5\text{OEt}$ , was obtained (Figure S3.1 in SI). This proves that the adsorbed  $\alpha$ -chymotrypsin layer catalyzes the condensation between KLOEt molecules. More interestingly, the reaction process localized at the substrate does not only form dimers but leads also to higher order of oligomers at a high enough rate to reach the critical concentration at which the gelation starts. The distribution of  $(\text{KL})_n\text{OEt}$  oligomers observed on the surface can be compared to the one obtained when  $\alpha$ -chymotrypsin is in solution.  $(\text{KL})_n\text{OEt}$  oligopeptides distribution extended up to  $n = 14$  when  $\alpha$ -chymotrypsin is in solution.<sup>13</sup> In our experimental conditions, confining  $\alpha$ -chymotrypsin on a surface results in a self-assembled architecture based on shorter  $(\text{KL})_n\text{OEt}$  oligomers in comparison to the ones obtained when  $\alpha$ -chymotrypsin is in solution.

The gelation growth process from the surface has also been followed by infrared spectroscopy in attenuated total reflection mode (IR-ATR). All the solutions were prepared in deuterated water to avoid water infrared band overlapping amide I band of peptides. After the buildup of the enzymatic precursor film, IR spectra were recorded for 17 h during the contact of KLOEt solution ( $1 \text{ mg.mL}^{-1}$ ) (Figure 3.2.a). Vibration bands at  $1614$  and  $1622 \text{ cm}^{-1}$  appear during the oligopeptides  $(\text{KL})_n\text{OEt}$  self-assembly, corresponding mainly to the carbonyl group stretching band, called amide I.<sup>17-18</sup> The secondary structure of the gel was revealed by circular dichroism (CD). Indeed, CD spectra of the gel obtained on the surface of the enzymatic precursor film showed one strong positive peak at  $198 \text{ nm}$  and a slight broad negative peak at  $215 \text{ nm}$  (Figure 3.2.b), characteristics of  $\beta$ -sheets structures.<sup>19</sup> A similar CD signal is obtained by Gross et al. for KLOEt hydrogel obtained in solution.<sup>13</sup>

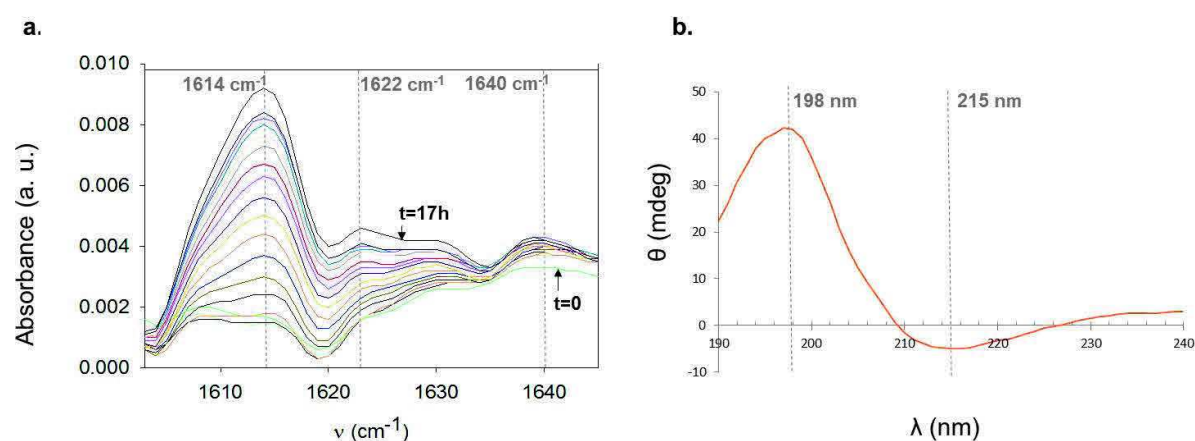


**Figure 3.2:** (a) Evolution of the IR-ATR spectra as a function of time during the contact of KLOEt solution ( $1 \text{ mg.mL}^{-1}$ ) with PEI/TA/ $\alpha$ -chymotrypsin precursor film. From the bottom to the top, each colored curve has been recorded every 10 min, except for the last black curve, measured at  $t = 17 \text{ h}$ ; (b) CD spectra measured of the gel obtained after 12 h of contact of KLOEt solution ( $1 \text{ mg.mL}^{-1}$ ) with PEI/TA/ $\alpha$ -chymotrypsin.

To get access to its morphology,  $(\text{KL})_n\text{OEt}$  oligopeptide gel, obtained after 12 h of contact of KLOEt solution ( $1 \text{ mg.mL}^{-1}$ ) on the enzymatic precursor film, was analyzed by wet scanning transmission electron microscopy (Wet STEM) and cryo-scanning electron microscopy (cryo-SEM). The advantage of these microscopies is to provide structural information in the presence of water. Using Wet STEM, the degree of humidity into the chamber containing the sample is controlled, allowing the morphological analysis in a wet state. Images of the surface of the self-assembled gel, obtained from Wet STEM, show the presence of a very dense network (figure S3.2

in SI). A cross-section of the hydrogel was observed by cryo-SEM using a specific cryo-holder designed in our mechanical facility. The sample is rapidly frozen in nitrogen slush and transferred under vacuum and low temperature in the cryo chamber attached to the SEM (see paragraph 3.5.1.7 SI for experimental details). As shown on Figure 3.3, a inhomogeneous full coverage of the surface by  $(KL)_nOEt$  gel is obtained with some areas of around 12  $\mu\text{m}$  and others with around 1  $\mu\text{m}$  in thickness. The morphology of the z-section displays thus two distinct parts: close to the substrate, a very dense network of nanofibers is anchored onto the surface (Figure 3.3.a, short black arrow and Figure 3.3.b) and roughly 2  $\mu\text{m}$  from the surface, this fibers nanoarchitecture disappears giving way to large oriented cavities (Figure 3.3.a, long black arrow).  $(KL)_nOEt$  fibers seem to be entangled together without crosslinking point, suggesting an organization close to a physical gel (Figure 3.3.b). The large oriented cavities, considered as artefacts, could be due to the formation of ice crystals during the freezing process. We observe these cavities at the surface of our samples were the freezing speed is the highest. An efficient freezing process can be achieved if the concentration of organic matter is high (or in presence of anti-freezing molecules). Thus, water rich regions are very badly preserved. As  $(KL)_nOEt$  gel is self-assembled from the surface by a bottom-up process, one can assume that the fiber density decreases as one moves away from the surface. Our hypothesis is that the artefacts appear in a region of the gel of small fiber density. This is confirmed by experiments performed with less concentrated  $KLOEt$  solutions ( $< 1\text{mg.mL}^{-1}$ ). Lower concentrations of  $KLOEt$  lead to a lower production of  $(KL)_nOEt$  oligopeptides from the enzymatic precursor film. In this case, only large cavities coming from freezing artefacts were visible (Figure S3.3 in SI).

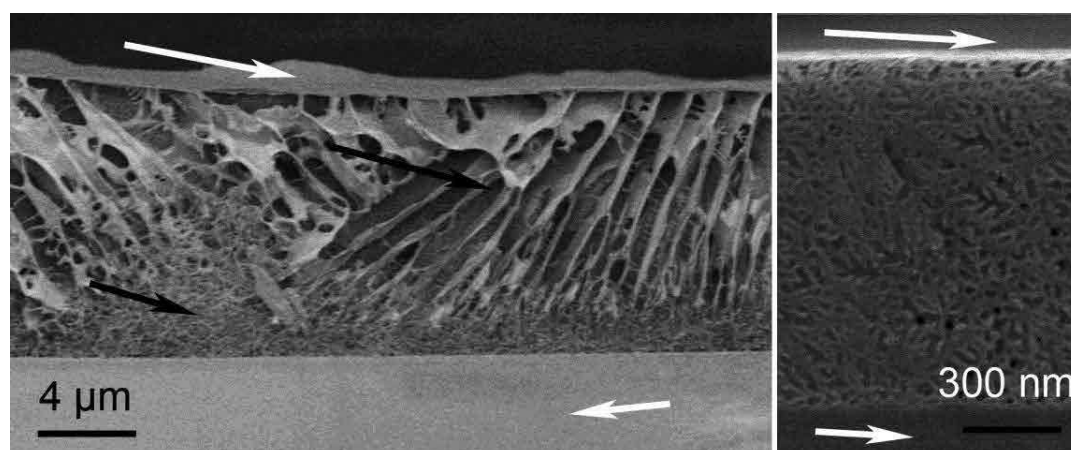


**Figure 3.3:** (a) Cryo-SEM image of a cross sectioned gel showing the  $(KL)_nOEt$  oligopeptide-based hydrogel obtained by contact of  $KLOEt$  solution ( $1 \text{ mg.mL}^{-1}$ ) for 12 h with the precursor enzymatic film adsorbed on a glass slide (short white arrow). The short black arrow points to the entangled fibers found at the glass interface. The long black arrow points to the water rich part of the gel appearing as cavities due to the slight etching performed before observation (see SI). The long white arrow indicate the air/gel interface (b) Cryo-SEM image highlighting the high density of entangled nanofibers located nucleated on the interface.

### 3.3.2 Toward the temporal control of the self-assembly and nanofibers growth

The time-evolution of the hydrogel growth from the enzymatic precursor film can be followed both by IR with the increase of the vibration band intensity measured at  $1614 \text{ cm}^{-1}$  (Figure S3.4 in SI) and by QCM with the increase of the fundamental frequency shift (Figure 3.1.c). In both cases, it appears that there is a lag time before the signal start to increase due to the self-assembly of  $(KL)_nOEt$ , which extends over several tens of minutes before reaching a plateau. Interestingly the self-assembly of oligopeptides is a process that does not occur instantaneously when the enzymatic precursor film is brought in contact with the  $KLOEt$  solution. The monitoring by IR-ATR reveals clearly a *lag time* of roughly 25 min before the detection of any matter adsorbed on the surface (Figure S3.4 in SI). Similarly, both the fundamental frequency shift and the dissipation remains unchanged for 9 min before starting to increase displaying finally a sigmoidal growth kinetic (Figure 3.1.c). This time frame is shorter than the one measured by IR-ATR, probably because of the higher sensitivity of QCM-D ( $\sim 1 \text{ ng/cm}^2$ ) compared to IR-ATR spectroscopy. The value of this *lag time*, corresponding to the period of time over which QCM-D signals are unchanged, can be estimated by taking the intersection of the tangent at the inflection point of the evolution curve of the fundamental frequency (or dissipation) with the time-abscissa (Figure S3.5 in SI). We observed that this lag time is strongly dependent upon the  $KLOEt$

concentration used for the buildup process (Figure 3.4.a and Figure S3.6 in SI). Below  $0.45 \text{ mg.mL}^{-1}$  of *KLOEt*, no gel buildup is observed. Above this critical concentration, the lag time decreases when the concentration of *KLOEt* increases: for instance, when the concentration of *KLOEt* is varied from 1.5 to  $0.45 \text{ mg.mL}^{-1}$ , the lag time varied from 6 to 13 min. In a physico-chemical point of view, the lag time corresponds to the time necessary to reach a critical concentration of oligopeptides  $(\text{KL})_n\text{OEt}$  near the surface required for the fibers formation. Furthermore, the kinetic of gelation (that can be appreciated by the slope of the change of the frequency shift at the inflection point) depends on the *KLOEt* concentration. Concentrated *KLOEt* solutions lead to more important slopes of the QCM signal (Figure 3.4.a). At longer time, the value in frequency shift at the plateau increases with the concentration of dipeptides in solution (Figure 3.4.b). Higher concentration of *KLOEt* in solution leads to higher density of self-assembled oligopeptides, and more encapsulated water, in the resulting gel.

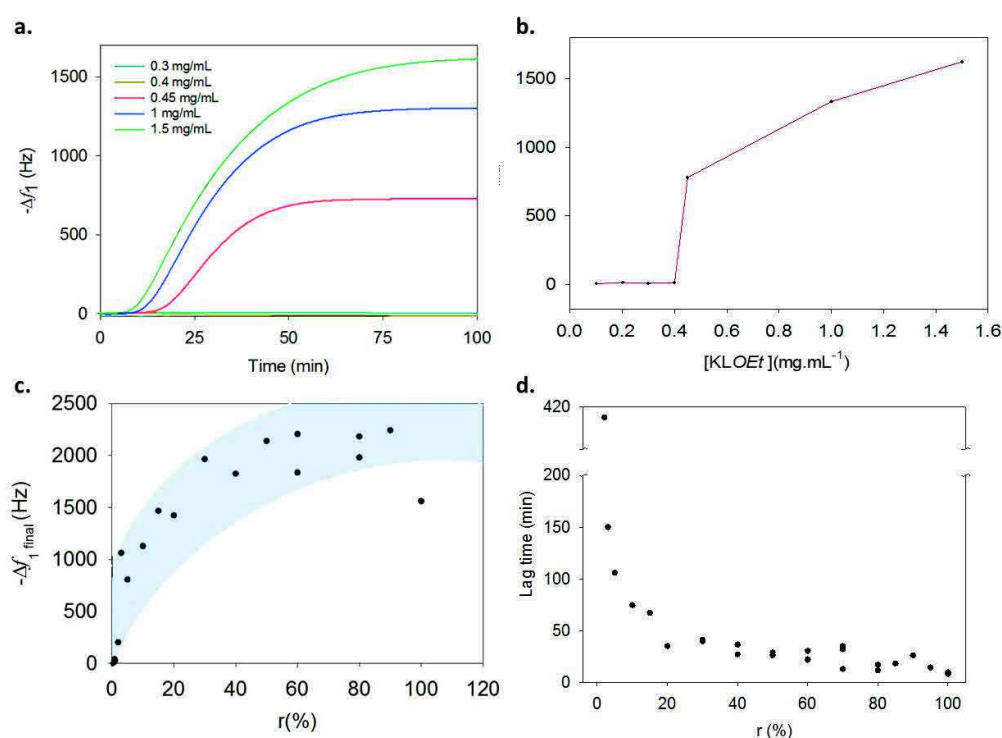


**Figure 3.4:** Evolution of (a) the fundamental frequency shift as a function of time and (b) the final value of the frequency shift obtained after 12 h when *KLOEt* solution, with different concentrations, is put in contact with the enzymatic PEI/TA/ $\alpha$ -chymotrypsin precursor film. Evolution of (c) the final value of the frequency shift obtained after 12 h and (d) the lag time, when *KLOEt* solution ( $1 \text{ mg.mL}^{-1}$ ) is put in contact with the PEI/TA/ $(\alpha$ -chymotrypsin( $r$ ) – BSA( $100-r$ )) precursor film, as a function of  $r$ , with  $r$  the molar ratio in  $\alpha$ -chymotrypsin in the solution deposited to build the precursor film.

To get a more precise control of the localized self-assembly process at the surface, we also varied another parameter, *i.e.* the composition of the enzymatic precursor film. For this purpose, protein mixtures of  $\alpha$ -chymotrypsin and bovine serum albumin (BSA), prepared at different molar ratio, were adsorbed on PEI/TA coated surface with  $r$  (%), the molar ratio defined as follows

$$r(\%) = \frac{[\alpha \text{ Chymotrypsin}]}{([\alpha \text{ Chymotrypsin}] + [\text{BSA}])} \times 100$$

We first determined the relative density of  $\alpha$ -chymotrypsin adsorbed on the surface by using rhodamine labelled  $\alpha$ -chymotrypsin,  $\alpha$ -chymotrypsin<sup>RHO</sup>, and non-labelled BSA in the protein mixture deposited on PEI/TA coated surface. Figure S3.7 (in SI) shows the fluorescence signal evolution measured on the surface as a function of the molar ratio  $r$  in solution.  $\alpha$ -Chymotrypsin<sup>RHO</sup> surface density increases steadily with the enzyme proportion in solution over the whole proportion range from 0 to 100% of  $\alpha$ -chymotrypsin<sup>RHO</sup>. The adsorption of BSA compared to  $\alpha$ -chymotrypsin<sup>RHO</sup> seems to be favored on PEI/TA film. Indeed for high values of  $r$ , the normalized fluorescence intensity measured is lower than the one expected in the case of similar adsorption of chymotrypsin<sup>RHO</sup> and BSA. In the following, all the results will be expressed as a function of  $\alpha$ -chymotrypsin molar ratio,  $r$ , in the protein solution used to be deposited on PEI/TA coated surface.

We first fixed the KLOEt concentration at 1 mg.mL<sup>-1</sup> to put in contact with PEI/TA/( $\alpha$ -chymotrypsin( $r$ ) – BSA(100- $r$ )) precursor film, at different  $r$  molar ratio. We were interested in the final value of the frequency shift after gelation, related to the amplitude of gelation, and the lag time, related to the kinetic formation of the gel. At the end of the gelation process (12 h of contact), the final value of the frequency shift remains almost constant when the molar ratio of  $\alpha$ -chymotrypsin is decreased from 100% to 30% and decreases strongly afterwards (Figure 3.4.c). In parallel, the lag time increases slowly from 9 min with  $r = 100\%$  to 40 min with  $r = 30\%$  and strongly afterwards until a value of 420 min with  $r = 2\%$  (Figure 3.4.d). As expected, the lag time diverges at 0% in  $\alpha$ -chymotrypsin (100% BSA) on the surface, no buildup is observed. Such a behavior is expected since the network buildup requires the synthesis of sufficient oligopeptides whose kinetic is directly dependent on the surface density in  $\alpha$ -chymotrypsin. Several kinetic studies have shown that the lag time may result from multiple nucleation that occurs before the propagation of the oligomerization and then the initiation of the self-assembly process.<sup>20</sup>

Next, we investigated the concomitant influence of two parameters on the gelation process (amplitude and kinetic): the *KLOEt* concentration and the composition of the precursor film, *i.e.* the surface density of  $\alpha$ -chymotrypsin. PEI/TA/ $(\alpha$ -chymotrypsin(*r*) – BSA(100-*r*)) precursor film were prepared at different *r* molar ratios from 5% to 100%. Different concentrations of *KLOEt* solutions, from 0.3 to 1.5 mg.mL<sup>-1</sup>, were put in contact with the precursor film for 12 h. Figure 3.5 represents in a 3D diagram the evolution of the lag time and of the final value of the frequency shift as a function of *KLOEt* concentration and molar ratio in  $\alpha$ -chymotrypsin *r*. The evolution of the dissipation is also represented in Figure S3.8 in SI.

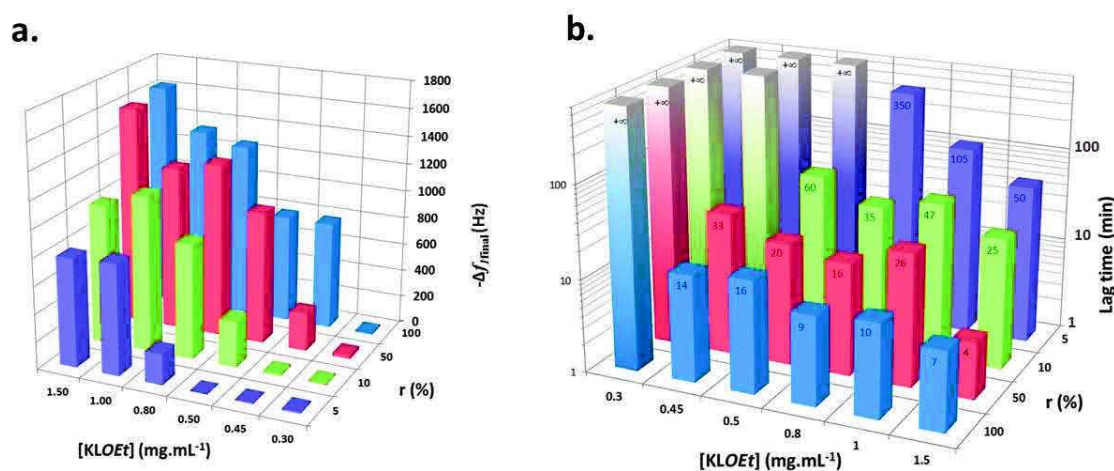


**Figure 3.5:** Evolution of (a) the fundamental frequency shift measured after 12 h of contact and (b) the lag time, in log scale, as a function of *KLOEt* concentration and *r*, molar ratio in  $\alpha$ -chymotrypsin in the solution deposited to build PEI/TA/ $(\alpha$ -chymotrypsin(*r*) – BSA(100-*r*)) precursor film. The symbol “+∞” means that the lag time is longer than 12 h.

Whatever the *KLOEt* concentration in solution, the self-assembly process is fairly similar for surfaces prepared by using solutions containing 100% and 50% of  $\alpha$ -chymotrypsin (Figure 3.5.a). The critical concentration in *KLOEt* required to obtain a self-assembly is about 0.45 mg.mL<sup>-1</sup>. In these cases, the surface density in  $\alpha$ -chymotrypsin is not the limiting parameter of the enzymatic reaction. For lower surface density, the critical *KLOEt* concentration increases until a value of 0.8 mg.mL<sup>-1</sup> with *r* = 5%. Moreover, the lag time increases with the decrease of *KLOEt* concentration or  $\alpha$ -chymotrypsin surface density (Figure 3.5.b). Such a behavior reflects the fact that a critical concentration of oligopeptides has to be present near the surface to start the self-assembly. Indeed, lower enzyme surface densities and/or lower *KLOEt* concentrations in solution

slow down the formation of  $(KL)_nOEt$  oligopeptides which delays the self-assembly process. Thus, the tuning of these two parameters allows to both easily and precisely control the time of the lag phase from few minutes to several hours kinetic of gelation and the resulting amplitude of hydrogel formed from the surface.

### 3.4 Conclusion

The development of chemical systems localized at an interface is an essential step toward the design of powerful nanoarchitectonic coatings. In this respect, the control in space and over time of the self-assembly process appears as a useful approach. In this work using LEASA strategy, we designed an enzymatic precursor film, using  $\alpha$ -chymotrypsin, on a surface to initiate the buildup of a hydrogel by condensation of KLOEt into oligomers. When  $(KL)_nOEt$  oligopeptides reach a critical concentration, they self-assemble into a dense fibrillar gel. LEASA allows to tune the amplitude (mass of hydrogel formed) and the kinetic (lag time) of the oligopeptides self-assembly by varying KLOEt concentration and/or  $\alpha$ -chymotrypsin surface density. These two parameters influence the local concentration of generated oligopeptides near the enzymatic precursor film affecting the self-assembly. These two parameters can be managed separately or concomitantly to tune the resulting hydrogel.

## 3.5 Supporting Information

### 3.5.1 Material and methods

#### 3.5.1.1 List of Chemicals

All chemicals used in this work are gathered in the following table.

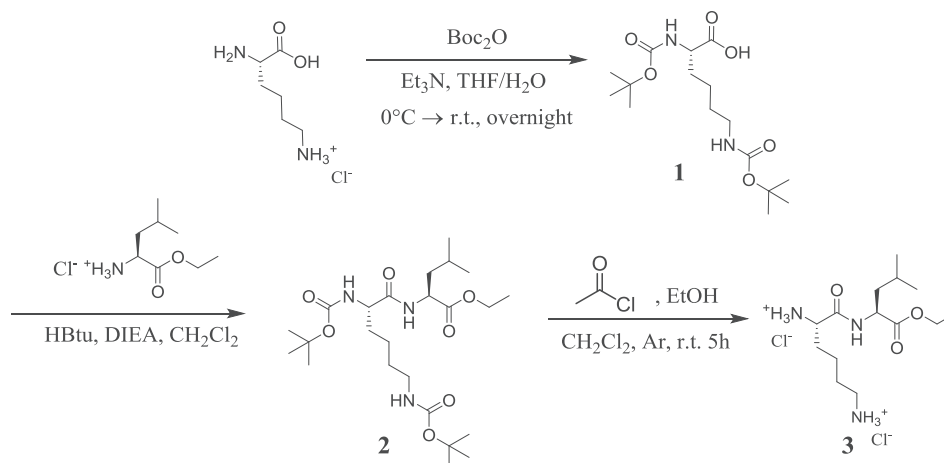
Name and Acronyme	Mw (g.mol <sup>-1</sup> )	Supplier	CAS number
Acetyl Chloride 98%	78.50	Alfa Aesar	75-36-5
Methylene Chloride (CH <sub>2</sub> Cl <sub>2</sub> )	84.93	Acros Organics	75-09-2
$\alpha$ -Chymotrypsin type II from Bovine Pancreas	25 kDa	Sigma Aldrich	9004-07-3
Albumin, bovine serum $\geq$ 99, essentially globulin free (BSA)		Sigma Aldrich	9048-46-8
L-Lysine.monohydrochloride	182.65	Sigma Aldrich	657-27-2
L-Leucine Ethyl Ester Hydrochloride 97%	195.69	Alfa Aesar	2743-40-0
Di-tert-butyl dicarbonate 97%	218.25	Fluka	24424-99-5
Tannic Acid (TA)	1701.23	Alfa Aesar	1401-55-4
Triethylamine (Et <sub>3</sub> N)	101.19	SDS	121-44-8
N,N'-diisopropylethylamine (DIEA)	129.25	Alfa Aesar	7087-68-5
		HiperSolv	
Ethanol	46.07	Chromatonorm	64-17-5
2 <sup>o</sup> -(1H benzotriazol-1-yl-1,1,3,3 tetramethyluronium hexafluorophosphate (HBTu)	379.24	Iris Biotech	94790-37-1
Rhodamine B isothiocyanate, mixed isomers	536.1	Sigma Aldrich	36877-69-7
Tetrahydrofuran (THF)	72.11	Acros Organics	109-99-9
Dimethyl sulfoxide (DMSO)	78.1	Acros Organics	67-68-5
Deuterated water (D <sub>2</sub> O)	20.03	Sigma Aldrich	7789-20-0
Deuterated Chloroform (CDCl <sub>3</sub> )	120.384	SDS	2206-27-1
Sodium Acetate	82.03	Sigma Aldrich	127-09-3
Sodium Phosphate	268.1	Sigma Aldrich	7782-85-2

Dibasic, heptahydrated			
Sodium Phosphate	138.0	Sigma Aldrich	10049-21-51
Monobasic, monohydrated			
Sodium Carbonate (Na <sub>2</sub> CO <sub>3</sub> )	105.9	Merk	497-19-8

### 3.5.1.2 Synthesis of Lysine-Leucine ethyl ester (KLOEt) and $\alpha$ -chymotrypsin<sup>RHO</sup>

#### General information

All starting materials were obtained from commercial suppliers and were used without further purification. <sup>1</sup>H NMR and <sup>13</sup>C NMR spectra were recorded on a Bruker Advance DPX400 (400 MHz) spectrometer. The NMR chemical shifts are reported in ppm relative to tetramethylsilane in CDCl<sub>3</sub> or *tert*-butanol (1.24 ppm) in D<sub>2</sub>O (s: singlet, t: triplet, q: quadruplet, dd: doublet of doublet, m: multiplet, br: broad. Reactions advancement was verified by thin layer chromatography (TLC) on Merck RP-18 F254S silica plates. TLC spots were revealed under UV light or after immersion into visualising agent solutions made of ninhydrin or 10% ethanolic phosphomolybdic acid. Column chromatography were performed with Geduran silica gel 60 (particle: 40 – 60  $\mu$ m).



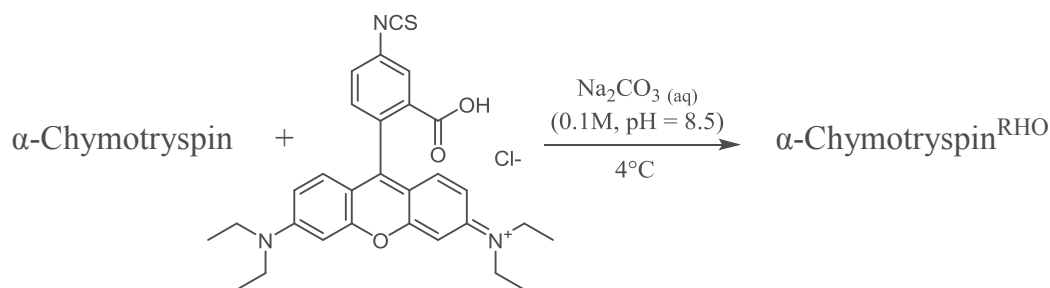
**Scheme 2:** Synthesis of Lysine Leucine-ethyl ester

**N<sub>α</sub>,N<sub>ε</sub>-Di-Boc-L-Lysine (1)** L-Lysine hydrochloride (1.600 g, 7.3 mmol, 1eq.) and triethylamine (4 mL, 29 mmol, 4eq.) were dissolved in milliQ water (27 mL) to be cold at 0°C. In a second round bottom flask, Di-*tert*-butyl dicarbonate (3.987 g, 18 mmol, 2.5 eq) was dissolved in THF (27 mL) and added dropwise to the L-Lysine monohydrochloride solution. The reaction

medium was stirred overnight at room temperature. Solvents were removed under vacuum to give a crude product engaged in next reaction without any further purifications. **<sup>1</sup>H NMR (CDCl<sub>3</sub>, 400 MHz):** 1.41 (s, 18H); 1.64 (m, 2H); 1.66 (m, 2H); 1.83 (m, 2H); 3.06 (m, 2H); 4.67 (br, 1H). **<sup>13</sup>C NMR (CDCl<sub>3</sub>, 100 MHz):**  $\delta$  22.4, 29.3, 33.2, 40.4, 54.8, 78.2, 78.5, 155.5, 155.9, 177.4. **FTIR (neat, cm<sup>-1</sup>):** 1691, 1475, 1395, 1171.

**N<sub>α</sub>,N<sub>ε</sub>-Di-Boc-L-Lysine Leucine-ethyl ester (2)** L-Leucine Ethyl Ester Hydrochloride (1.213 g, 6.203 mmol, 1.1 eq) and **1** (2.527 g, 5.639 mmol, 1 eq) were dissolved in dry CH<sub>2</sub>Cl<sub>2</sub> (115 mL). DIEA (2.0 mL, 11.2 mmol, 2eq) was added to the mixture and cooled at 0°C before addition of HBTU (3.208 g, 8.459 mmol, 1.5 eq). The reaction was stirred overnight and monitored by TLC in SiO<sub>2</sub> (Hexanes/EtOAc 5:5). The mixture was washed twice with NaHCO<sub>3</sub> (aq) and milliQ water in a separatory funnel. The organic layer was dried on Na<sub>2</sub>SO<sub>4</sub> and organic solvents were removed under reduced pressure. The crude product was purified by silica gel chromatography (Hexanes/EtOAc: 65/35) to afford a white powder as product (2.225, 81 % yield). **<sup>1</sup>H NMR (CDCl<sub>3</sub>, 400 MHz):**  $\delta$  0.91 (s, 3H); 0.92 (s, 3H); 1.26 (t,  $J = 7.1$  Hz, 3H); 1.38 (m, 2H); 1.42 (s, 18H); 1.57 (m, 1H); 1.63 (m, 2H); 1.82 (m, 2H); 3.09 (m, 2H); 4.05 (br, 1H); 4.17 (q,  $J = 7.1$  Hz, 2H); 4.68 (br, 1H). **<sup>13</sup>C NMR (CDCl<sub>3</sub>, 100 MHz):**  $\delta$  14.1, 21.8, 22.5, 22.8, 24.8, 28.8, 29.6, 31.9, 40.1, 41.4, 50.8, 54.2, 60.4, 61.3, 79.1, 80.0, 155.7, 156.1, 171.9, 172.7. **FTIR (neat, cm<sup>-1</sup>):** 1732, 1675, 1657, 1257, 1163.

**Lysine Leucine-ethyl ester (3)** Compound **2** (2.225 g, 4.56 mmol, 1eq.) was dissolved in dry DCM (46mL) under inert atmosphere. Acetyl Chloride (3.02mL, 43.14 mmol, 9.4 eq) and Absolute Ethanol (4.3 mL, 73.81 mmol, 16.7 eq) were injected dropwise to the solution. The reaction was stirred for 2 days at room temperature. Solvents were removed under vacuum and product **3** was obtained as a white powder (1.49 g, 93 % yield) by precipitation in cold EtOAc. **<sup>1</sup>H NMR (D<sub>2</sub>O, 400 MHz):**  $\delta$  0.94 (d,  $J = 5.9$  Hz, 3H); 0.98 (d,  $J = 5.9$  Hz, 3H); 1.31 (t,  $J = 7.1$  Hz, 3H); 1.53 (m, 2H); 1.71 (m, 1H); 1.74 (m, 2H); 1.76 (m, 2H); 1.97 (m, 2H); 3.06 (t,  $J = 7.6$  Hz, 2H); 4.06 (t,  $J = 5.9$  Hz, 1H); 4.26 (q,  $J = 7.0$  Hz, 2H); 4.49 (t,  $J = 7.0$  Hz, 1H). **<sup>13</sup>C NMR (D<sub>2</sub>O, 100 MHz):**  $\delta$  13.8, 20.8, 20.9, 22.4, 24.8, 26.1, 30.1, 39.7, 51.6, 53.3, 61.7, 168.4, 172.6. **FTIR (neat, cm<sup>-1</sup>):** 1709, 1682, 1555, 1470, 1294, 1255.



**Labeled  $\alpha\text{-Chymotrypsin}^{\text{RHO}}$**  was obtained by coupling  $\alpha\text{-Chymotrypsin}$  (10 mg) dissolved in 5mL of  $\text{Na}_2\text{CO}_3$  (0.1M; pH = 8.5) with Rhodamine B isocyanate (1mg) solubilized in 0.5mL of DMSO. The mixture was stirred overnight at  $4^\circ\text{C}$  and protected from light. Rhodamine B isocyanate excess was removed by dialysis (Zellultrans Roth, Co., MW 3500) against  $\text{NaCl}$ (aq) (0.5M) solution and milliQ water. Dialysis was realized at  $4^\circ\text{C}$  and kept away from light to avoid Rhodamine B bleaching. The dialysate was dried-freeze to give  $\alpha\text{-Chymotrypsin}^{\text{RHO}}$  as a pink powder.

### 3.5.1.2 Multilayer film preparation and hydrogel self-assembly

The preparation of the enzymatic precursor film and the hydrogel self-assembly was identical for all type of surfaces used in the different experimental techniques of characterization: quartz crystal for QCM-D, ZnSe crystal for IR-ATR and glass slide for fluorescence spectroscopy, cryo-SEM and ETEM and 300 mesh carbon-coated formvar-covered for TEM. All the solutions used to build the enzymatic precursor films were prepared in sodium acetate buffer (10 mM, pH = 6.0) and all hydrogelation experiments were realized in phosphate buffer (186 mM, pH = 8.7), *i.e.* *KLOEt* solutions were prepared in phosphate buffer. The enzymatic precursor films were obtained by dipping process: a first adsorption of a PEI layer ( $1 \text{ mg.mL}^{-1}$ ) for 5 min, followed by sodium acetate buffer rinsing step (5 min) with and the adsorption of TA layer ( $1.125 \text{ mg.mL}^{-1}$ ) for 5 min, followed sodium acetate buffer rinsing step (5 min). Then, protein solution, *i.e.*  $\alpha\text{-chymotrypsin}$  ( $0.2 \text{ mg.mL}^{-1}$ ), BSA ( $0.53 \text{ mg.mL}^{-1}$ ) or ( $\alpha\text{-chymotrypsin}(r)\text{-BSA}(100-r)$ ) mixture solution with  $r$  the molar ratio of  $\alpha\text{-chymotrypsin}$ , were adsorbed for 5 min on PEI/TA film followed by a rinsing step sodium acetate buffer. A second rinsing step (5 min) was performed with phosphate buffer (186 mM, pH = 8.7) before the contact with *KLOEt* ( $1 \text{ mg.mL}^{-1}$ ) solution. In the case of infrared spectroscopy, all solutions used were prepared with  $\text{D}_2\text{O}$  instead of water.

### **3.5.1.3 Fluorescence Microscopy**

All fluorescence intensities were measured by using Nikon Eclipse Ti-S with a 10× PL Fluor (0.30 NA) objective equipped with Nikon Digital Camera (with NIS-Elements software). Excitations of Rhodamine labelled  $\alpha$ -chymotrypsin were set between 542-582 nm and emission wavelengths was measured between 604-644 nm. The images were processed with ImageJ.

### **3.5.1.4 Circular Dichroism (CD)**

Circular dichroism spectra were recorded using a Jasco J-810 spectropolarimeter with a data pitch of 1 nm on the light wavelength. CD spectra are obtained by shining the polarized light beam perpendicularly through a silicone sheet covered by the PEI/Tannic Acid/ $\alpha$ -Chymotrypsin precursor film, immersed in a KLOEt solution for 12h. The CD spectra show the ellipticity expressed as an angle as a function of the wavelength.

### **3.5.1.5 Matrix-Assisted Laser Desorption/Ionization Time-of-Flight (MALDI-TOF)**

Mass measurements were carried out on an Autoflex<sup>TM</sup> MALDI-TOF mass spectrometer (Bruker Daltonics GmbH, Bremen, Germany). This instrument was used at a maximum accelerating potential of 20 kV in positive mode and was operated in mode reflector at 19 kV. The delay extraction was fixed at 110 ns and the frequency of the laser (nitrogen 337 nm) was set at 5 Hz. The acquisition mass range was set to 500-5000 m/z with a matrix suppression deflection (cut off) set to 500 m/z. The equipment was first externally calibrated with a standard peptide calibration mixture that contained 7 peptides (Bruker Peptide Calibration Standard #206196, Bruker Daltonics GmbH, Bremen, Germany) covering the 1000-3200 m/z range. Each raw spectrum was opened with flexAnalysis 2.4 build 11 (Bruker Daltonics GmbH, Bremen, Germany) software and processed using the following parameters: signal-to-noise threshold of 1, Savitzky-Golay algorithm for smoothing, median algorithm for baseline subtraction, and SNAP algorithm for monoisotopic peak detection and labelling. In all cases, resolution was higher than 9000.

The analyzed (KL)<sub>n</sub>OEt hydrogel, was grown for 12 h on a PEI/TA/ $\alpha$ -chymotrypsin film. The hydrogel sample was collected directly on the surface with a pipette to be dried via the droplet method. Mixture of 0.5  $\mu$ l of sample with 0.5  $\mu$ l of matrix solution dry at room temperature. The

first matrix solution was prepared from a saturated solution of  $\alpha$ -cyano-4-hydroxycinnamic acid in water/acetonitrile 50/50 diluted three times in water/acetonitrile/trifluoroacetic acid: 50/49.9/0.1

### 3.5.1.6 Cryo-Scanning Electron Microscopy (*cryo*-SEM)

To observe cross-sectioned gels, a specific cryo-holder was designed and manufactured by mechanical facility of Charles Sadron Institute (see the image below). The glass slide, covered by the enzymatic precursor film and the self-assembled gel, was inserted in the jaws of the vise. As by design the center of the holder is invariable (the two jaws can be displaced by screws and springs), the sample was in the optical axis of the SEM after introduction in the microscope (Hitachi SU 8010 FEG SEM) and was observed at 1 kV and at  $-170^{\circ}\text{C}$ .



*Specific home-made cryo-holder*

The holder with the sample is then rapidly plunged in a nitrogen slush in the cryo preparation chamber of the Quorum PT 3010 machine. As the sample is free standing over the holder, during the plunging, the sample is rapidly frozen by direct contact with the nitrogen slush. The sample is then transferred into the chamber attached to the microscope and fractured with the razor blade. A slight etching at  $-80^{\circ}\text{C}$  is performed to render the fibers more visible. Finally a layer of Pt is deposited.

### 3.5.1.7 Wet Scanning Transmission Electron Microscopy (Wet STEM)

We realized direct bilk observations, by Wet Scanning Transmission Electron Microscopy (Wet STEM), of the suspension dispersed in a thin film on a 300 mesh carbon-coated formvar-covered Transmission Electron Microscopy (TEM) grid as support. A solid-state STEM detector allows detection of electrons transmitted through of the specimen in the native state.

Contrast is due to the relatively low accelerating voltage of the electrons compared to TEM. Samples were cooled at 5°C and imaged, with a Quanta 250 FEG environmental Scanning electron microscope (FEI, Eindhoven, The Netherlands), at 30 kV, a relative humidity of about 70 % and at a specimen chamber pressure of 600 Pa.

### 3.5.3 Supporting figures

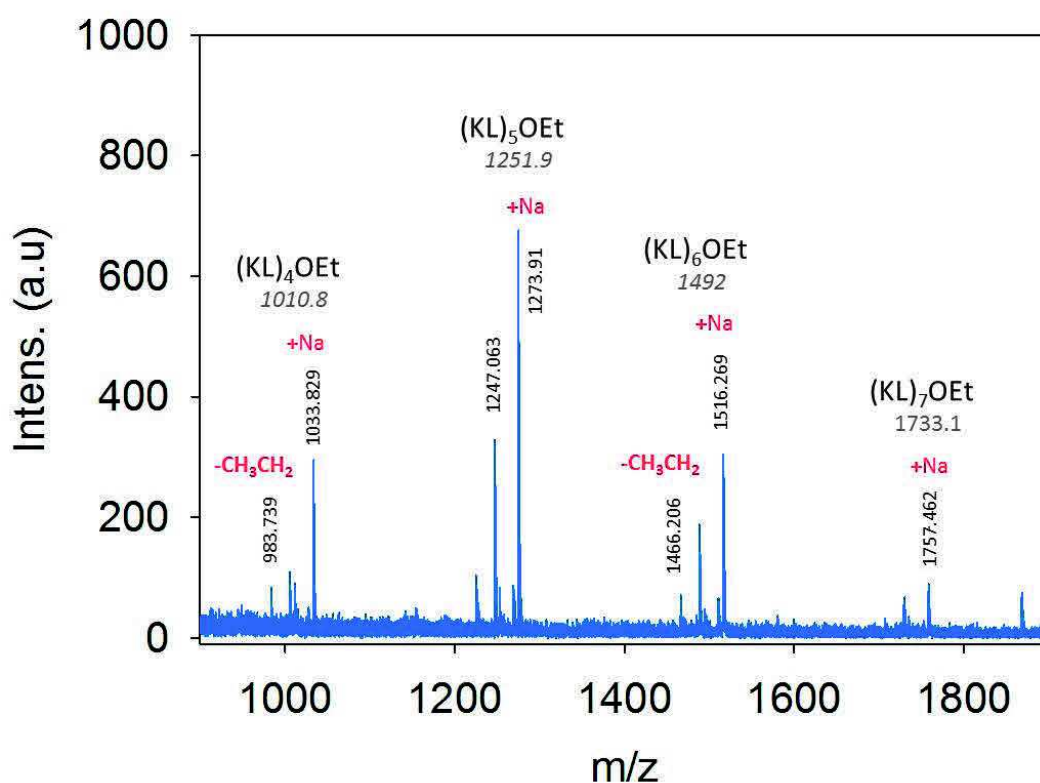


**Figure S3.1:** MALDI-TOF spectra of  $(KL)_xOEt$  hydrogel grown on PEI/TA/ $\alpha$ -chymotrypsin precursor film. A KLOEt solution ( $1\text{mg}\cdot\text{mL}^{-1}$ ) prepared in phosphate buffer (186 mM, pH=8.7) was put in contact with the precursor enzymatic film.

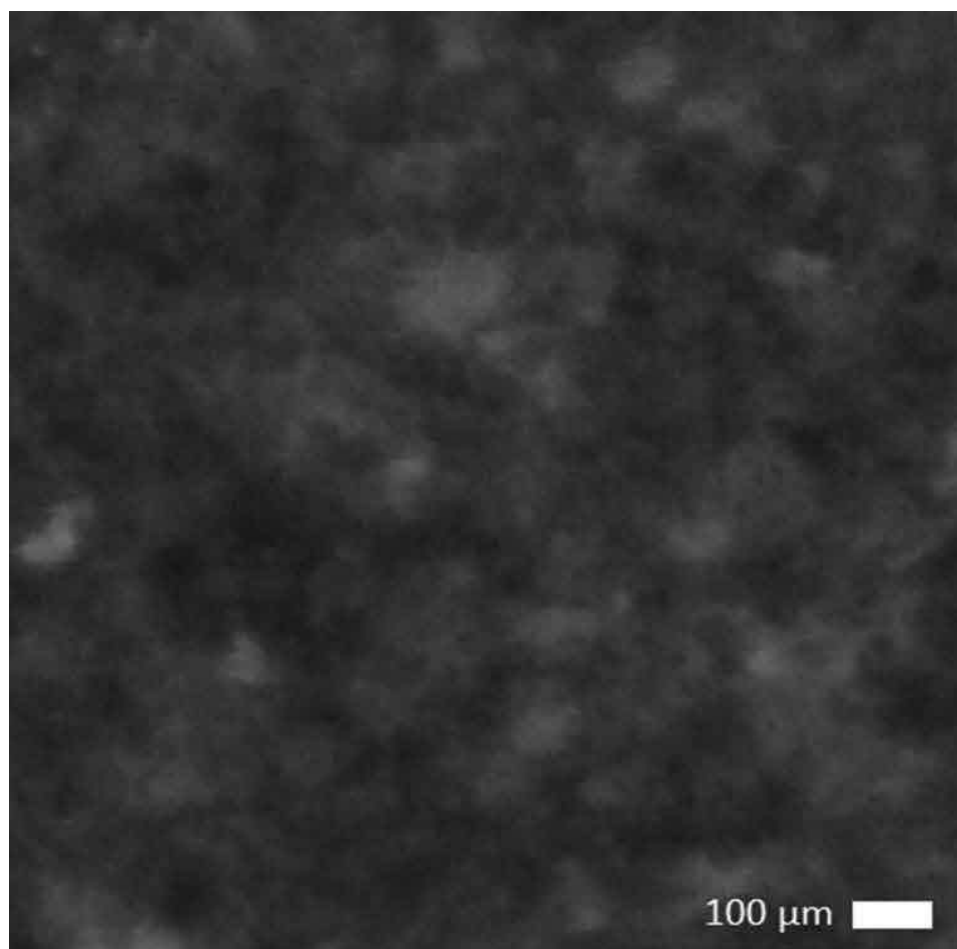


**Figure S3.2:** Environmental Transmission Electron Microscopy (Wet STEM) image of hydrogel built from enzymatic precursor film after 12 h in contact with KLOEt solution ( $1 \text{ mg}\cdot\text{mL}^{-1}$ ). This image has been taken with 66% of humidity and 580 Pa.

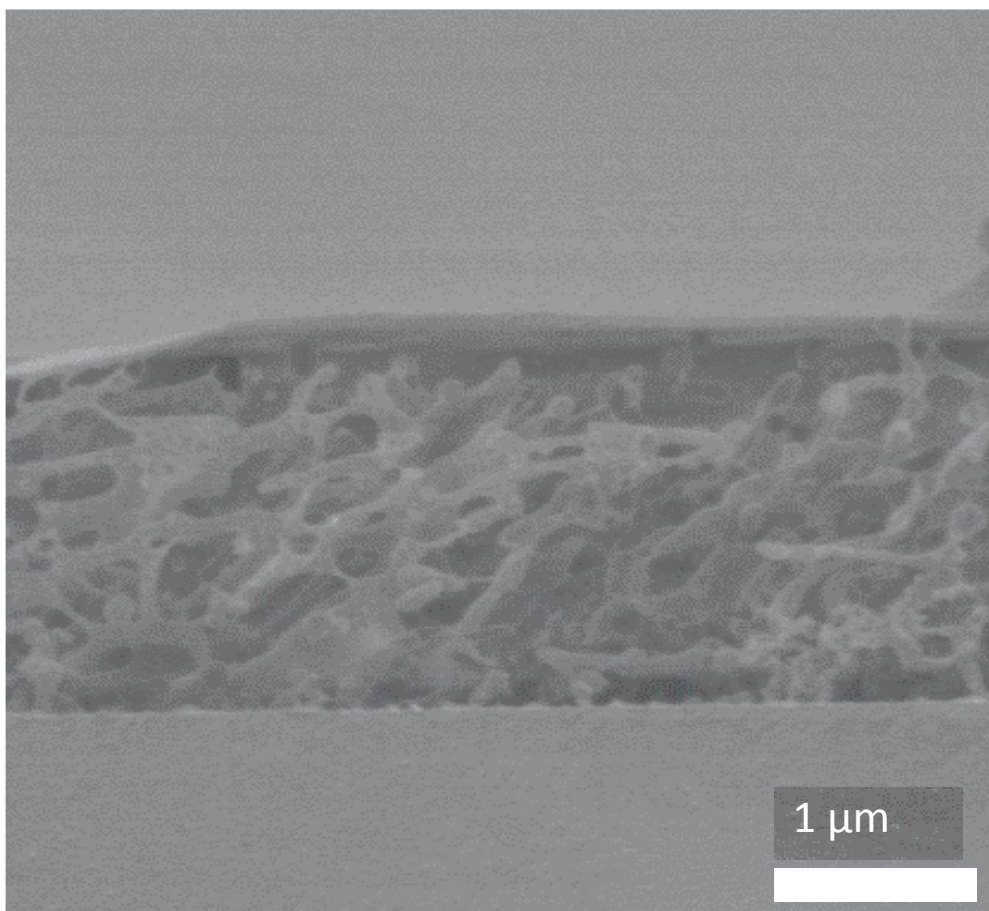


**Figure S3.3:** Cryo-SEM image of a cross sectioned gel showing the  $(KL)_nOEt$  oligopeptide-based hydrogel obtained from the enzymatic precursor film adsorbed on glass when brought in contact with  $KLOEt$  ( $< 1\text{mg.mL}^{-1}$ ) during 12h.

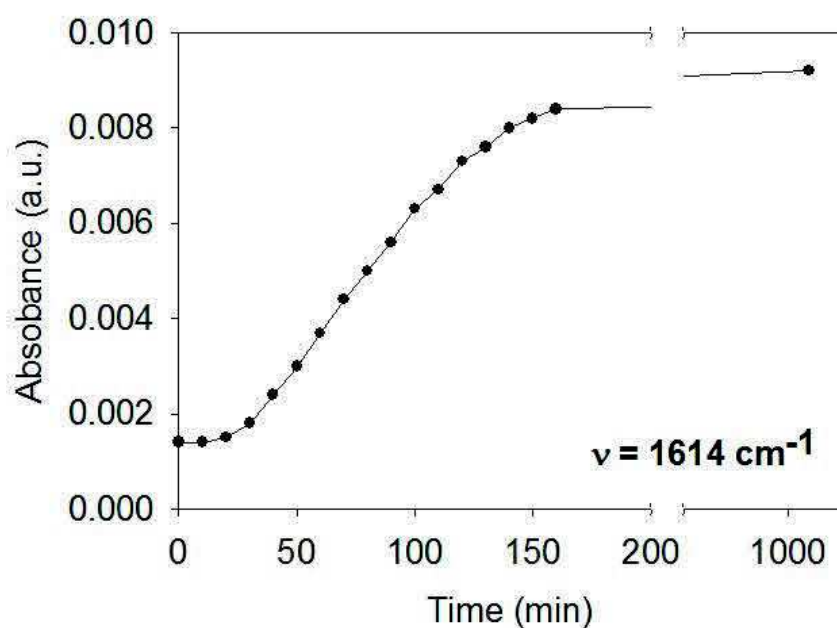


**Figure S3.4:** Evolution of the amide I ( $\nu = 1614 \text{ cm}^{-1}$ ) band intensity as a function of time measured by IR-ATR when the enzymatic precursor film is brought in contact with a KLOEt solution ( $1 \text{ mg.mL}^{-1}$ ).

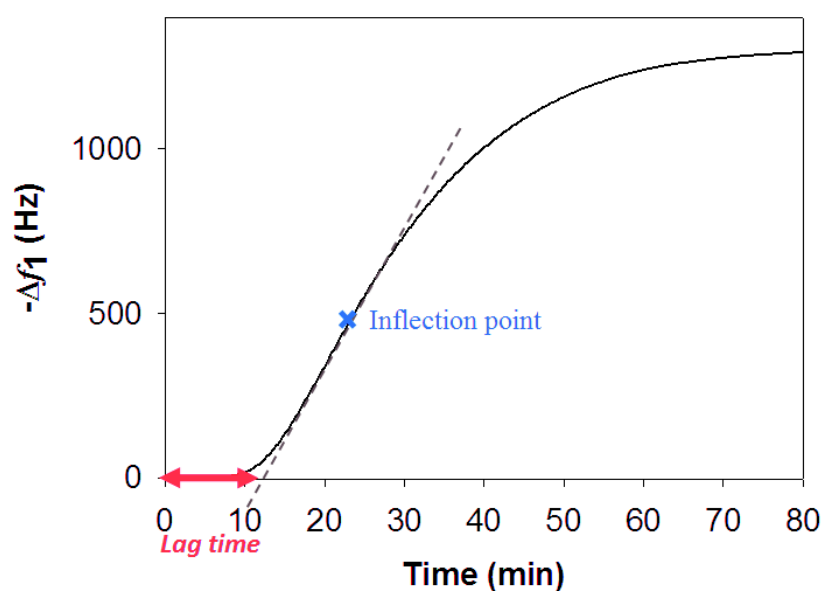


**Figure S3.5:** Schematic representation of the lag time estimation: intersection of time-abscissa with tangent at the inflection point.

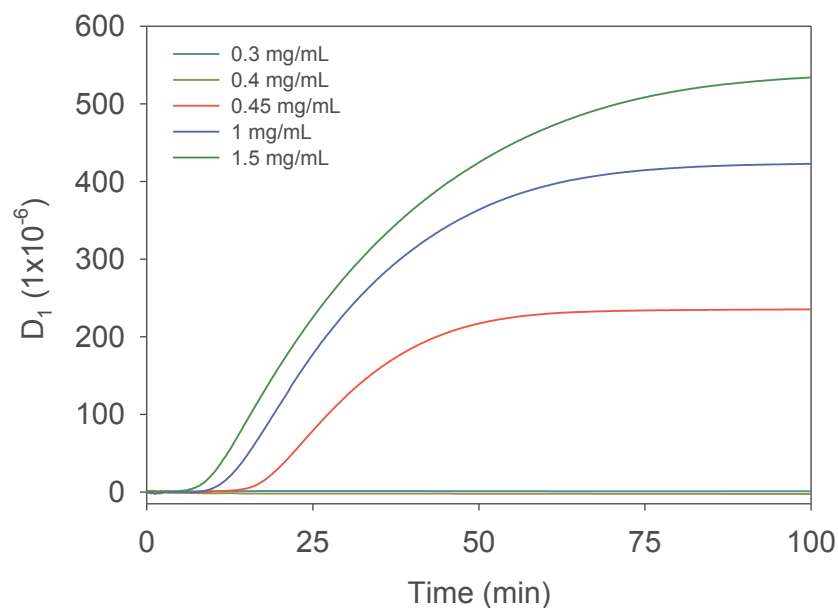


**Figure S3.6:** Evolution of dissipation, measured by QCM-D, as a function of time when different KLOEt concentrations are brought in contact with the enzymatic precursor film.

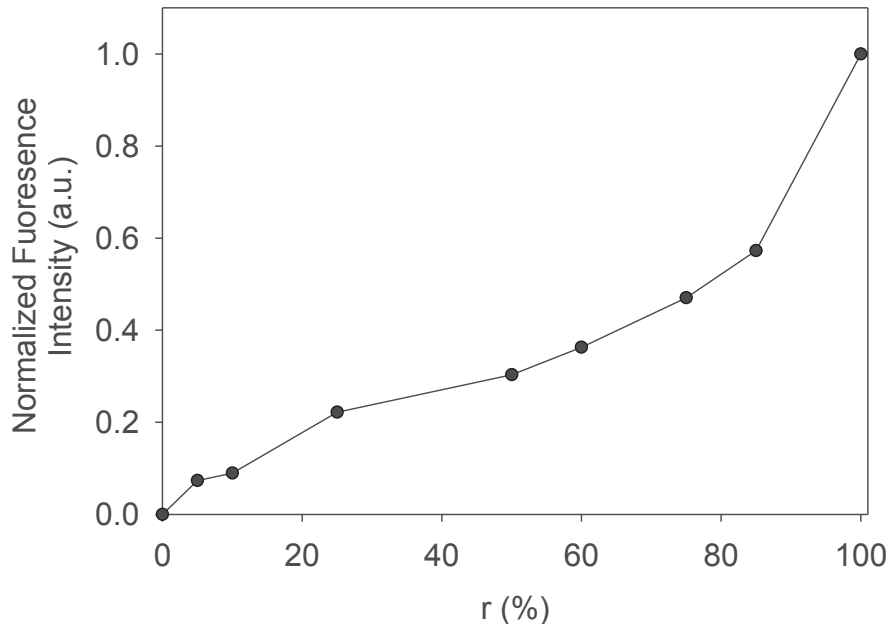


**Figure S3.7:** Evolution of the fluorescence intensity, measured at 572 nm, on PEI/TA coated surface, after the deposition of  $\alpha$ -chymotrypsin<sup>RHO</sup> ( $r$ ) – BSA(100- $r$ ) mixture, prepared at different molar ratio  $r$  in solution.

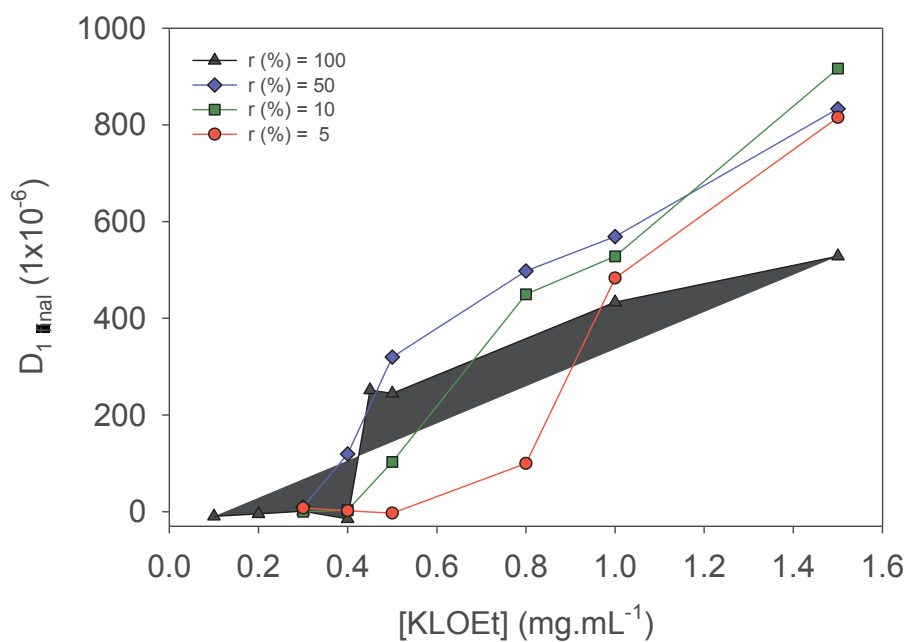


**Figure S3.8:** Evolution of the final value of the dissipation, measured at 5 MHz by QCM-D, as a function of KLOEt concentration after 12 h of contact of KLOEt solutions with PEI/TA/ $(\alpha$ -chymotrypsin( $r$ )–BSA( $1-r$ )) precursor film, with  $r$  the molar ratio in  $\alpha$ -chymotrypsin in the solution deposited to build the precursor film.

## References

1. Barral, J. M.; Epstein, H. F. Protein machines and self assembly in muscle organization. *Bioessays* **1999**, *21* (10), 813.
2. Li, R.; Albertini, D. F. The road to maturation: somatic cell interaction and self-organization of the mammalian oocyte. *Nature Reviews Molecular Cell Biology* **2013**, *14* (3), 141.
3. Olive, A. G. L.; Abdullah, N. H.; Ziemecka, I.; Mendes, E.; Eelkema, R.; van Esch, J. H. Spatial and Directional Control over Self-Assembly Using Catalytic Micropatterned Surfaces. *Angew. Chem.-Int. Edit.* **2014**, *53* (16), 4132.
4. Wong, I. Y.; Footer, M. J.; Melosh, N. A. Electronically activated actin protein polymerization and alignment. *J. Am. Chem. Soc.* **2008**, *130* (25), 7908.
5. Rydzek, G.; Jierry, L.; Parat, A.; Thomann, J. S.; Voegel, J. C.; Senger, B.; Hemmerle, J.; Ponche, A.; Frisch, B.; Schaaf, P.; Boulmedais, F. Electrochemically Triggered Assembly of Films: A One-Pot Morphogen-Driven Buildup. *Angew. Chem.-Int. Edit.* **2011**, *50* (19), 4374.
6. Johnson, E. K.; Adams, D. J.; Cameron, P. J. Directed Self-Assembly of Dipeptides to Form Ultrathin Hydrogel Membranes. *J. Am. Chem. Soc.* **2010**, *132* (14), 5130.
7. Kuang, Y.; Shi, J. F.; Li, J.; Yuan, D.; Alberti, K. A.; Xu, Q. B.; Xu, B. Pericellular Hydrogel/Nanonets Inhibit Cancer Cells. *Angew. Chem.-Int. Edit.* **2014**, *53* (31), 8104.
8. Williams, R. J.; Smith, A. M.; Collins, R.; Hodson, N.; Das, A. K.; Ulijn, R. V. Enzyme-assisted self-assembly under thermodynamic control. *Nat. Nanotechnol.* **2009**, *4* (1), 19.
9. Yang, Z. M.; Gu, H. W.; Fu, D. G.; Gao, P.; Lam, J. K.; Xu, B. Enzymatic formation of supramolecular hydrogels. *Adv. Mater.* **2004**, *16* (16), 1440.
10. Toledano, S.; Williams, R. J.; Jayawarna, V.; Ulijn, R. V. Enzyme-triggered self-assembly of peptide hydrogels via reversed hydrolysis. *J. Am. Chem. Soc.* **2006**, *128* (4), 1070.
11. Hirst, A. R.; Roy, S.; Arora, M.; Das, A. K.; Hodson, N.; Murray, P.; Marshall, S.; Javid, N.; Sefcik, J.; Boekhoven, J.; van Esch, J. H.; Santabarbara, S.; Hunt, N. T.; Ulijn, R. V. Biocatalytic induction of supramolecular order. *Nat. Chem.* **2010**, *2* (12), 1089.
12. Johnson, E. K.; Chen, L.; Kubiak, P. S.; McDonald, S. F.; Adams, D. J.; Cameron, P. J. Surface nucleated growth of dipeptide fibres. *Chemical Communications* **2013**, *49* (77), 8698.
13. Qin, X.; Xie, W. C.; Tian, S.; Cai, J. L.; Yuan, H.; Yu, Z.; Butterfoss, G. L.; Khuong, A. C.; Gross, R. A. Enzyme-triggered hydrogelation via self-assembly of alternating peptides. *Chem. Commun.* **2013**, *49* (42), 4839.

14. Ui, N. Isoelectric points and conformation of proteins. II. Isoelectric focusing of alpha-chymotrypsin and its inactive derivative. *Biochim Biophys Acta* **1971**, 229 (3), 582.
15. Lomova, M. V.; Brichkina, A. I.; Kiryukhin, M. V.; Vasina, E. N.; Pavlov, A. M.; Gorin, D. A.; Sukhorukov, G. B.; Antipina, M. N. Multilayer Capsules of Bovine Serum Albumin and Tannic Acid for Controlled Release by Enzymatic Degradation. *ACS Applied Materials & Interfaces* **2015**, 7 (22), 11732.
16. Sauerbrey, G. Verwendung von Schwingquartzen zur Wägung dünner Schichten und zur Mikrowägung. *Z. Phys.* **1959**, 155, 206.
17. Guiffo-Soh, G.; Hernández, B.; Coïc, Y.-M.; Boukhalfa-Heniche, F.-Z.; Fadda, G.; Ghomi, M. Vibrational Analysis of Amino Acids and Short Peptides in Hydrated Media. 3. Successive KL Repeats Induce Highly Stable  $\beta$ -Strands Capable of Forming Non-H-Bonded Aggregates. *The Journal of Physical Chemistry B* **2008**, 112 (4), 1282.
18. Kong, J.; Yu, S. Fourier Transform Infrared Spectroscopic Analysis of Protein Secondary Structures. *Acta Biochimica et Biophysica Sinica* **2007**, 39 (8), 549.
19. Hernández, B.; Boukhalfa-Heniche, F. Z.; Seksek, O.; Coïc, Y.-M.; Ghomi, M. Secondary conformation of short lysine- and leucine-rich peptides assessed by optical spectroscopies: Effect of chain length, concentration, solvent, and time. *Biopolymers* **2006**, 81 (1), 8.
20. Arosio, P.; Knowles, T. P. J.; Linse, S. On the lag phase in amyloid fibril formation. *Physical Chemistry Chemical Physics* **2015**, 17 (12), 7606.

Chapter 4:  
Bioactive seed layer for surface confined  
self-assembly of peptides

---

---

## Chapter 4: Bioactive Seed layer for Surface Confined Self- Assembly of Peptides

---

### Summary

<b>4.1 Abstract</b> .....	<b>105</b>
<b>4.2 Introduction</b> .....	<b>106</b>
<b>4.3 Results and discussion</b> .....	<b>107</b>
<b>4.4 Conclusion</b> .....	<b>112</b>
<b>4.5 Supporting information</b> .....	<b>113</b>
4.5.1 Materials and methods.....	113
4.5.1.1 List of chemicals .....	113
4.5.1.2 Peptides characterization and preparation of modified PAA-CGGG-Fmoc and PAA-CFF-Fmoc	114
4.5.1.3 Preparation of modified PAA: PAA-CFF-Fmoc and PAA-CGGG-Fmoc .....	116
4.5.1.4 Multilayer film preparation and hydrogel self-assembly.....	120
4.5.1.5 Fluorescence spectroscopy.....	120
4.5.2 Preliminary tests of gelation in vials .....	121
4.5.3 Influence of the decrease of ALP density on the hydrogel formation .....	122
4.5.4 Supporting figures .....	123
<b>References</b> .....	<b>127</b>

## 4.1 Abstract

The design and control of molecular systems that self-assemble spontaneously and exclusively at or near an interface represents a real scientific challenge. We present here a new concept, an *active seed-layer* that allows overcoming this challenge. It is based on *enzyme-assisted self-assembly*. An enzyme, alkaline phosphatase, which transforms an original peptide, Fmoc-FFY( $\text{PO}_4^{2-}$ ), into an efficient gelation agent by dephosphorylation, is embedded in a polyelectrolyte multilayer and constitutes the "reaction motor". A *seed-layer* composed of a polyelectrolyte covalently modified by anchoring hydrogelator peptides constitutes the top of the multilayer. This layer plays the role of nucleation site for the Fmoc-FFY peptide self-assembly. When such a film is brought in contact with a Fmoc-FFY( $\text{PO}_4^{2-}$ ) solution, a nanofiber network starts to form almost instantaneously which extends up to several micrometers into the solution after several hours. We demonstrate that the *active seed-layer* allows convenient control over the self-assembly kinetics and the geometric features of the fiber network simply by changing its peptide density.

## 4.2 Introduction

Self-assembly has become over the last years one of the most active fields in chemistry and materials science with more than 120000 references responding to this key word on Web of Science. When restricting the research to the two topics "surface-confined" and "self-assembly" only slightly more than 100 references remain and most of them address independently the two topics. This clearly demonstrates that the design of molecular systems that self-assemble spontaneously and exclusively at or near an interface represents a real scientific challenge. The most valuable approach developed so far to address this problem is to use non-self-assembling entities (molecules or macromolecules) that undergo a chemical change at the interface and thereby acquire a self-assembling propensity. Confining this chemical change at the interface can be achieved by using chemical reactions or physical processes catalyzed by molecular entities called *morphogens* (such as protons or metallic cations) that diffuse from the surface towards the solution, creating a concentration gradient, a strategy used by Nature.<sup>1</sup> In synthetic approaches, the generation of these morphogens require the continuous application of an external stimulus such as light<sup>2</sup> or electrochemistry<sup>3-4</sup> to maintain the self-assembly process alive.

In 2004, a new way to initiate gel formation in the bulk was introduced and called *enzyme-assisted self-assembly* (EA-SA).<sup>5</sup> The authors used alkaline phosphatase (ALP) to dephosphorylate a short Fmoc-protected peptide which becomes instantaneously an hydrogelator in the reaction medium due to the decrease of its water solubility. EA-SA was intensively developed by several groups who extended the concept to many more enzyme/peptide systems, getting success in fields such as inhibition of cancer cell lines,<sup>6</sup> intracellular imaging and intratumoral chemotherapy<sup>7</sup> or biocatalysis.<sup>8</sup> In 2009, the group of Ulijn grafted enzymes onto a substrate and observed the formation of localized peptide-based fibers originating from microscopic globules that were identified as enzyme clusters.<sup>9</sup>

Herein, we present the design of a new generation of surface localized EA-SA allowing the control of the hydrogel formation exclusively at and from a surface. The ability of the surface to initiate and to tune its own coating is based on the use of polyelectrolyte multilayer architectures that offer the possibility to design highly organized and enzymatically active nanometer size films.<sup>10-11</sup> Polyelectrolyte multilayers are organized structures obtained by the alternate deposition of polyanions and polycations onto a substrate.<sup>12</sup> They constitute an ideal tool to functionalize surfaces. The general architecture we propose is represented in Figure 4.1.a. It is composed of three main film components: (1) a precursor multilayer deposited on the

substrate, rendering the whole process substrate independent; (2) an enzyme layer deposited onto the precursor layer and (3) a *seed-layer* composed of polyelectrolytes modified by anchoring hydrogelator peptides. When precursor peptides, *i.e.* peptides that do not interact with each other in solution, reach the multilayer, an enzymatic reaction occurs at the film/solution interface,<sup>13</sup> generating effective hydrogelator peptides at the film/solution interface. An increase of the concentration of hydrogelator peptides occurs near the film/solution interface and induces their spontaneous self-assembly initiated from, what can be called, a *bioactive seed-layer*. Gel formation thus starts exclusively from the surface. In this work, we demonstrate the validity of this approach and the control of the formation of a gel on the surface through the presence of the *active seed-layer*

### 4.3 Results and discussion

Inspired by hydrogelator/enzyme systems introduced by Yang and Ulijn,<sup>14</sup> we designed an original peptide Fmoc-FFY( $\text{PO}_4^{2-}$ ) with a phosphorylated phenol group of the tyrosine at C-terminal position as model to validate our concept (Figure 4.1.b). Alkaline phosphatase (ALP, 150 kDa) was used as catalytically active enzyme inducing the dephosphorylation of Fmoc-FFY( $\text{PO}_4^{2-}$ ) leading to the local production of the hydrogelator Fmoc-FFY.

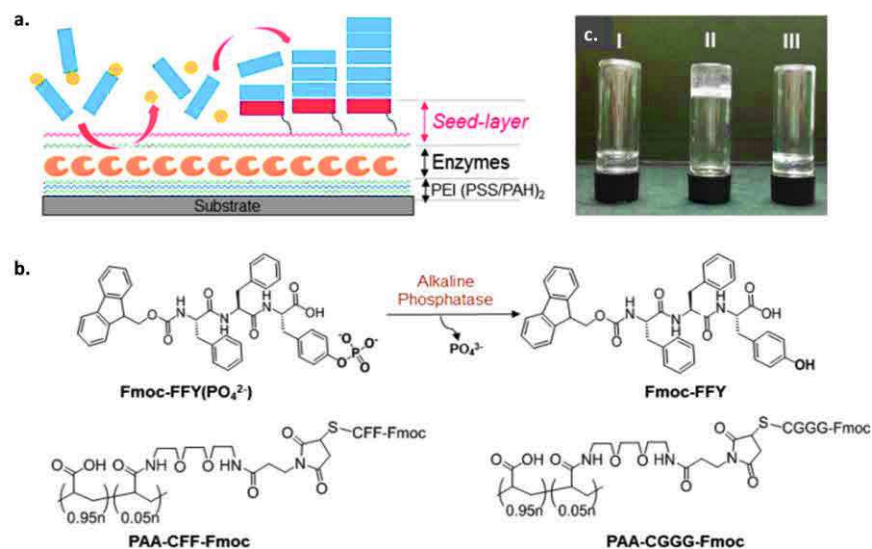


**Figure 4.1:** (a) Schematic representation of the surface localized EA-SA concept; (b) Chemical structures of all peptides and modified polyelectrolytes involved in this work (C = Cysteine, F = Phenylalanine, G = Glycine, Y = Tyrosine, Fmoc = Fluorenylmethyloxycarbonyl group); (c) Gelation tests realized in vials with different solutions: (I) 0.90 mM Fmoc-FFY( $\text{PO}_4^{2-}$ ) and ALP (1 U.mL<sup>-1</sup>); (II) 0.60 mM Fmoc-FFY( $\text{PO}_4^{2-}$ ), PAA-CFF-Fmoc (0.30 mM of “CFF-Fmoc”) and ALP (1 U.mL<sup>-1</sup>); (III) 0.90 mM Fmoc-FFY( $\text{PO}_4^{2-}$ ), PAA and ALP (1 U.mL<sup>-1</sup>). The vials were turned upside down after 15 min.

The *seed-layer* is composed of poly(acrylic acid) chains (PAA,  $M_n = 100$  kDa) modified with the hydrogelator Fmoc-FFC through a short spacer (Figure 4.1.b). The presence of the cysteine at C-terminal position allows clicking the peptide Fmoc-FFC through the thiol-ene reaction onto a maleimide-modified PAA. The grafting ratio of PAA-CFF-Fmoc is around 5% according to  $^1\text{H}$  NMR spectroscopy. Syntheses and characterization of all compounds used in this work are reported in the Supporting Information (see paragraph 4.5.1.2 and 4.5.1.3 in SI). We first verified in solution (*i*) that gelation can be induced by dephosphorylation of Fmoc-FFY( $\text{PO}_4^{2-}$ ) in the presence of ALP, (*ii*) that Fmoc-FFY, generated *in situ*, is an efficient hydrogelator and (*iii*) that PAA-CFF-Fmoc interacts with the peptide Fmoc-FFY, promoting gel formation. All the experiments were performed at  $25^\circ\text{C}$  and at pH 9.5 using a borax buffer solution (see paragraph 4.5.1.4 in SI).

Next we wanted to validate the concept of *seed-layer* acting as a "nucleating agent" and favoring the self-assembly of a gel on the surface. For this purpose we built a PEI-(PSS/PAH)<sub>2</sub>-PAA-CFF-Fmoc film (PEI: poly(ethylene imine); PSS: poly(styrene sulfonate); PAH: poly(allylamine hydrochloride)) that was brought in contact with a mixture solution containing Fmoc-FFY( $\text{PO}_4^{2-}$ ) at 0.90 mM and ALP at  $0.33 \text{ mg}\cdot\text{mL}^{-1}$  (or  $1 \text{ U}\cdot\text{mL}^{-1}$ ). The process taking place at the interface was followed *in situ* by Quartz Crystal Microbalance (QCM) by monitoring the evolution of the opposite of the fundamental resonance frequency shift  $-\Delta f_1$  and the corresponding dissipation  $D_1$ . Whereas no gel is observed in solution in these conditions (Figure 4.1.c), a strong increase of  $-\Delta f_1$  is observed at the injection of (Fmoc-FFY( $\text{PO}_4^{2-}$ ), ALP) mixture up to a value of 1200 Hz after 8 min of buildup (Figure S4.2). In the same time, an important increase of the dissipation  $D_1$  is measured, up to a high value of  $900 \times 10^{-6}$ . This indicates the formation of a thick viscoelastic gel on top of the multilayer. As a control experiment, the PAA-CFF-Fmoc *seed-layer* was replaced by a modified PAA grafted with 5% of Fmoc-GGGC, a sequence recently described as an ideal non-gelating peptide (we also verified this result in solution (Figure S4.2)).<sup>15</sup> When the Fmoc-FFY( $\text{PO}_4^{2-}$ ) and ALP mixture was brought in contact with a PAA-CGGG-Fmoc ended multilayer, only a small increase of the QCM signals were observed ( $-\Delta f_1$  increases by 20 Hz and  $D_1$  by  $180 \times 10^{-6}$ , Figure S4.2). When a PAA-CFF-Fmoc ended multilayer film was brought in contact with ALP in the absence of Fmoc-FFY( $\text{PO}_4^{2-}$ ), almost no variations of  $-\Delta f_1$  and  $D_1$  were observed by QCM (Figure S4.3). These results prove that the layer of PAA-CFF-Fmoc deposited on the multilayer serves indeed as an effective *seed-layer*. In this configuration, the gel buildup is initiated at the surface of the multilayer but the reaction takes place all over the solution that contains ALP.

Let us now go one step further and see if one can create a *bioactive seed-layer* by incorporating the "reaction motor", *i.e.* ALP, in the multilayer instead of having it in the solution.

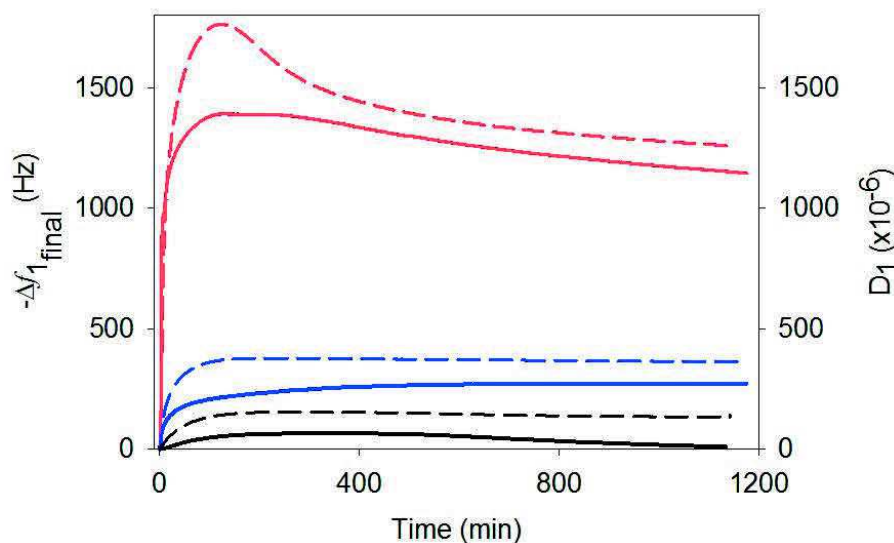


**Figure 4.2:** Comparison of the evolution of the opposite of the fundamental frequency shift (full curve) and dissipation (dashed curve), measured at 5 MHz by QCM-D, as function of time when 0.90 mM Fmoc-FFY( $\text{PO}_4^{2-}$ ) solution is brought in contact with the multilayers PEI-(PSS/PAH)<sub>2</sub>-ALP-(PAH/PAA-CFF-Fmoc) (red), PEI-(PSS/PAH)<sub>2</sub>-ALP (blue) and (PEI-(PSS/PAH)<sub>2</sub>-ALP-(PAH/PAA-CGGG-Fmoc) (black);

For this purpose, we built the multilayer architecture PEI-(PSS/PAH)<sub>2</sub>-ALP-(PAH/PAA-CFF-Fmoc), represented in Figure 4.1.a and followed its buildup by QCM (Figure S4.4). The calculated thickness of this film is about 53 nm according to Sauerbrey's relation.<sup>16</sup> When this film was brought in contact with 0.90 mM of Fmoc-FFY( $\text{PO}_4^{2-}$ ) solution, an increase of  $-\Delta f_1$  and  $D_1$  occurred within 10 min after the injection of Fmoc-FFY( $\text{PO}_4^{2-}$ ) and reached respectively 1400 Hz and  $1200 \times 10^{-6}$  after 12h (Figure 4.2). This indicates the buildup of a gel at the interface. These values are even larger than those observed when ALP was in solution (Figure S4.2 in SI). When a Fmoc-FFY( $\text{PO}_4^{2-}$ ) solution (0.90 mM) was brought in contact with a film containing ALP and ending by PAA-CGGG-Fmoc, only a small increase of  $-\Delta f_1$  (10 Hz) and of  $D_1$  ( $135 \times 10^{-6}$ ) took place (Figure 4.2). We verified, using *para*-nitrophenol phosphate as chromogenic enzyme substrate, that when PAA-CFF-Fmoc is replaced by PAA-CGGG-Fmoc the enzymatic activity of the film does not change (Figure S4.5). In order to get an idea about the synergy between the presence of the *enzyme layer* and the *seed-layer* we performed also an experiment with the multilayer PEI-(PSS/PAH)<sub>2</sub>-ALP ending with a bare enzyme layer. When bringing this film in contact with a Fmoc-FFY( $\text{PO}_4^{2-}$ ) solution at 1 mg/mL one observes an

increase of  $-\Delta f_1$  of 271 Hz. This shows that a "bare" enzyme layer allows getting a gel at the interface as first shown by Ulijn et al<sup>9</sup> yet with a lesser efficacy. But the major drawback of the bare enzyme layer is the absence of possibility to tune and control the activity of this layer.

The gel buildup with a PAA-CFF-Fmoc *seed-layer* was also followed by Fourier transform infrared spectroscopy in attenuated total reflection mode in deuterated water. After the injection of Fmoc-FFY( $\text{PO}_4^{2-}$ ), the intensity of the vibration bands at 1630  $\text{cm}^{-1}$  and 1688  $\text{cm}^{-1}$  increase and then level off after 60 min (Figure S4.6 in SI). The band at 1630  $\text{cm}^{-1}$  correspond to the carbonyl groups of the amide I involved in  $\beta$ -sheet assemblies<sup>17 18</sup> and the band at 1688  $\text{cm}^{-1}$  can be assigned to carbamates present in the antiparallel  $\beta$ -sheets composed of Fmoc-FFY self-assembly<sup>19-20</sup>. A fluorescence spectroscopy study during the self-assembly of the gel shows the presence of Fmoc group excimer at 331 nm, in accordance with the  $\beta$ -sheet assembly characteristic of peptide-based hydrogel (Figure S4.7 in SI).<sup>18</sup>

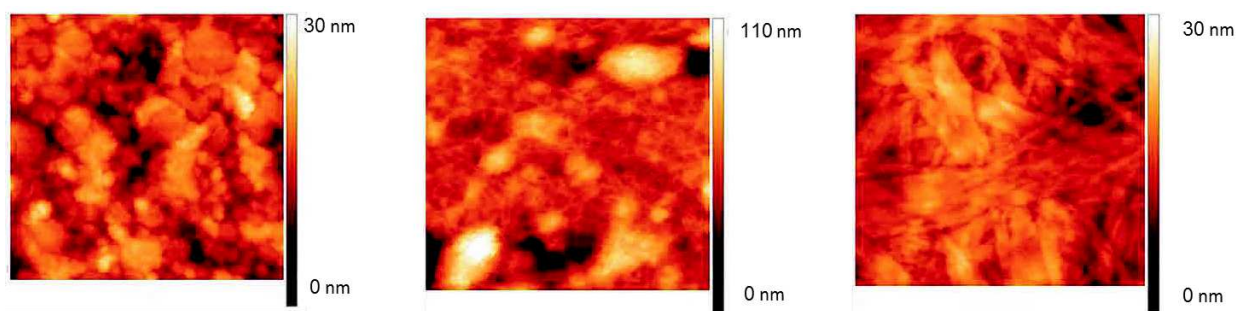


**Figure 4.3:** Typical AFM images ( $1 \times 1 \mu\text{m}^2$ ), obtained in contact mode and dry state, of gel obtained after 5 min (z-scale = 76 nm), 120 min (z-scale = 40 nm) and 12 h (z-scale = 15 nm) of contact with Fmoc-FFY( $\text{PO}_4^{2-}$ ) solution.

Using Atomic Force Microscopy (AFM) in dry state, we imaged the obtained gel after 2, 4, 20, 120 min and 12 h of contact of Fmoc-FFY( $\text{PO}_4^{2-}$ ) solution with PEI-(PSS/PAH)<sub>2</sub>-ALP-(PAH/PAA-CFF-Fmoc) film (Figure 4.3 and Figure S4.8). After 4 and 20 min, nanofibers appear over the whole coated substrate with entanglements and local bundles. After 120 min and 12 h, the nanofibrous structure appears as growing flat ribbons with a diameter of about 100 nm. Less than 4 min are necessary to the surface nucleation process to form fibers and the internal architecture of the gel changes overtime despite the fact that the QCM signals level off after 20 min.

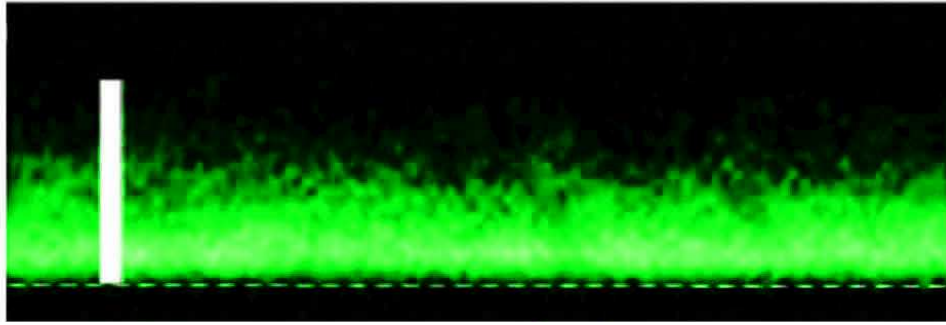


**Figure 4.4:** Confocal microscopy cross-section image of the gel self-assembled from Fmoc-FFY( $\text{PO}_4^{2-}$ ) on PAA-CFF-Fmoc seed-layer ended film in the presence of  $\text{BSA}^{\text{FITC}}$ . The dashed line represents the substrate and the scale bar represents  $5 \mu\text{m}$ .

Confocal microscopy was used to determine the thickness of the gel after 12 h. PEI-(PSS/PAH)<sub>2</sub>-ALP-(PAH/PAA-CFF-Fmoc) was spin-coated step-by-step on a glass substrate and then brought in contact for 12 h with a mixture of Fmoc-FFY( $\text{PO}_4^{2-}$ ) and fluorescein-labeled albumin ( $\text{BSA}^{\text{FITC}}$ ).  $\text{BSA}^{\text{FITC}}$  was used for visualization purposes to be trapped in the gel during its growth. A gradient of fluorescence extending over several micrometers appears from the surface, suggesting a gradient of  $\text{BSA}^{\text{FITC}}$  and thus also of fiber density extending from the multilayer to the solution (Figure 4.4).

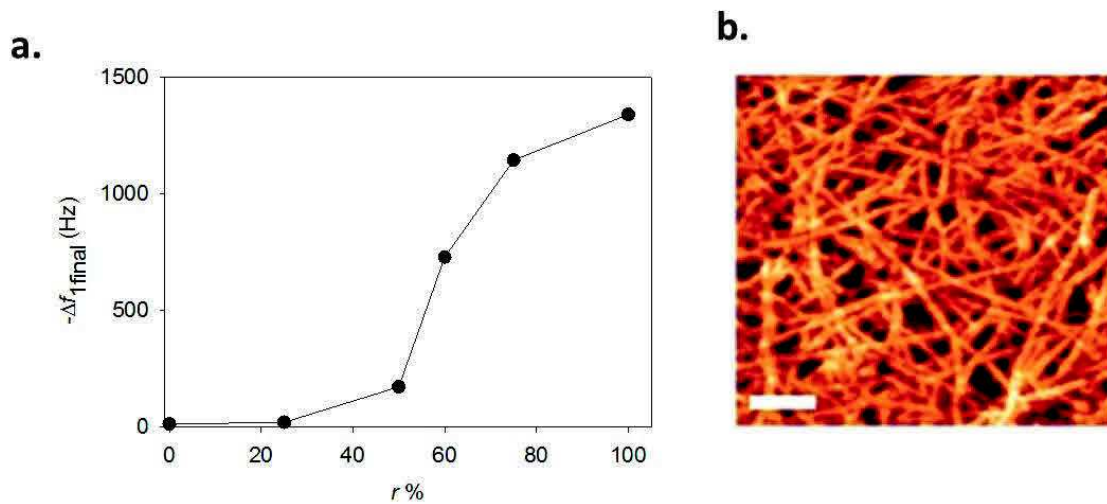


**Figure 4.5:** (a) Evolution the opposite of the fundamental frequency shift, measured at 5 MHz by QCM-D after 12 h of contact of PEI-(PSS/PAH)<sub>2</sub>-ALP-(PAH/(PAA-CFF-Fmoc; PAA-CGGG-Fmoc with Fmoc-FFY( $\text{PO}_4^{2-}$ ) solution, as a function of the mass ratio  $r = [\text{PAA-CFF-Fmoc}]/([\text{PAA-CGGG-Fmoc}] + [\text{PAA-CFF-Fmoc}])$  in the buildup solution. (b) Typical AFM image ( $1 \times 1 \mu\text{m}^2$ ) obtained in contact mode and dry state after 12 h of self-assembly of gel from Fmoc-FFY( $\text{PO}_4^{2-}$ ) on multilayer ended with a ratio  $r = 0.75$ . The z scale is 34 nm and the scale bar represent  $0.15 \mu\text{m}$ .

Next, we looked at whether the concept of *active seed-layer* allows precisely controlling the film buildup by modifying the density of “Fmoc-FF” peptide moieties on the surface. This was done by adsorbing the *seed layer* from a solution containing a mixture of PAA-CFF-Fmoc and PAA-CGGG-Fmoc. Thus, the multilayer film PEI-(PSS/PAH)<sub>2</sub>-ALP-(PAH/(PAA-CFF-Fmoc; PAA-CGGG-Fmoc)) was prepared with various mass ratios equal to  $r = 0, 0.25, 0.50, 0.60, 0.75$  and  $1.0$  with  $r = [\text{PAA-CFF-Fmoc}]/([\text{PAA-CGGG-Fmoc}] + [\text{PAA-CFF-Fmoc}])$ . The value of  $-\Delta f_1$  measured after 12 h for each ratio  $r$  is given in Figure 4.5.a By decreasing the proportion of PAA-CFF-Fmoc in the buildup solution of the *seed-layer*, the opposite of the fundamental frequency shift relative to the gel buildup decreases correlatively. With  $r$  values below 1 after 12h, the resulting gels show a less dense network of fibers, without formation of large ribbons (Figure 4.5.b). In addition, by decreasing the density of ALP in the multilayer, one observes correlatively a quasi linear decrease of the kinetic gel buildup when the film is brought in contact with the initiating Fmoc-FFY(PO<sub>4</sub><sup>2-</sup>) solution peptide (see paragraph 4.5.3 in SI).

## 4.4 Conclusion

To sum up, we have introduced the concept of *bioactive seed-layer* that triggers the buildup of a self-assembling peptide fiber network exclusively at the film/solution interface. Furthermore, by using confinement of enzymes through multilayer film design, the self-assembly process is maintained continuously and autonomously “alive” without any intervention of external stimuli. These two features rendering our concept fully original. In addition, the use of a *bioactive seed-layer* allows controlling and tuning both the network kinetics and the fiber morphologies. Currently, the research carried out in the field of self-assembly systems focuses on the development of increasingly complex architectures organized onto a surface, going closer to systems developed by nature. We believe that our bottom-up approach can significantly contribute to the design of sophisticated and smart nanoarchitecture systems.

## 4.5 Supporting information

### 4.5.1 Materials and methods

#### 4.5.1.1 List of chemicals

All chemicals used in this work are gathered in the following table.

Name and Acronyme	Mw (g.mol <sup>-1</sup> )	Supplier	CAS number
Borax Anhydrous	201.22	Fluka	1330-43-4
Sodium Chloride	58.44	VWR Chemicals	7647-14-5
Bovine serum albumine labelled with Fluorescein (BSA <sup>FITC</sup> )	-	Sigma Aldrich	-
Poly(ethylene imine) (PEI)	750 000	Sigma Aldrich	9002-98-6
Poly(acrylic acid) (PAA)	100 000	Sigma Aldrich	9003-01-4
Poly(styrene sulfonate) (PSS)	70 000	Sigma Aldrich	25704-18-1
Poly(allylamine) hydrochloride (PAH)	15 000	Sigma Aldrich	71-550-12
Alkaline Phosphatase (ALP)	-	TCI europe	9001-78-9
Deuterated Water (D <sub>2</sub> O)	20.03	Sigma Aldrich	7789-20-0
$\beta$ -alanine, 98%	89.09	Alfa Aesar	107-95-9
Maleic anhydride	98.06	Alfa Aesar	108-31-6
Dimethylformamide (DMF)	73.09	Acros Organics	68-12-2
<i>N</i> -hydroxysuccinimide (NHS)	115.09	Alfa Aesar	6066-82-6
<i>N,N'</i> -Dicyclohexylcarbodiimide (DCC)	206.33	Alfa Aesar	538-75-0
Dichloromethane (CH <sub>2</sub> Cl <sub>2</sub> )	84.93	Acros Organics	75-09-2
Sodium Hydrogenocarbonate NaHCO <sub>3</sub>	84.01	VWR Chemicals	144-55-8
Magnesium Sulfate MgSO <sub>4</sub>	120.37	VWR Chemicals	7487-88-9
Chloroform CHCl <sub>3</sub>	119.34	Carlo Erba	67-66-3
<i>n</i> -Hexane	86.18	Carlo Erba	110-54-3

Trifluoroacetic acid (TFA)	114.02	Alfa Aesar	76-05-1
Deuterated DMSO (DMSO-d <sub>6</sub> )	84.17	SDS	2206-27-1
N (3-Dimethylaminopropyl)-N'-ethylcarbodiimide hydrochloride (EDC.HCl)	191.70	Iris Biotech	25952-53-8
Fmoc-FFY(PO <sub>4</sub> <sup>2-</sup> )	777.85	Proteogenix	-
Fmoc-FFC	636.81	Proteogenix	-
Fmoc-GGGC	514.61	Proteogenix	-
Deuterated Chloroform (CDCl <sub>3</sub> )	120.384	Sigma Aldrich	865-49-6
MES Free Acid Monohydrate	191.24	Fisher Scientific	4432-31-9
4-nitrophenyl phosphate disodium salt hexahydrate, 98 %	371.15	Alfa Aesar	4264-83-9
N-Boc-2,2'-(ethylenedioxy)diethylamine	248.32	Sigma Aldrich	153086-78- 3

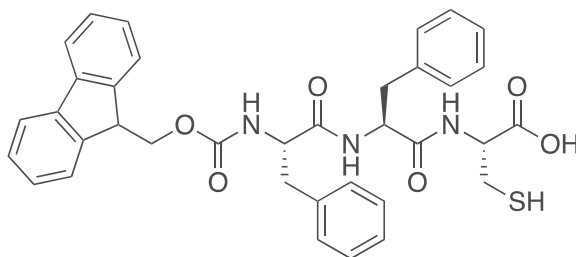
#### 4.5.1.2 Peptides characterization and preparation of modified PAA-CGGG-Fmoc and PAA-CFF-Fmoc

##### General Informations

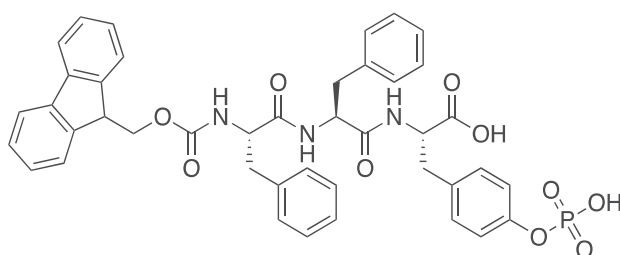
All starting materials were obtained from commercial suppliers and were used without further purification. All dried solvents were purchased from Acros Organics. <sup>1</sup>H NMR and <sup>13</sup>C NMR spectra were recorded on Bruker Advance DPX400 (400 MHz) spectrometers. The NMR chemical shifts are reported in ppm relative to tetramethylsilane (DMSO-*d*<sub>6</sub>, CDCl<sub>3</sub> or MeO-*d*<sub>4</sub>) or *tert*-butanol (1.24 ppm) in D<sub>2</sub>O (s: singlet, t: triplet, q: quadruplet, dd: doublet of doublet, m: multiplet, br: broad). Infrared spectra were obtained on a Vertex 70 spectrometer (Bruker, Germany). The spectra were recorded in the Attenuated Total Reflection (ATR) mode. Merck RP-18 F254S plates were used for analytical thin layer chromatography. Silica gel 60 (particle: 40 – 60 μm) was used for flash chromatography. High-resolution mass spectra (HRMS) were recorded with an MicroTOF-Q (BRÜKER) mass spectrometer at the *Service de Spectrométrie de Masse de la Faculté de Chimie (University of Strasbourg)* and are given in m/z.

##### *Characterization of peptides Fmoc-FFY(PO<sub>4</sub><sup>2-</sup>), Fmoc-FFC and Fmoc-GGGC*

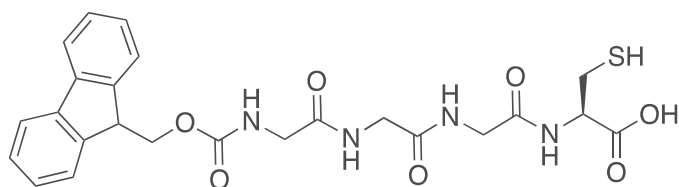
All three peptides Fmoc-FFY(PO<sub>4</sub><sup>2-</sup>), Fmoc-FFC and Fmoc-GGGC were purchased from Proteogenix company with a chemical purity of ≥ 95%. These peptides were further analyzed by <sup>1</sup>H/<sup>13</sup>C NMR, infrared spectroscopy and mass spectroscopy (high resolution).



**Fmoc-FFC.**  $^1\text{H}$  NMR (DMSO-*d*<sub>6</sub>, 400 MHz) :  $\delta$  12.95 (s, 1H), 7.87 (d,  $J$  = 7.7 Hz, 2H), 7.61 (t,  $J$  = 7.7 Hz, 2H), 7.4 (td,  $J$  = 7.2 Hz,  $J$  = 3.1 Hz, 2H), 7.25 (m, 10H), 7.16 (m, 2H), 4.64 (m, 1H), 4.45 (m, 1H), 4.23 (m, 1H), 4.17 (m, 1H), 4.11 (m, 2H), 3.09 (dd,  $J$  = 13.8 Hz,  $J$  = 4.6 Hz, 1H), 2.81 (m, 5H);  $^{13}\text{C}$  NMR (DMSO-*d*<sub>6</sub>, 100 MHz) :  $\delta$  171.4, 171.3, 171.0, 155.7, 143.8, 140.6, 138.1, 137.8, 129.3, 128.0, 127.6, 127.0, 126.3, 125.3, 120.0, 65.6, 56.1, 54.4, 53.7, 46.5, 37.4, 25.6; FTIR (neat,  $\text{cm}^{-1}$ ) 1689, 1642, 1533, 1259, 739, 696; HR ESI MS Calcd for  $\text{C}_{36}\text{H}_{35}\text{N}_3\text{O}_6\text{S}$  [ $\text{M}+\text{Na}^+$ ] : 660.2144 found: 660.2156.

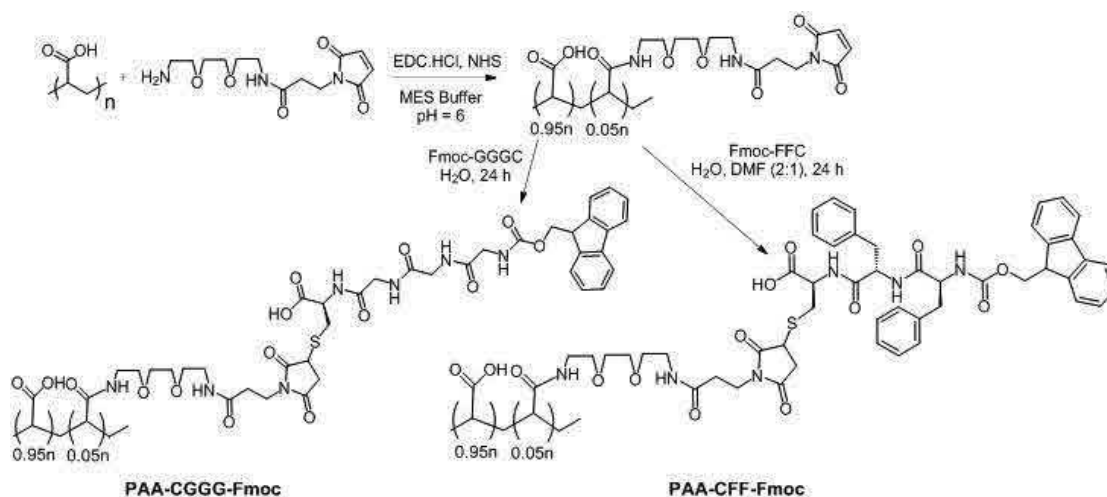


**Fmoc-FFY( $\text{PO}_4^{2-}$ ).**  $^1\text{H}$  NMR (DMSO-*d*<sub>6</sub>, 400 MHz):  $\delta$  7.88 (d,  $J$  = 7.5 Hz, 2H), 7.61 (m,  $J$  = 7.4 Hz), 7.41 (m, 2H), 7.2 (m, 12H), 7.15 (m, 2 H), 7.09 (d,  $J$  = 8.1 Hz, 2H), 4.60 (m, 1H), 4.43 (m, 1H), 4.21 (m, 1H), 4.17 (m, 1H), 4.10 (m, 2H), 3.04 (m, 2H), 2.81 (m, 2H), 2.96 (m, 2H);  $^{13}\text{C}$  NMR (DMSO-*d*<sub>6</sub>, 100 MHz):  $\delta$  172.6, 171.3, 171.2, 155.6, 143.6, 140.6, 137.7, 129.2, 127.9, 127.6, 127.0, 126.1, 125.2, 120.0, 65.6, 56.0, 53.6, 46.5, 37.6, 37.4; FTIR (neat,  $\text{cm}^{-1}$ ): 1692, 1646, 1536, 1508, 1450, 1260, 1223, 1034, 972, 738, 696; HR ESI MS Calcd for  $\text{C}_{42}\text{H}_{40}\text{N}_3\text{O}_{10}\text{P}$  [ $\text{M}+\text{H}^+$ ] : 778.2529 found: 778.2574.

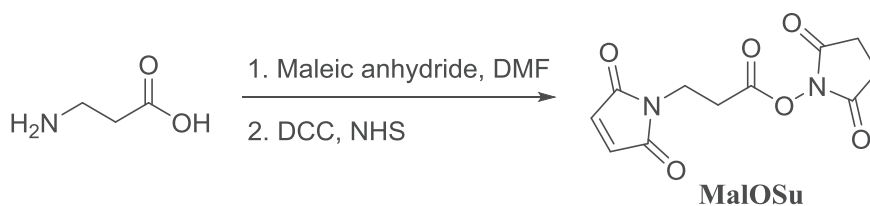


**Fmoc-GGGC.**  $^1\text{H}$  NMR (DMSO- $d_6$ , 400 MHz):  $\delta$  7.9 (d,  $J=7.4$  Hz, 2H), 7.73 (d,  $J=7.4$  Hz, 2H), 7.43 (t,  $J=7.5$  Hz, 2H), 7.34 (t,  $J=7.5$  Hz, 2H), 4.42 (m, 1H), 4.31 (m, 2H), 4.24 (m, 1H), 3.8 (t,  $J=5.0$  Hz), 3.76 (d,  $J=5.4$  Hz, 2H), 3.68 (d,  $J=6.1$  Hz, 2H);  $^{13}\text{C}$  NMR (DMSO- $d_6$ , 100 MHz):  $\delta$  171.4, 169.5, 169.1, 168.8, 156.5, 143.8, 140.7, 127.6, 127.1, 125.2, 120.1, 65.7, 54.3, 46.6, 43.5, 42.0, 41.7, 25.6; FTIR (neat,  $\text{cm}^{-1}$ ) 1657, 1534, 1254, 755, 738; HR ESI MS Calcd for  $\text{C}_{24}\text{H}_{26}\text{N}_4\text{O}_7\text{S}$  [ $\text{M}+\text{Na}^+$ ]: 537.1419 found: 537.1441.

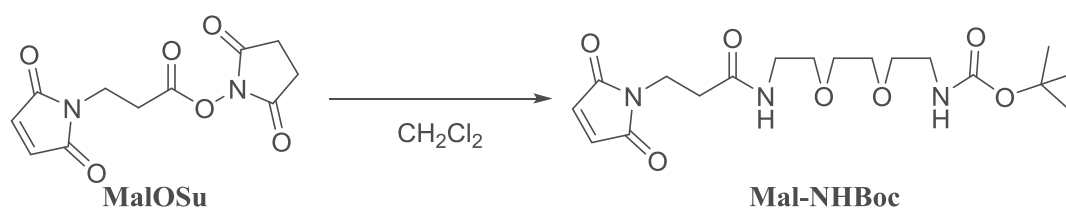
#### 4.5.1.3 Preparation of modified PAA: PAA-CFF-Fmoc and PAA-CGGG-Fmoc



Polyelectrolytes PAA-CGGG-Fmoc and PAA-CFF-Fmoc were prepared according the following synthetic pathway.

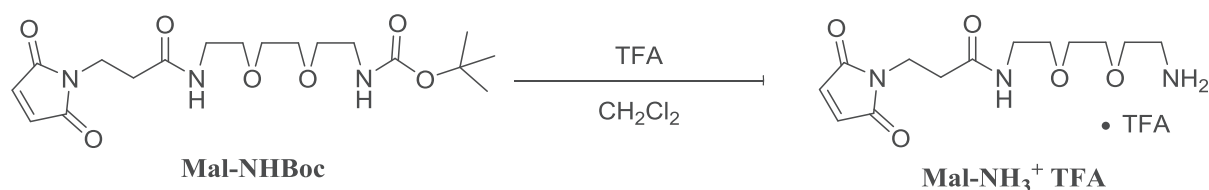


**3-Maleimidopropionic acid *N*-hydroxysuccinimide ester (MalOSu) prepared according to literature.**<sup>21</sup>  $\beta$ -alanine (9.142 g, 102.6 mmol, 1.0 eq.) was added in one portion to a solution of maleic anhydride (10.063 g, 102.6 mmol, 1.0 eq.) in dry DMF (60 mL) under Ar and the mixture was stirred during 5h. The reaction mixture was cooled at 0 °C and *N*-hydroxysuccinimide (NHS, 14.763 g, 128.23 mmol, 1.25 eq.) was added and then, dicyclohexylcarbodiimide (DCC, 42.348 g, 205.24 mmol, 2.0 eq.). This mixture was allowed to warm up to room temperature and stirred overnight. The crude was filtered through Celite to remove the resulting dicyclohexylurea (DCU) and rinse with CH<sub>2</sub>Cl<sub>2</sub>. The filtrate was diluted with additional CH<sub>2</sub>Cl<sub>2</sub> and washed with saturated aqueous NaHCO<sub>3</sub> solution. The aqueous layer was then extracted twice with CH<sub>2</sub>Cl<sub>2</sub> and the combined organic layers were washed five times with brine. The organic layer was dried over MgSO<sub>4</sub>, filtered and evaporated. The crude was diluted in CHCl<sub>3</sub> (1.5 L) and addition of cold *n*-hexane allowed the precipitation of the desired product (named **MalOSu**) which was recovered by filtration (20.365 g, 76%). FTIR (neat, cm<sup>-1</sup>): 1712, 1704, 1211; <sup>1</sup>H NMR (CDCl<sub>3</sub>, 400 MHz):  $\delta$  2.82 (s, 4H), 3.02 (t, *J* = 6.9 Hz, 2H), 3.94 (t, *J* = 7.0 Hz, 2H), 6.73 (s, 2H); <sup>13</sup>C NMR (CDCl<sub>3</sub>, 100 MHz):  $\delta$  170.0, 168.7, 166.0, 134.3, 32.9, 29.7, 25.5.

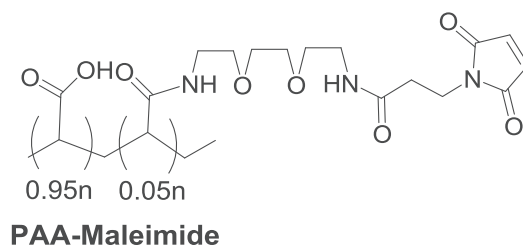


***tert*-butyl(2-(2-(2-(3-(2,5-dioxo-2,5-dihydro-1*H*-pyrrol-1-yl)propanamido)ethoxy)ethoxy)ethyl)carbamate (Mal-NHBoc).** MalOSu (205 mg, 772  $\mu$ mol, 0.9 eq.) was added in one portion to a solution of *N*-Boc-2,2'-(ethylenedioxy)diethylamine (213 mg, 858  $\mu$ mol, 1.0 eq.) in anhydrous CH<sub>2</sub>Cl<sub>2</sub> (5 mL) and the resulting mixture was stirred overnight. The reaction was quenched with 10 mL of saturated aqueous NaHCO<sub>3</sub> and extracted 3 times with CH<sub>2</sub>Cl<sub>2</sub>. The combined organic layers were washed with brine, dried over MgSO<sub>4</sub>, filtered and evaporated

to give the desired product Mal-NHBoc as a white solid (305 mg, 99%) which was used in the next step without further purification. FTIR (neat,  $\text{cm}^{-1}$ ): 3345, 3315, 2977, 2872, 1697, 1684, 1535;  $^1\text{H}$  NMR ( $\text{CDCl}_3$ , 400 MHz):  $\delta$  1.44 (s, 9H), 2.53 (t,  $J = 7.3$  Hz, 2H), 3.32 (bs, 2H), 3.43 (q,  $J = 5.1$  Hz, 2H), 3.52-3.62 (m, 8H), 3.85 (t,  $J = 7.2$  Hz, 2H), 6.69 (s, 2H);  $^{13}\text{C}$  NMR ( $\text{CDCl}_3$ , 100 MHz):  $\delta$  170.4, 169.7, 156.0, 134.1, 79.3, 70.2, 70.1, 70.1, 69.7, 40.3, 39.2, 34.5, 34.3, 28.3.

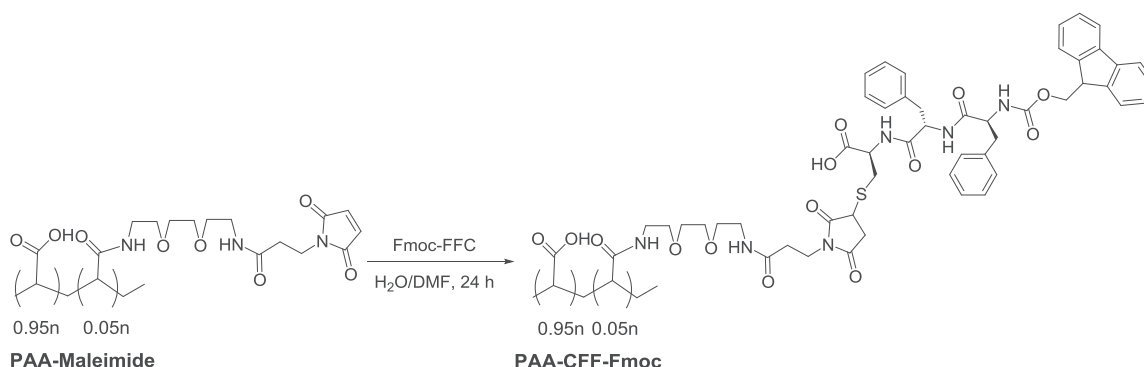


**Trifluoroacetate salt of N-(2-(2-(2-aminoethoxy)ethoxy)ethyl)-3-(2,5-dioxo-2,5-dihydro-1H-pyrrol-1-yl)propanamide (Mal-NH<sub>3</sub><sup>+</sup>TFA).** Mal-NHBoc (533 mg, 1.334 mmol, 1.0 eq.) was dissolved in  $\text{CH}_2\text{Cl}_2$  (15 mL) and treated with TFA (1.5 mL) for 2h. The resulting reaction mixture was then concentrated under reduced pressure leading to the desired product Mal-NH<sub>3</sub><sup>+</sup>TFA as a colourless oil (560 mg, quantitative yield). This compound was used in the next step without further purification.  $^1\text{H}$  NMR ( $\text{CDCl}_3$ , 400 MHz):  $\delta$  2.60 (t,  $J = 6.8$  Hz, 2H), 3.30 (bs, 2H), 3.41-3.50 (m, 2H), 3.56-3.63 (m, 4H), 3.68-3.72 (m, 2H), 3.77-3.83 (m, 4H), 6.71 (s, 2H).

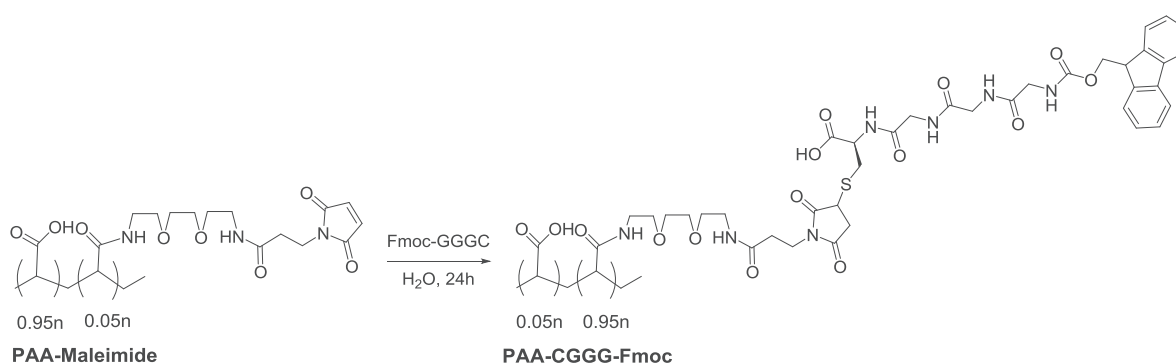


**PAA-Maleimide.** Poly(acrylic acid) (921 mg, 4.35 mmol, 1.0 eq.) was dissolved in MES buffer at pH=6. EDC.HCl (250 mg, 1.3 mmol, 0.3 eq.) and NHS (500 mg, 4.35 mmol, 1.0 eq.) were added in one portion to the solution and stirred for 2h. Mal-NH<sub>3</sub><sup>+</sup>TFA (489 mg, 0.87 mmol, 0.2 eq.) was added to the previous mixture and let stirred overnight at room temperature. The reaction mixture was purified by dialysis (Zellultrans Roth, Co., MW 12000-14000) against aqueous 0.5M NaCl solution and milliQ water. The dialysate was freeze-dry providing PAA-Maleimide as a white powder. FTIR (neat,  $\text{cm}^{-1}$ ): 1705, 1559, 1450, 1403;  $^1\text{H}$  NMR ( $\text{D}_2\text{O}$ , 400 MHz):  $\delta$  1.65 (br m, 2H,  $\text{CH}_2(\beta)$  PAA), 2.30 (br s, 1H,  $\text{CH}(\alpha)$  PAA), 2.65 (br t, 2H,  $\text{CH}_2$  ethylene linker), 3.05-3.30 (br m, H,  $\text{CH}_2$  ethylene and ethylene oxide linker), 3.35-3.60 (br m, H,  $\text{CH}_2$  ethylene oxide linker), 6.90 (br s, 2H,  $\text{CH}=\text{CH}$  maleimide group). The integration of

the signal at 6.90 ppm (br s, 2H, CH=CH maleimide group) in comparison with the integration of the broad signal at 2.30 ppm (br s, 1H, CH( $\alpha$ ) PAA) gives 5% of modification degree.



**PAA-CFF-Fmoc.** PAA-Maleimide (90.4 mg, 0.2 mmol, 1.0 eq.) was dissolved in milliQ water. In a spare vial, Fmoc-FFC (7.8 mg, 0.12 mmol, 0.05 eq.) previously dissolved in dimethylformamide was added dropwise to the polymer solution. The reaction mixture was stirred for 24h at room temperature. The crude product was dialyzed against water and brine (0.5M) to result a with solid dried under vacuum. FTIR (neat,  $\text{cm}^{-1}$ ) 1705, 1646, 1559, 1450, 1250, 1166, 1081, 1020, 791;  $^1\text{H}$  NMR ( $\text{D}_2\text{O}$ , 400 MHz):  $\delta$  1.70 (br m, 2H,  $\text{CH}_2(\beta)$  PAA), 2.30 (br s, 1H, CH( $\alpha$ ) PAA), 2.50 (br s), 2.90 (br s), 3.10-3.80 (br m), 4.05-4.20 (br m), 5.4 (br s), 7.05-7.80 (br m, CH aromatic of Fmoc group). The singlet at 6.90 ppm corresponding to CH=CH of the maleimide group of PAA-Maleimide is no longer present in the  $^1\text{H}$  NMR spectra of PAA-CFF-Fmoc. The integration of the broad signal at 7.05-7.80 ppm (br m, CH aromatic of Fmoc group) in comparison with the integration of the broad signal at 1.70 ppm (br m, 2H,  $\text{CH}_2(\beta)$  PAA) gives 5% of modification degree.



**PAA-CGGG-Fmoc.** PAA-Maleimide (80 mg, 0.2 mmol, 1.0 eq.) and commercial Fmoc-GGGC (27.4 mg, 0.05 mmol, 0.2 eq.) were diluted in milliQ water and stirred for 24h. The reaction mixture was dialyzed for several days against brine (0.5M) and water and dried under vacuum to obtain a white solid. FTIR (neat,  $\text{cm}^{-1}$ ) 1705, 1646, 1541, 1450, 1404, 1250, 1166,

791;  $^1\text{H}$  NMR ( $\text{D}_2\text{O}$ , 400 MHz):  $\delta$  1.70 (br m, 2H,  $\text{CH}_2(\beta)$  PAA), 2.30 (br s, 1H,  $\text{CH}(\alpha)$  PAA), 3.30-4.60 (br m), 7.10-7.80 (br m, CH aromatic of Fmoc group). Because the singlet at 6.90 ppm corresponding to  $\text{CH}=\text{CH}$  of the maleimide group of PAA-Maleimide is no longer present in the  $^1\text{H}$  NMR spectra of PAA-CGGG-Fmoc, we have considered this polymer modified with 5% of grafting ratio.

#### 4.5.1.4 Multilayer film preparation and hydrogel self-assembly

All polyelectrolytes and proteins were prepared in Borax buffer (25 mM, pH = 9.5). Different substrates were used depending on the characterization techniques used: QCM quartz crystal for QCM, ZnSe crystal for ATR-FTIR and silica glass for UV, fluorescence spectroscopy and confocal microscopy. After the deposition of a PEI ( $1 \text{ mg}\cdot\text{mL}^{-1}$ ) precursor layer on the substrate, the multilayer film was performed by alternatively exposing the substrate to PSS ( $1 \text{ mg}\cdot\text{mL}^{-1}$ ) and PAH ( $1 \text{ mg}\cdot\text{mL}^{-1}$ ) for 5 min with an intermediate rinsing with Borax buffer after each polymer for 5 min. Alkaline phosphatase ( $1 \text{ mg}\cdot\text{mL}^{-1}$ ), PAA-CFF-Fmoc ( $0.2 \text{ mg}\cdot\text{mL}^{-1}$ ) or PAA-CGGG-Fmoc ( $0.2 \text{ mg}\cdot\text{mL}^{-1}$ ) were adsorbed for 20 min followed by 5 min of rinsing step with Borax buffer. In the case of infrared spectroscopy, all solutions used were prepared with  $\text{D}_2\text{O}$  instead of water.

#### 4.5.1.5 Fluorescence spectroscopy

All fluorescence intensities were measured by using the spectrofluorometer FluoroMax-4 from HORIBA JOBIN YVON at 290 nm of excitation wavelength and measured between 300 – 440 nm. A special support was used to measure the fluorescence in solution during the self-assembly of gel when PEI-(PSS/PAH)<sub>2</sub>-ALP-(PAH/PAA-CFF-Fmoc) film was put in contact with 0.90 mM Fmoc-FFY( $\text{PO}_4^{2-}$ ) solution.

#### 4.5.2 Preliminary tests of gelation in vials

All the following experiments were realized in Borax Buffer (25mM, pH 9.5).

1. Fmoc-FFY( $\text{PO}_4^{2-}$ ) (0.9 mM) and Alkaline Phosphatase ( $25 \text{ U.mL}^{-1}$ ) were dissolved in 1 mL of Buffer. After 15 min, the vial was turned upside down showing a stable hydrogel (Vial 1 in the picture below).
2. Fmoc-FFY( $\text{PO}_4^{2-}$ ) (0.9 mM) and Alkaline Phosphatase ( $1 \text{ U.mL}^{-1}$ ) were dissolved in 1 mL of Buffer. No gel was formed after 15 min (Vial 2 in the picture below).
3. Fmoc-FFY( $\text{PO}_4^{2-}$ ) (0.6 mM) and ( $0.5 \text{ mg.mL}^{-1}$ ) PAA-CFF-Fmoc mixture (corresponding to 0.3 mM of peptides “Fmoc-FF”), was added to Alkaline Phosphatase ( $1 \text{ U.mL}^{-1}$ ) in 1 mL of buffer. After 15 min, the vial was turned upside down showing a stable hydrogel (Vial 3 in the picture below).
4. Fmoc-FFY( $\text{PO}_4^{2-}$ ) (0.6 mM), PAA-CGGG-Fmoc ( $0.5 \text{ mg.mL}^{-1}$ , corresponding to 0.3 mM of peptides “Fmoc-GGG”) and Alkaline Phosphatase ( $1 \text{ U.mL}^{-1}$ ) were dissolved in 1 mL of buffer. 15 min after Alkaline Phosphatase addition, no gel was observed (Vial 4 in the picture below).
5. Fmoc-FFY( $\text{PO}_4^{2-}$ ) (0.9 mM), PAA ( $0.5 \text{ mg.mL}^{-1}$ ) and Alkaline Phosphatase ( $1 \text{ U.mL}^{-1}$ ) were dissolved in 1 mL of buffer. No gel was observed after 15 min (Vial 5 in the picture below).



### 4.5.3 Influence of the decrease of ALP density on the hydrogel formation

We also modulated the catalytic activity of the film by decreasing the amount of ALP in the film. This was done by using various concentrations of ALP during the film buildup (0, 0.25, 0.50, 1 mg.mL<sup>-1</sup>). First of all, we checked by QCM-D that the mass of ALP adsorbed for each concentration used is proportional to the variation of the opposite of the fundamental frequency shift measured after contact with a 0.90 mM of Fmoc-FFY(PO<sub>4</sub><sup>2-</sup>) solution (Figure below). Thus, by decreasing the density of ALP in the multilayer, one observes correlatively a quasi linear decrease of the gel buildup when the film is brought in contact with the initiating Fmoc-FFY(PO<sub>4</sub><sup>2-</sup>) solution peptide (Figure below).

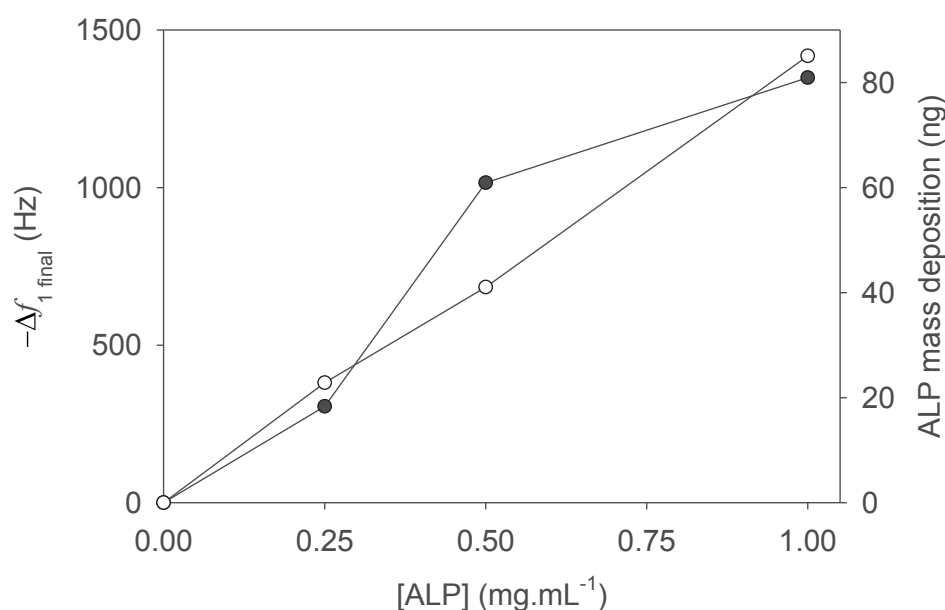


**Figure S4.1:** (●Black dots) Evolution of the opposite of the fundamental frequency shift, measured at 5 MHz by QCM-D, after 12 h of self-assembly of gel from Fmoc-FFY(PO<sub>4</sub><sup>2-</sup>) on PAA-CFF-Fmoc ended film as a function of the concentration of ALP deposited onto the film. (○White dots) Mass adsorbed of ALP in PEI-(PSS/PAH)-ALP-(PAH/PAA-CFF-Fmoc) film, measured by QCM-D using Sauerbrey equation, as a function of the concentration of ALP used

## 4.5.4 Supporting figures

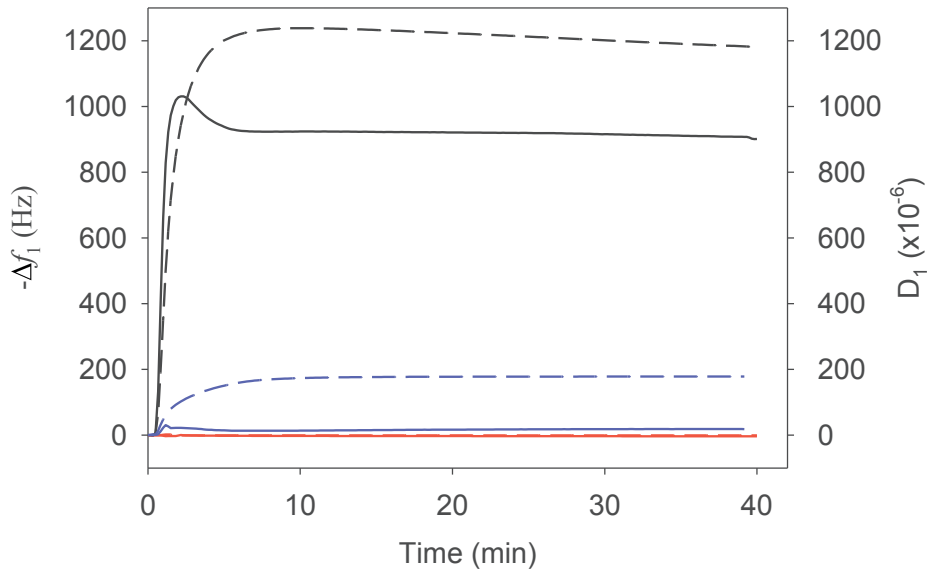


**Figure S4.2:** Evolution of the fundamental frequency shift (full line) and dissipation (dashed line), measured at 5 MHz by QCM-D, as function of time after 0.90 mM Fmoc-FFY( $\text{PO}_4^{2-}$ ) solution injection on (red) PEI-(PSS/PAH)<sub>2</sub>-PAA-CFF-Fmoc and after 0.90 mM Fmoc-FFY( $\text{PO}_4^{2-}$ ) and 0.33 mg.mL<sup>-1</sup> (1 U.mL<sup>-1</sup>) ALP mixture solution injection on (black) PEI-(PSS/PAH)<sub>2</sub>-PAA-CFF-Fmoc film and (blue) PEI-(PSS/PAH)<sub>2</sub>-(PAH/PAA-CGGG-Fmoc).

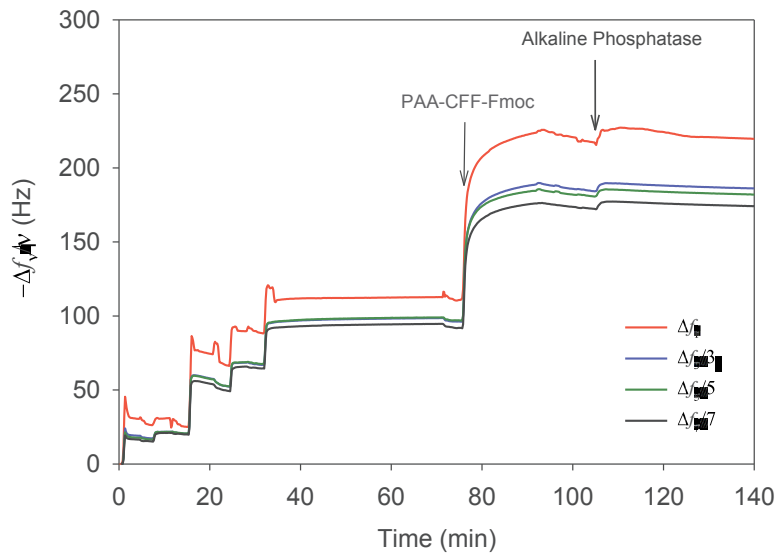


**Figure S4.3:** Evolution of the opposite of the fundamental frequency shift and the harmonics, measured at 5, 15, 25 and 35 MHz by QCM-D, as function of time during the buildup of PEI-(PSS/PAH)<sub>2</sub>-(PAA-CFF-Fmoc) multilayer films brought in contact with 0.33 mg.mL<sup>-1</sup> ALP solution (1 U.mL<sup>-1</sup>).

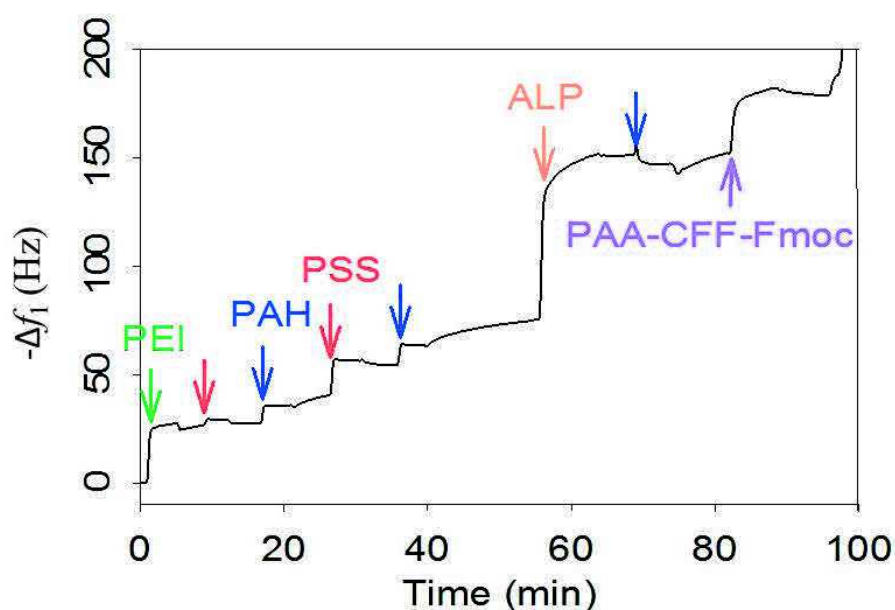


**Figure S4.4:** Evolution of the opposite of the fundamental frequency shift, measured at 5 MHz by QCM-D during the buildup of the multilayer PEI-(PSS/PAH)<sub>2</sub>-ALP-(PAH/(PAA-CFF-Fmoc)).

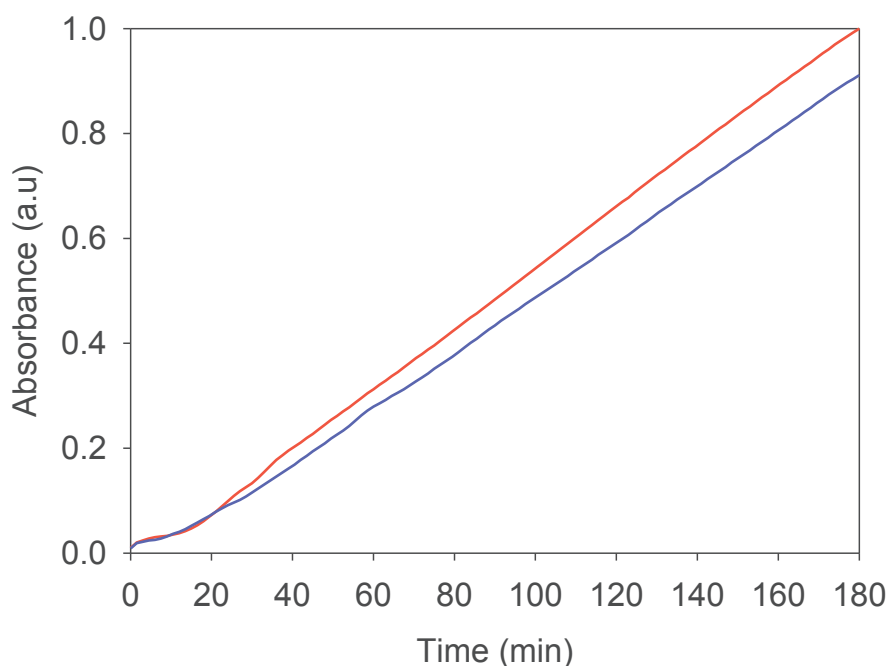


**Figure S4.5:** Evolution of the optical density (OD) as a function of time of a paranitrophenyl phosphate (PNP) solution brought in contact with (red curve) PEI-(PSS/PAH)<sub>2</sub>-ALP-(PAH/PAA-CFF-Fmoc) and (blue curve) PEI-(PSS/PAH)<sub>2</sub>-ALP-(PAH/PAA-CGGG-Fmoc) multilayer. The absorbance was measured at 405 nm. PNP is transformed into paranitrophenol ( $\lambda_{\max} = 405$  nm) and phosphate ions by ALP immobilized into the film. The measurement was performed with a microplate reader (see Materials and Methods section described above in SI). The value of the slopes are  $4.3 \times 10^{-3}$  and  $3.9 \times 10^{-3}$  for PAA-CFF-Fmoc and PAA-CGGG-Fmoc ended films, respectively.

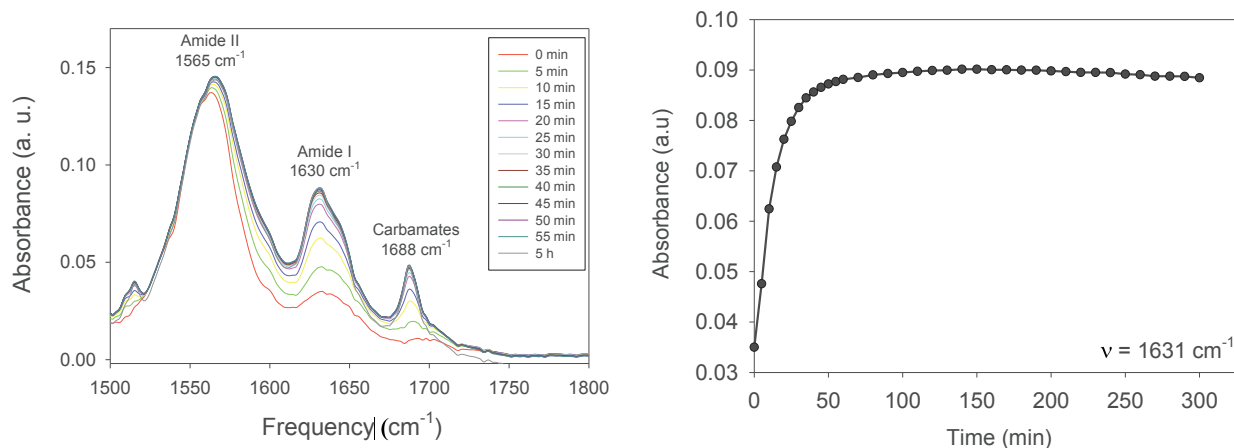


**Figure S4.6:** (a) Evolution of ATR-FTIR spectra as a function of time after 0.90 mM Fmoc-FFY( $\text{PO}_4^{2-}$ ) solution injection on PEI-(PSS/PAH)-ALP-(PAH/PAA-CFF-Fmoc) multilayer. (b) Evolution of the intensity of absorbance measured at  $1631\text{ cm}^{-1}$ , assigned to carbonyl groups of the amide I band involved in  $\beta$ -sheet structures. Prior to the injection of the 0.90 mM Fmoc-FFY( $\text{PO}_4^{2-}$ ) solution, the initial IR spectrum of the film PEI-(PSS/PAH)-ALP-(PAH/PAA-CFF-Fmoc) shows amide I band and carbamate peak due to PAA-CFF-Fmoc layer.

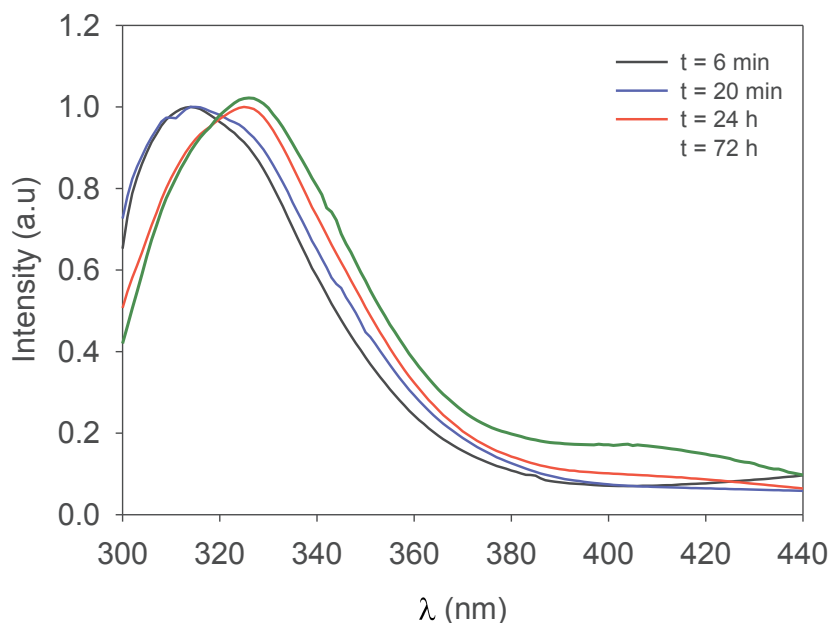


**Figure S4.7:** Evolution of the fluorescence intensity over time, at excitation wavelength of 290 nm, when the film PEI-(PSS/PAH)-ALP-(PAH/PAA-CFF-Fmoc) is brought in the contact with 0.90 mM Fmoc-FFY( $\text{PO}_4^{2-}$ ) solution.

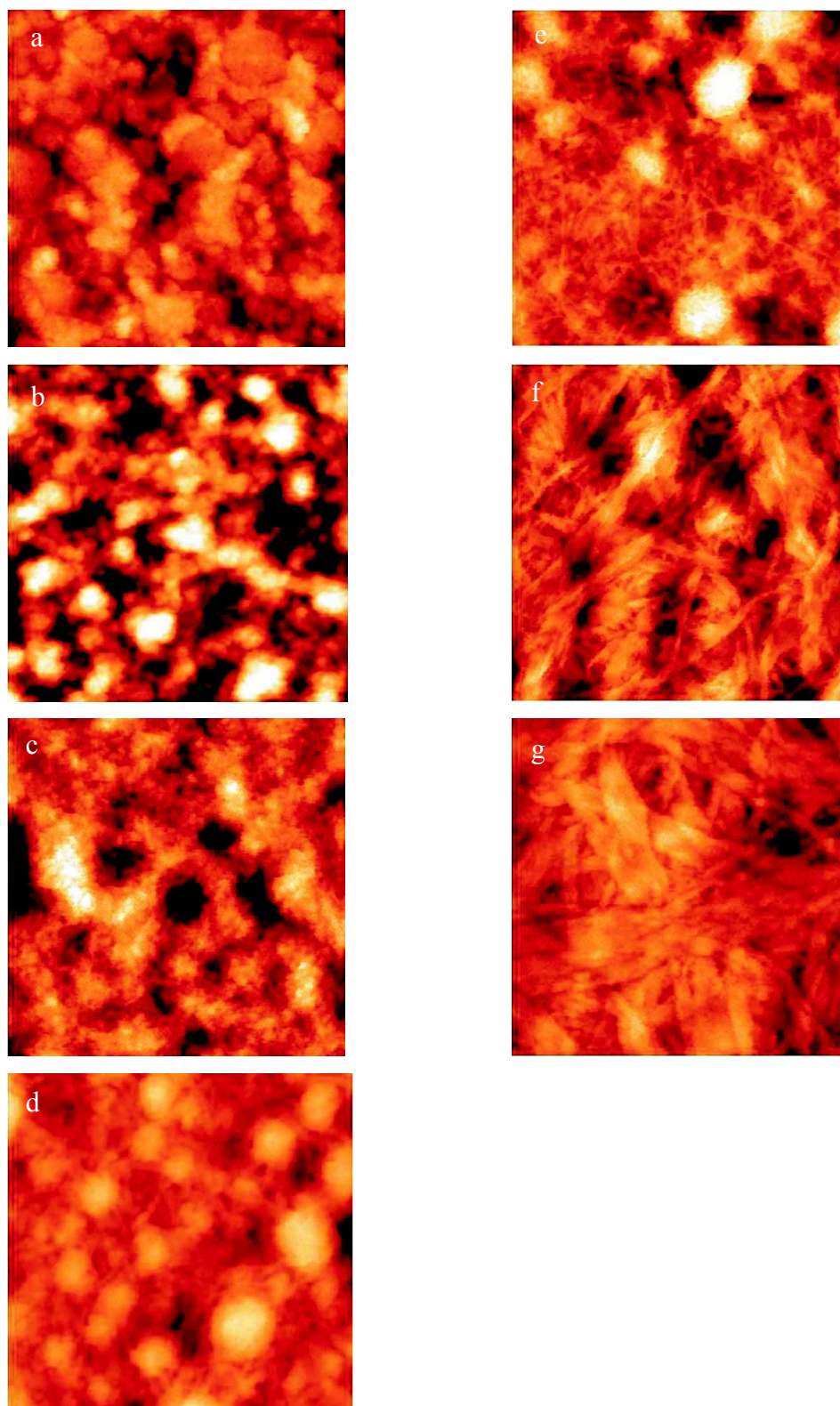


**Figure S4.8:** Typical AFM images, obtained in contact mode and dry state, of the gel built from the multilayer PEI-(PSS/PAH)-ALP-(PAH/PAA-CFF-Fmoc) when brought in contact with 0.90 mM Fmoc-FFY( $PO_4^{2-}$ ) solution during: (a) 0 s (z-scale = 30 nm), (b) 30 s (z-scale = 30 nm), (c) 2 min (z-scale = 30 nm), (d) 5 min (z-scale = 76 nm), (e) 20 min (z-scale = 70 nm), (f) 120 min (z-scale = 40 nm) and (g) 12 h (z-scale = 15 nm).

## References

1. Rydzek, G.; Jierry, L.; Parat, A.; Thomann, J. S.; Voegel, J.-C.; Senger, B.; Hemmerlé, J.; Ponche, A.; Frisch, B.; Schaaf, P.; Boulmedais, F. Electrochemically Triggered Assembly of Films: A One-Pot Morphogen-Driven Buildup. *Angew. Chem.-Int. Edit.* **2011**, *50* (19), 4374.
2. Maity, C.; Hendriksen, W. E.; van Esch, J. H.; Eelkema, R. Spatial Structuring of a Supramolecular Hydrogel by using a Visible-Light Triggered Catalyst. *Angew. Chem. Int. Ed.* **2015**, *54* (3), 998.
3. Shi, X.-W.; Tsao, C.-Y.; Yang, X.; Liu, Y.; Dykstra, P.; Rubloff, G. W.; Ghodssi, R.; Bentley, W. E.; Payne, G. F. Electroaddressing of Cell Populations by Co-Deposition with Calcium Alginate Hydrogels. *Adv. Funct. Mater.* **2009**, *19* (13), 2074.
4. Johnson, E. K.; Adams, D. J.; Cameron, P. J. Directed Self-Assembly of Dipeptides to Form Ultrathin Hydrogel Membranes. *J. Am. Chem. Soc.* **2010**, *132* (14), 5130.
5. Yang, Z. M.; Gu, H. W.; Fu, D. G.; Gao, P.; Lam, J. K.; Xu, B. Enzymatic formation of supramolecular hydrogels. *Adv. Mater.* **2004**, *16* (16), 1440.
6. Kuang, Y.; Shi, J.; Li, J.; Yuan, D.; Alberti, K. A.; Xu, Q.; Xu, B. Pericellular Hydrogel/Nanonets Inhibit Cancer Cells. *Angew. Chem. Int. Ed.* **2014**, *53* (31), 8104.
7. Li, J.; Gao, Y.; Kuang, Y.; Shi, J.; Du, X.; Zhou, J.; Wang, H.; Yang, Z.; Xu, B. Dephosphorylation of d-Peptide Derivatives to Form Biofunctional, Supramolecular Nanofibers/Hydrogels and Their Potential Applications for Intracellular Imaging and Intratumoral Chemotherapy. *J. Am. Chem. Soc.* **2013**, *135* (26), 9907.
8. Wang, Q.; Yang, Z.; Gao, Y.; Ge, W.; Wang, L.; Xu, B. Enzymatic hydrogelation to immobilize an enzyme for high activity and stability. *Soft Matter* **2008**, *4* (3), 550.
9. Williams, R. J.; Smith, A. M.; Collins, R.; Hodson, N.; Das, A. K.; Ulijn, R. V. Enzyme-assisted self-assembly under thermodynamic control. *Nat. Nanotechnol.* **2009**, *4* (1), 19.
10. Tang, Z. Y.; Wang, Y.; Podsiadlo, P.; Kotov, N. A. Biomedical applications of layer-by-layer assembly: From biomimetics to tissue engineering. *Adv. Mater.* **2006**, *18* (24), 3203.
11. Ariga, K.; Mori, T.; Hill, J. P. Control of nano/molecular systems by application of macroscopic mechanical stimuli. *Chemical Science* **2011**, *2* (2), 195.
12. Decher, G. Fuzzy nanoassemblies: Toward layered polymeric multicomposites. *Science* **1997**, *277* (5330), 1232.
13. Lvov, Y.; Ariga, K.; Ichinose, I.; Kunitake, T. Assembly of multicomponent protein films by means of electrostatic layer-by-layer adsorption. *J. Am. Chem. Soc.* **1995**, *117*, 6117.
14. Javid, N.; Roy, S.; Zelzer, M.; Yang, Z.; Sefcik, J.; Ulijn, R. V. Cooperative Self-Assembly of Peptide Gelators and Proteins. *Biomacromolecules* **2013**, *14* (12), 4368.
15. FrederixPim, W. J. M.; Scott, G. G.; Abul-Haija, Y. M.; Kalafatovic, D.; Pappas, C. G.; Javid, N.; Hunt, N. T.; Ulijn, R. V.; Tuttle, T. Exploring the sequence space for (tri-)peptide self-assembly to design and discover new hydrogels. *Nat Chem* **2015**, *7* (1), 30.

- 
16. Sauerbrey, G. Verwendung von Schwingquartzen zur Wägung dünner Schichten und zur Mikrowägung. *Z. Phys.* **1959**, *155*, 206.
  17. Kong, J.; Yu, S. Fourier Transform Infrared Spectroscopic Analysis of Protein Secondary Structures. *Acta Biochimica et Biophysica Sinica* **2007**, *39* (8), 549.
  18. Smith, A. M.; Williams, R. J.; Tang, C.; Coppo, P.; Collins, R. F.; Turner, M. L.; Saiani, A.; Ulijn, R. V. Fmoc-Diphenylalanine Self Assembles to a Hydrogel via a Novel Architecture Based on  $\pi$ - $\pi$  Interlocked  $\beta$ -Sheets. *Adv. Mater.* **2008**, *20* (1), 37.
  19. Fleming, S.; Frederix, P. W. J. M.; Ramos Sasselli, I.; Hunt, N. T.; Ulijn, R. V.; Tuttle, T. Assessing the Utility of Infrared Spectroscopy as a Structural Diagnostic Tool for  $\beta$ -Sheets in Self-Assembling Aromatic Peptide Amphiphiles. *Langmuir* **2013**, *29* (30), 9510.
  20. Yamada, N.; Ariga, K.; Naito, M.; Matsubara, K.; Koyama, E. Regulation of  $\beta$ -Sheet Structures within Amyloid-Like  $\beta$ -Sheet Assemblage from Tripeptide Derivatives. *J. Am. Chem. Soc.* **1998**, *120* (47), 12192.
  21. Ede, N. J.; Tregear, G. W.; Haralambidis, J. Routine Preparation of Thiol Oligonucleotides: Application to the Synthesis of Oligonucleotide-Peptide Hybrids. *Bioconjugate Chemistry* **1994**, *5* (4), 373.

## General Conclusion and outlooks

Over the last century, the self-assembly of small chemical units into complex structures was mainly driven by the development of functional materials. In this context, we took the challenge to modify surfaces in order to give them **the ability to initiate and to control over space and time the chemical interactions between peptide hydrogelators and their neighboring environment**. We developed surfaces coated with enzymatic nanofilms using the layer-by-layer method. These enzymatic precursor films were able to trigger the chemical transformation of peptides into self-assembling building blocks. By tuning the composition of the enzymatic precursor film or the initial experimental conditions (concentration in peptides), it is possible to tune the nucleation process and the growth of the hydrogel structure exclusively from the surface.

The bibliographic chapter I introduced the chemical basis required to design stimuli-responsive gelators using sonication, temperature, pH or catalysis as a trigger. A short review of the chemical system developed on surface is given: articles published roughly in the ten last years and more specifically during the period of my PhD. This mini-review is thus fully original. A brief description of LbL is given.

Since October 2013, I developed two approaches related to the localized enzyme-assisted self-assembly (LEASA) process. In a first approach described in Chapter three, the self-assembly of peptides was assisted by  $\alpha$ -chymotrypsin immobilized on a surface through electrostatic interactions and hydrogen bonds. This localized enzymatic stimulus catalyzed the condensation of *KLOEt* peptides to form  $(KL)_nOEt$  oligomers. These oligopeptides are gradually released from the surface and then self-assemble into nanofibers growing from the surface. This strategy based on LEASA allows to tune the amplitude and kinetic of oligopeptides self-assembly by the modification of the initial concentration of *KLOEt* or the surface density in  $\alpha$ -chymotrypsin. In a second approach (Chapter four), I have designed a thin film promoting both the enzymatic production and the seeding of hydrogelator-based peptides to nucleate the self-assembly process exclusively from the surface. A bioactive seeding multilayer film embedding alkaline phosphatase

in its architecture was built. This nanofilm catalyzes the formation of Fmoc-FFY hydrogelators in the close vicinity of the surface. The seeding layer displaying the “gelating” sequence (Fmoc-FFC) was deposited on the top of the enzymatic precursor film to pattern local aggregation of hydrogelators. The enzymatic film ensured the continuous chemical transformation of the peptide into hydrogelator and the seeding layer the spatial control of the nucleation process of the self-assembly. Indeed in the absence of the seeding layer, no gelation occurs. Thus, we have introduced a sophisticated and smart *bioactive seed-layer* that triggers buildup of a fibrous network and controls spatiotemporally its self-assembly.

Spatiotemporal control over peptide self-assembly could result in highly order structures exhibiting different functionalities, in particular different catalytic activities. As outlooks of my PhD. work, one interesting project would be to build a **functional hydrogels** with catalytic properties, provided either by an enzyme embedded into the self-assembled gel or via the artificial catalysis of a short peptide sequence.

In a first strategy, the encapsulation of natural enzymes in a peptide based-hydrogel through LEASA could activate the self-assembly of a second peptide-based hydrogel. Hydrogels thus will growth successively one **from** the other. This process could be repeated several times to obtain alternated layers of two different kinds of catalytic hydrogels (Figure 5.1). To this aim, each gel chosen must be prepared with a different peptide and initiated with a different enzyme. The development of a spatiotemporal control over the self-assembly of alternated hydrogels can lead to the design of spatially resolved materials with specific region of functionality. Preliminary tests of alternated hydrogelation were realized in solution as presented in annexe 1.

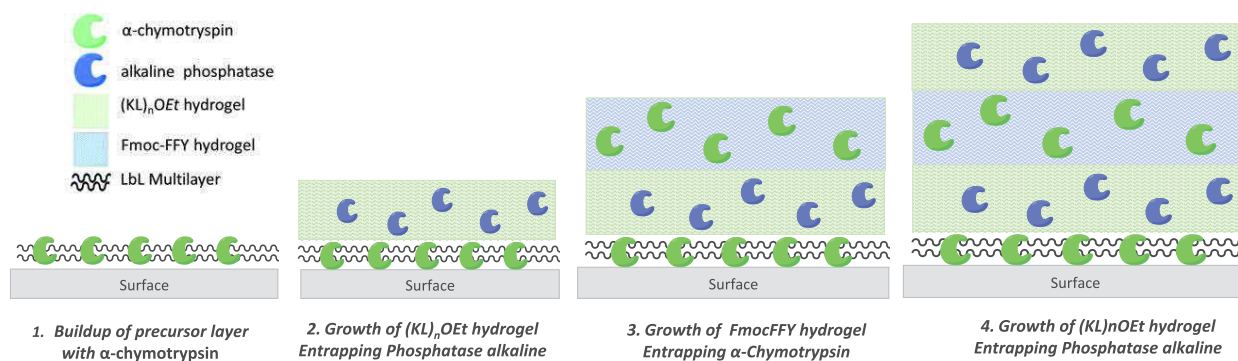


**Figure 5.1:** Schematic representation of alternated hydrogels entrapping enzymes initiating the next self-assembly of peptides from the bottom to the top.

The second strategy can be based on the design of a peptide able to self-assemble through localized catalytic assisted self-assembly (LCASA) that can further induced a second self-assembled hydrogel. Artificial enzyme-like catalysis is interesting in order to overcome the drawbacks of natural enzymes, such as denaturation causing a loss of activity. As a preliminary study, we selected from the literature Ac-IHIHIQI-NH<sub>2</sub> peptide sequence which has the property to self-assemble into  $\beta$ -sheet-amyloids in the presence of Zn<sup>2+</sup> and has a “esterase-like” catalytic activity. In a preliminary study presented in annexe 2, we evaluated this catalytic activity of Ac-IHIHIQI-NH<sub>2</sub> complexes by monitoring transformation of a model substrate.

Confinement of catalytic Ac-IHIHIQI-NH<sub>2</sub> with Zn<sup>2+</sup> on the surface, will be develop using concept of polyelectrolyte seeding layer (Chapter four). As seed layer, poly (acrylic acid) can be modified by two peptide seeding sequences: the catalyst precursor (derived from Ac-IHIHIQI-NH<sub>2</sub>) and a second peptide **P** that will play the role the hydrogelator (Figure 5.2). After the immobilisation of the polyelectrolyte seeding layer, the addition of a mixture of Zn<sup>2+</sup> and Ac-IHIHIQI-NH<sub>2</sub> will induce the formation of “esterase-like” catalyst confined on the surface. The second peptide **P** will be designed to have the property to be transformed into a hydrogelator by an esterase. When **P** solution will be put in contact with the confined “esterase-like” catalyst, a gelation will be induced.

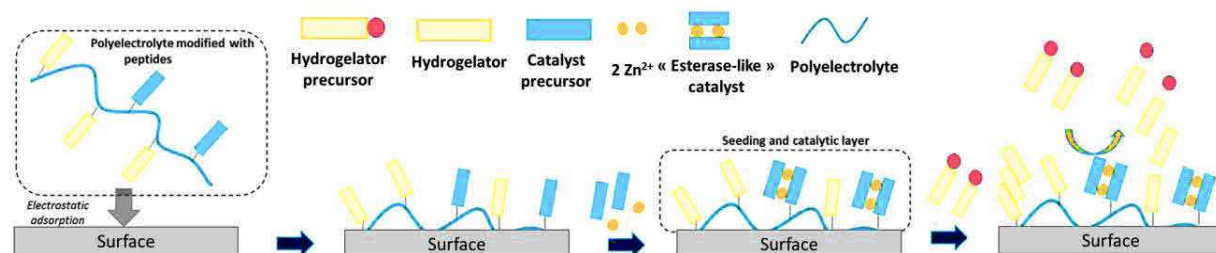


**Figure 5.2:** Schematic representation of LCASA induced by a confined artificial catalysis using a bi-functionalized polyelectrolyte seeding layer: the confined artificial “enzyme-like” activity of the first self-assembled peptide allows to initiate the transformation of a second peptidic precursor into a supramolecular hydrogels.

The idea of these two outlooks is to use catalytic properties of a first peptide hydrogel to design newly formed catalytic architectures. The spontaneous formation of catalytic hydrogels suggests a very high degree of control over materials formation.

Annexes:  
Preliminary results

---

# Annexes

## Preliminary results

---

### **Summary**

<b>Annexe 1: Alternated superposition of multi-component gels .....</b>	<b>135</b>
<b>Annexe 2: Catalytic assay of Ac-IHIHIQI-NH<sub>2</sub> catalyst.....</b>	<b>136</b>

## Annexe 1: Alternated superposition of multi-component gels

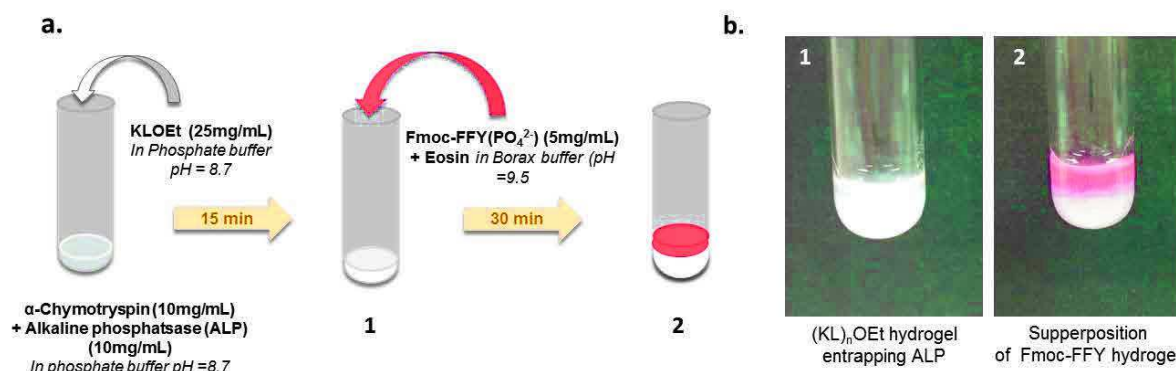


**Figure 5.1:** (a) Schematic representation of experimental settings to build up a bilayered hydrogel; (b) Pictures of 1 (KL)<sub>n</sub>OEt hydrogel layer loaded with alkaline phosphatase and 2 showing the two layers of (KL)<sub>n</sub>OEt hydrogel (bottom) and Fmoc-FFY based hydrogel, labelled by eosin (red dye) (top).

Herein, preliminary results are presented on the alternated hydrogelation in solution using both peptide/enzyme systems developed during my Ph.D. work (Figure A). Both enzymes,  $\alpha$ -chymotrypsin and alkaline phosphatase (ALP), were solubilized into phosphate buffer (pH=8.7) in a test tube. KLOEt peptides were added to the enzyme mixture solution to encapsulate ALP inside (KL)<sub>n</sub>OEt hydrogel. After 15 min, a white (KL)<sub>n</sub>OEt hydrogel is formed, holding to the test tube when it is turned upside-down. To create the second hydrogel layer, a Fmoc-FFY(PO<sub>4</sub><sup>2-</sup>) solution, containing a red dye (eosin), was added on the top of the first gel layer. After 30 min, a second gel is formed on the top of the first one, displaying a red-pink color. When the test tube is turned upside down, both hydrogel layers do not separate one from the other, and the pink color has no yet diffused (Figure 5.1.b). Several hours later, eosin still stays in the second gel, without diffusing in the first gel.

## Annexe 2: Catalytic assay of Ac-IHIHIQI-NH<sub>2</sub> with Zn<sup>2+</sup>

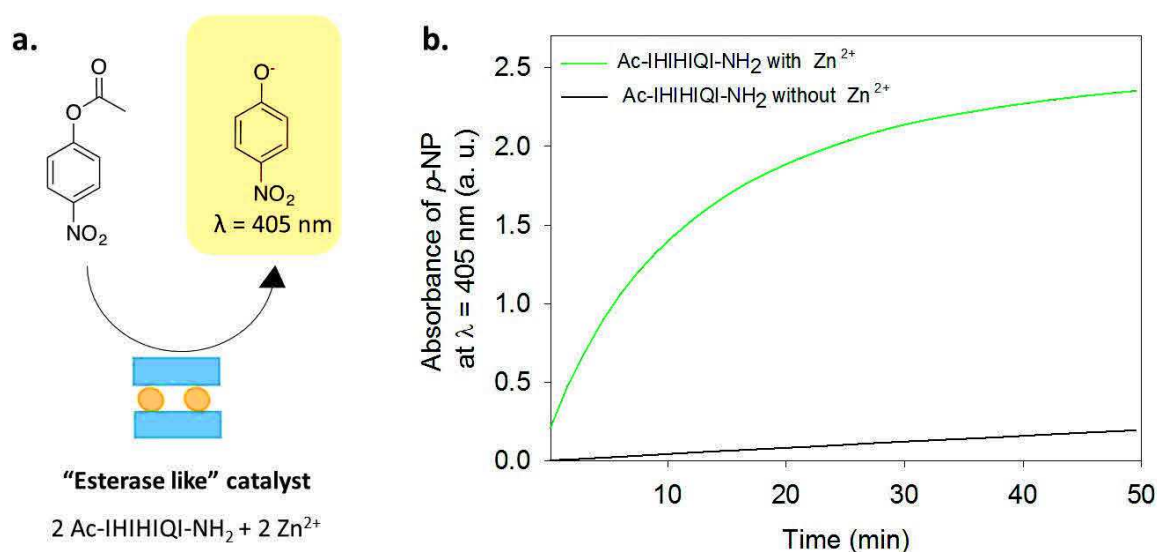


**Figure 5.2:** (a) Schematic representation of *p*-nitrophenylacetate (*p*-NPA) hydrolysis into *p*-nitrophenol (*p*-NP) by C<sub>2</sub> complex; (b) Evolution of absorbance at  $\lambda=405 \text{ nm}$  as function of time for Ac-IHIHIQI-NH<sub>2</sub> in TRIS buffer (25mM, pH=8) in presence or absence of Zn<sup>2+</sup>.

The esterase-like activity of Ac-IHIHIQI-NH<sub>2</sub> peptide, purchased from a commercial supplier, was evaluated using a chromogenic substrate *p*-nitrophenylacetate (*p*-NPA) (Figure 5.2.a). Hydrolysis of *p*-NPA ester leads to acetate and *p*-nitrophenol (*p*-NP) which shows a strong absorbance in UV-visible domain ( $\lambda=405 \text{ nm}$ ). Ac-IHIHIQI-NH<sub>2</sub> was dissolved in a TRIS buffer (25 mM, pH=8) with 1 mM of ZnCl<sub>2</sub>. After the addition of *p*-NPA substrate, absorbance at 405 nm rapidly increased reaching a plateau after 50 min (Figure 5.2.b). Without Zn<sup>2+</sup> in solution, almost no shift of absorbance was observed. The catalytic activity of Ac-IHIHIQI-NH<sub>2</sub> peptides is only effective in presence of Zn<sup>2+</sup>, as described in the literature.

## Résumé de thèse

### Introduction

La modification de surface est une méthode efficace permettant de conférer une grande variété de propriétés spécifiques à un matériau. L'existence d'un large éventail de méthodes de fonctionnalisation permet le contrôle des interactions entre un revêtement en surface composé de diverses molécules et/ou biomolécules et son environnement. Ce choix de revêtement ouvre le champ à de multiples applications dans le secteur du textile, du stockage d'énergie, de l'électronique, des biomatériaux, de la conception de bio-senseur et bien d'autres...

Au début des années 1990 une nouvelle méthode de fonctionnalisation de surface émerge basée sur la déposition alternée d'espèces chargées positivement et négativement sur une surface.<sup>1</sup> Cette nouvelle approche dite du « couche par couche », principalement utilisée pour le dépôt de polyélectrolytes, permet la construction d'un film multicouche avec un contrôle précis de son épaisseur grâce au nombre de couches et à différents paramètres physico-chimiques (pH, force ionique, nature des macromolécules...). Cette technique permet de fonctionnaliser un grand nombre de supports en leur conférant différentes propriétés selon le type de (bio)molécules ou macromolécules adsorbées. Malgré de nombreux avantages, la fonctionnalisation de surface par la technique « couche par couche » est chronophage et/ou fastidieuse lorsqu'il s'agit de construire des films multicouches d'épaisseur importante.

Depuis 2011, notre équipe a développé différentes stratégies d'autoconstructions « tout en un » (en anglais « one pot ») de films organiques et inorganiques à la surface d'un support conducteur. Déclenché par l'application d'un stimulus électrique qui génère la formation d'un gradient de catalyseur (ions métalliques ou protons) proche de la surface, l'autoconstruction de films a été développée à base d'oligomères, polymères, petites molécules, ou nanoparticules inorganiques.<sup>2</sup> Cette méthode de fonctionnalisation est avantageuse puisqu'elle permet la réaction (ou l'interaction) contrôlée de tous les constituants présents au départ par voie ascendante (stratégie « bottom-up ») depuis la surface.

La nature fournit de multiples exemples de petites unités biologiques qui s'auto-assemblent pour former des structures complexes et fonctionnelles. Le facteur clé de cette stratégie d'organisation ascendante est basé sur le contrôle localisé d'interactions entre les briques de construction moléculaire et leur environnement local. Afin de développer cette approche, nous avons choisi d'utiliser des peptides comme briques moléculaires. Les peptides présentent des propriétés d'interaction ajustables utiles pour programmer l'auto-assemblage des molécules sous forme de nano architectures tels que des fibres, sphères, tubes ou micelles.

**L'objectif de ma thèse est de mettre au point des surfaces intelligentes capables d'initier et de contrôler le processus d'auto-assemblage ascendant de peptides dans le temps et dans l'espace.** Cette stratégie est basée sur le développement de surface enzymatique active avec une enzyme catalysant la formation d'un substrat peptidique choisi. La fonctionnalisation enzymatique des surfaces a été développée par la méthode du « couche par couche », permettant d'induire une transformation de peptides substrat en peptide activé, capables de s'auto-assembler spontanément depuis la surface.

Dans ce projet, l'auto-assemblage ascendant (stratégie « bottom-up ») est initié depuis la surface (*espace*) par un stimulus enzymatique qui engendre la formation d'une architecture fibrillaire en milieu aqueux, ossature d'un hydrogel. L'utilisation d'une surface fonctionnalisée de façon adéquate permet la régulation dans le *temps* de la construction de l'édifice auto-assemblé.

Le manuscrit de thèse se compose de quatre chapitres. Le premier chapitre présente l'état de l'art de l'auto-assemblage d'hydrogels à base de peptides ou molécules à bas poids moléculaire. Pour comprendre ce procédé nous avons résumé quels facteurs structuraux et environnementaux sont impliqués. Ces paramètres sont déterminants dans la programmation de l'auto-assemblage de peptides *via des* interactions supramoléculaires.

Le deuxième chapitre décrit le matériel et les méthodes utilisées au cours de cette thèse. Les chapitres trois et quatre exposent deux stratégies distinctes d'auto-assemblage enzymatique en surface. Ces deux procédés de gélification sont basés sur l'utilisation d'une surface enzymatique capable d'induire l'auto-assemblage de peptides et de contrôler la croissance des fibres depuis la surface. L'enzyme confinée en surface transforme des

précurseurs peptidiques inertes en gélateurs capables de s'auto-assembler sous la forme de nanofibres (Figure 1).

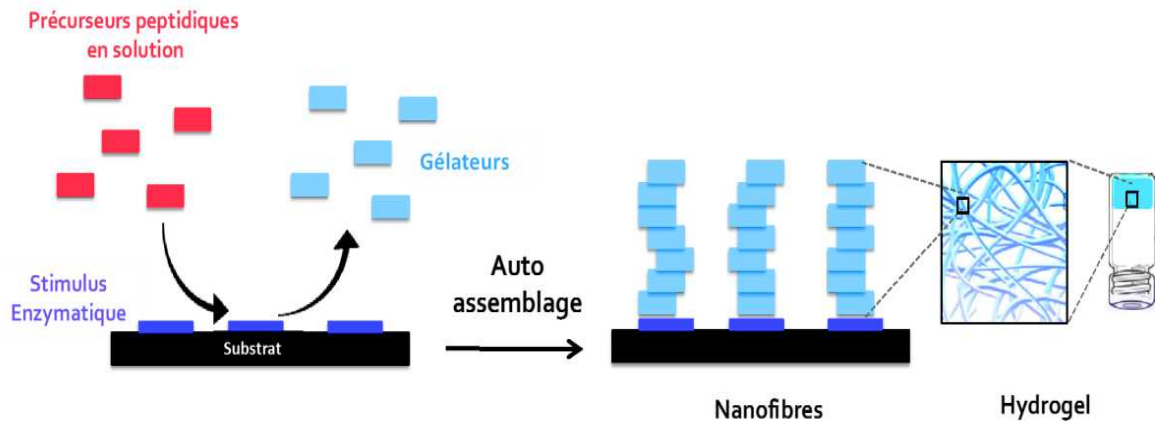


**Figure 1:** Représentation schématique de la formation d'un hydrogel obtenu par auto-assemblage de précurseurs peptidiques. Au contact d'une surface modifiée présentant une enzyme, ces précurseurs sont transformés en gélateurs efficaces.

Deux stratégies permettant le contrôle d'un processus d'auto-assemblage à partir de la surface sont envisagées :

- Le premier système catalyse la **formation de liaisons covalentes** entre des précurseurs peptidiques pour former des chaînes courtes d'acide aminés. L'auto-assemblage de ces oligopeptides au voisinage de la surface est un processus dépendant de la concentration. Si celle-ci est suffisamment importante (*concentration critique de gélation*), la formation des nanofibres se produit alors spontanément à partir de la surface et engendre la croissance d'un gel.
- Dans le second système, l'**hydrolyse de groupements chimiques** spécifiques, présents dans la structure de précurseurs peptidiques, induit l'auto-assemblage du gel. Dans les conditions utilisées, l'enzyme confinée en surface ne permet pas de produire suffisamment de peptides gélateurs, à partir des peptides précurseurs. Pour atteindre la concentration critique de gélation à proximité de la surface, des «

peptides initiateurs» ont été immobilisés à la surface du film enzymatique en utilisant un polyélectrolyte fonctionnalisé.

## 1. L'état de l'art : Auto-assemblage de peptides en solution

Une grande diversité de petites molécules comme les acides nucléiques, les sucres et autres dérivés de composés aromatiques peuvent être choisis pour former un hydrogel. Parmi eux, les peptides composés d'acides aminés sont des molécules de choix. La vingtaine d'acides aminés naturels existant proposent un large choix de fonctions latérales impliquées dans la formation de liaisons intra- ou inter- moléculaires ou covalentes source d'une organisation sous forme de structures secondaires (hélices, feuilletts, etc...). Cette organisation conduit à la formation d'un grand nombre d'objets nanométriques : fibres, tubes, sphères ou feuilletts (Figure 2)

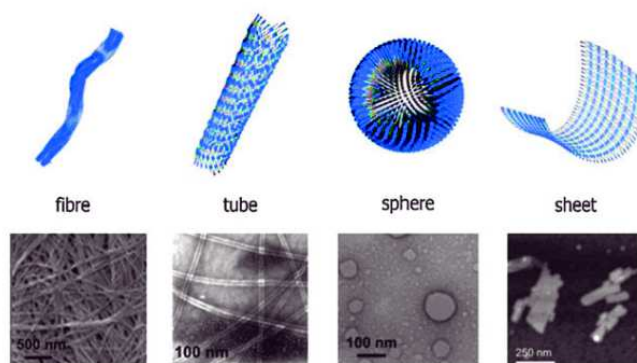


**Figure 2 :** Exemples de nanostructures supramoléculaires obtenues via un auto-assemblage supramoléculaire.

Les séquences peptidiques impliquées dans le processus d'auto-assemblage sont souvent décrites comme étant des molécules amphiphiles. Elles sont constituées de régions hydrophiles augmentant la solubilité des molécules dans l'eau et de régions hydrophobes qui accroissent les interactions entre les gélateurs. Ainsi la conception des séquences a un effet sur la hiérarchisation de l'auto-assemblage. Par conséquent, le juste équilibre doit être trouvé entre les propriétés hydrophobes et hydrophiles du peptide amphiphile. Ce

manuscrit présente une liste non exhaustive de trois catégories de peptides amphiphiles : les peptides aliphatiques, alternés, et aromatiques (Figure 3).

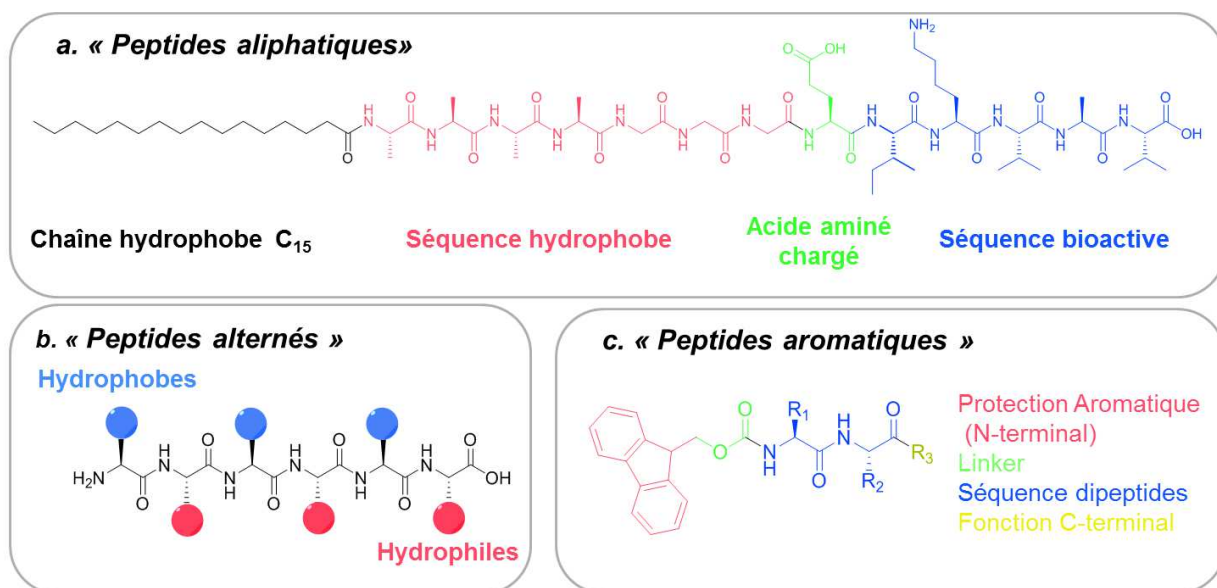


**Figure 3 :**(a) Séquence moléculaire de peptides amphiphiles aliphatiques (b) structure de peptides amphiphiles alternés, (c) Structure générique de peptides amphiphiles aromatiques constituée de 4 segments.

### Peptides aliphatiques amphiphiles

Ces peptides amphiphiles sont des molécules linéaires présentant une tête hydrophile et une queue hydrophobe avec quatre régions caractéristiques (Figure 3a) : La région 1 est impliquée dans la formation d'interactions de type van der Waals, la région 2 est une séquence hydrophobe, la région 3 améliore la solubilité globale du peptide et la région 4 peut être ajoutée pour jouer un rôle de vecteur biologique. Des micelles cylindriques et sphériques ou des structures lamellaires sont quelques exemples de nano-objets qui s'auto-assemblent en solution. Malgré la complexité de tels systèmes chimiques, ce type de peptides amphiphiles requiert une stratégie de synthèse sur support solide.

### Peptides amphiphiles alternés

Cette deuxième classe est caractéristique de séquences peptidiques alternant résidus acides aminés polaires et non polaires (Figure 3b). Ces séquences sont également nommées peptides amphipathiques.<sup>3</sup> Ils s'auto-assemblent sous forme de feuillets  $\beta$  formant des fibres.

L'organisation de ces structures primaires est dirigée par la ségrégation des chaînes latérales hydrophiles et hydrophobes conduisant à la formation de structures secondaires en bicouche. En milieu aqueux, les chaînes latérales hydrophiles sont alors exposées au solvant tandis que les résidus hydrophobes se regroupent pour former un « feuillet interne ». Zhang *et al.* ont pour la première fois décrit que l'auto-assemblage de ces peptides sous forme de feuillets  $\beta$  et fibres pouvait mener à la formation d'hydrogel.<sup>4</sup> Dans ces systèmes, la propension d'assemblage des peptides semble être dépendante de la séquence alternée choisie, de leur concentration et des facteurs environnementaux tels que le pH.<sup>5</sup>

### *Peptides amphiphiles aromatiques*

En parallèle du développement de peptides aliphatiques et amphipatiques, une troisième catégorie de peptides a été décrite pour la première fois par Vergner en 1995. Cette classe regroupe de courtes séquences peptidiques comprenant des acides aminés et des groupements protecteurs aromatiques (Figure 3c). Depuis une dizaine d'années, l'intérêt pour ce type de peptides grandit notamment grâce aux investigations de Bing Xu, qui ont mises en évidence l'auto-assemblage de cette catégorie de peptide en 2004.<sup>6</sup> Par analogie avec les peptides aliphatiques, les propriétés amphiphiles de ces séquences reposent sur quatre régions clés : Un groupement aromatique protecteur placé en position N-terminal, une liaison entre le groupement aromatique et la séquence peptidique qui peut être fonctionnalisée en C-terminal.

## **2. Auto-assemblage d'oligomères peptidiques contrôlé par une enzyme en surface**

Le premier système que nous avons étudié catalyse la **formation de liaisons covalentes** entre des précurseurs peptidiques pour former des chaînes courtes d'acide aminés. Nous avons choisi l' $\alpha$ -chymotrypsine comme enzyme modèle. En milieu basique, cette enzyme<sup>7</sup> est capable de catalyser la formation d'une liaison amide (CO-NH) entre les dipeptides lysine-leucine éthyle ester (KLOEt) (Figure 4a). Les chaînes oligopeptidiques  $(KL)_nKLOEt$  (avec  $4 \leq n \leq 7$ ) formées sont capables de s'auto-assembler en feuillets  $\beta$  via des liaisons hydrogènes et par des interactions hydrophobe.



quelques minutes (Figure 4b, courbe bleue). Ce phénomène est liée au processus d'auto-assemblage des oligopeptides  $(KL)_nKLOEt$  depuis la surface enzymatique ( $\alpha$ -chymotrypsine). Le suivi cinétique de l'auto-assemblage, par spectroscopie infrarouge à transformée de Fourier en mode réflexion totale atténuée, indique une organisation structurée en feuillets  $\beta$  de l'hydrogel obtenu. En remplaçant l' $\alpha$ -chymotrypsine par l'albumine (protéine non enzymatique), aucune variation de fréquence n'est observée lorsque la surface est au contact de la solution de KLOEt (Figure 4b courbe noire).

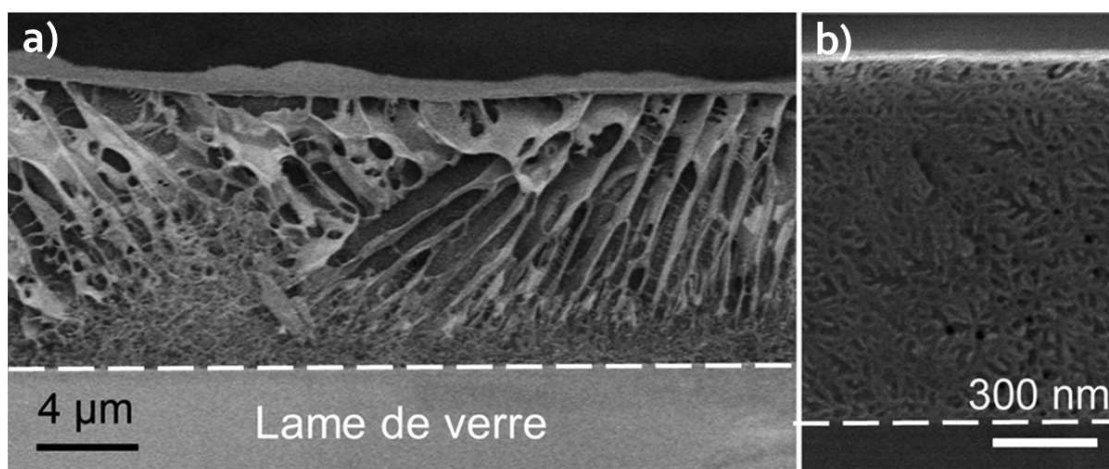


**Figure 5** : Images de cryo-microscopie électronique à balayage (a) d'une section de gel de  $(KL)_nOEt$  obtenue après contact avec la solution de KLOEt ( $1mg.mL^{-1}$ ) pendant 12 h (b) d'une partie de la section du gel ayant une forte densité de nanofibres interpénétrées localisées à la surface.

Pour caractériser la morphologie de l'hydrogel à base d'oligopeptides  $(KL)_nOEt$  une section en z de l'échantillon a été imagée par cryo-microscopie électronique à balayage. L'échantillon a été rapidement congelé dans un bain d'azote liquide et ensuite placé sous vide, à basse température dans une chambre reliée au microscope électronique. Comme le montre la Figure 5a, un revêtement hétérogène recouvre la totalité de la surface. Le gel de  $(KL)_nOEt$  atteint à certains endroits une épaisseur d'environ 12 µm et à d'autres seulement 1 µm. On observe sur la coupe deux morphologies distinctes: une zone de fibres dense, ancrée et proche de la surface, et au-delà de 2 µm d'épaisseur un réseau de fibres moins dense avec de larges cavités orientées. Les fibres de  $(KL)_nOEt$  semblent être enchevêtrées sans points d'attache, ce qui suggère une organisation proche du gel physique (figure 5b). Les cavités observées sont considérées comme des artefacts dus à la présence de cristaux

de glace formés lors de la congélation de l'échantillon qui sont favorisées par la faible densité du gel lorsque l'on s'éloigne de la surface enzymatique. En effet à une concentration plus faible en KLOEt ( $< 1\text{mg/mL}$ ), produisant moins d'oligopeptides au contact de la surface enzymatique et donc un hydrogel moins dense, les cavités se retrouvent dans la totalité de la section du gel.

Afin de contrôler l'auto-assemblage des oligopeptides en surface, deux paramètres ont été étudiés : la concentration en précurseur peptidique et la densité surfacique en  $\alpha$ -chymotrypsine. Lorsque la densité de surface en enzyme est de 100%, une concentration en précurseur peptidique, KLOEt, supérieure ou égale à  $0.4\text{ mg/mL}$  est nécessaire pour obtenir la formation de l'édifice supramoléculaire (Figure 6a, courbes rouge, bleue et verte). Le temps de « nucléation », temps à partir duquel la fréquence de résonance augmente significativement, diminue avec l'augmentation de la concentration en KLOEt utilisée.

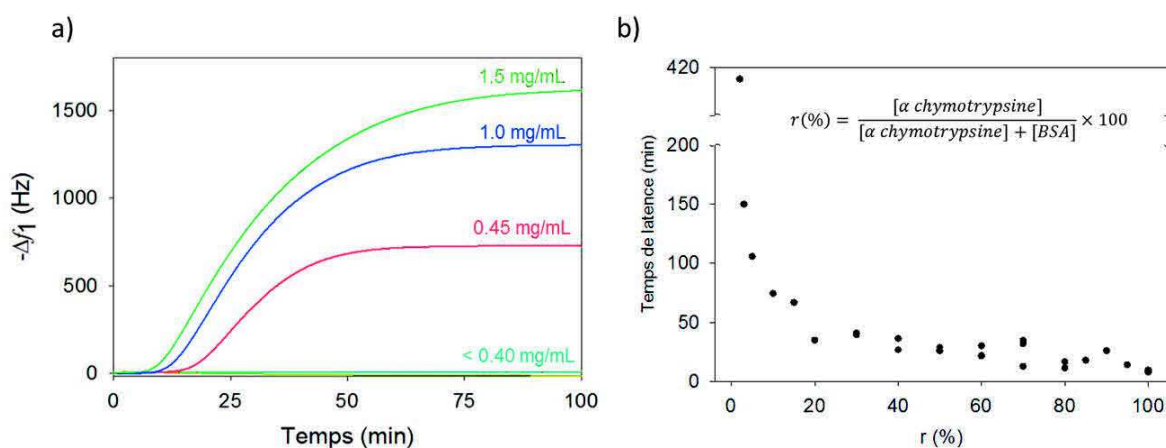


**Figure 6 :** (a) Evolution de l'opposée de la fréquence fondamentale de résonance, mesurée par QCM, lors du contact du film PEI/AcT/ $\alpha$ -chymotrypsine avec une solution de KLOEt à différentes concentrations; (b) Evolution du temps de nucléation pour différents ratios  $r$  (%) d' $\alpha$ -chymotrypsine adsorbés en surface au contact avec une concentration de  $1\text{ mg/mL}$  de KLOEt.

Pour une concentration de  $1\text{ mg/mL}$  en KLOEt, la densité surfacique d' $\alpha$ -chymotrypsine a été modifiée en adsorbant en surface un mélange d' $\alpha$ -chymotrypsine/albumine à différents ratios  $r$  (%). Lorsque la surface est entièrement fonctionnalisée par l' $\alpha$ -chymotrypsine ( $r = 100\%$ ), l'auto-assemblage est obtenu au bout

d'environ 5 minutes (Figure 6b) alors qu'avec 5% en densité surfacique d'enzyme, le temps de nucléation augmente jusqu'à 400 minutes. Par conséquent, la variation de la concentration surfacique en  $\alpha$ -chymotrypsine et la concentration en substrat KLOEt permettent de contrôler la cinétique de nucléation et d'auto-assemblage peptidique.

### 3. Auto-assemblage de peptides depuis une surface contrôlé par une couche d'ensemencement

Dans le second système, l'**hydrolyse de groupements chimiques** spécifiques, présents dans la structure de précurseurs peptidiques, induit l'auto-assemblage du gel. Cette approche utilise la phosphatase alcaline (PA)<sup>8</sup> comme enzyme modèle. Le substrat peptidique original conçu est le Fmoc-FFY-PO<sub>4</sub><sup>2-</sup> hydrolysé par la PA en Fmoc-FFY (Figure 7). Ce dernier s'auto-assemble spontanément en nanofibres d'environ 10 nm de diamètre qui engendrent la formation d'un hydrogel. La présence d'interactions de van der Waals, d'empilements  $\pi$ - $\pi$  et l'effet hydrophobe assure la cohésion des peptides Fmoc-FFY entre eux.

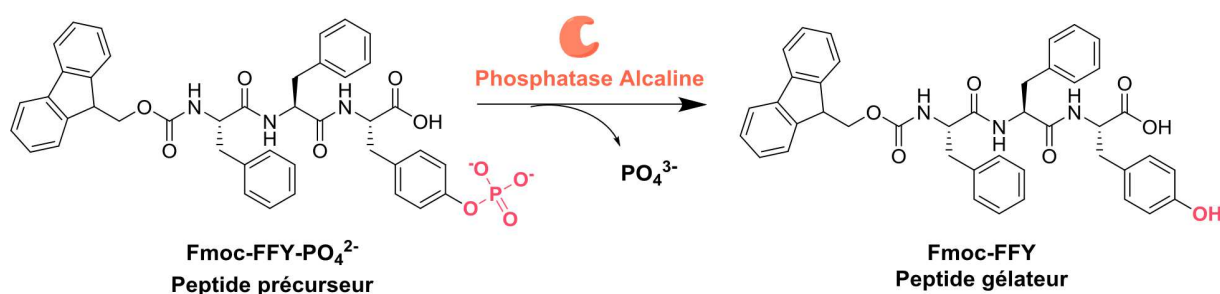


**Figure 7 :** Transformation enzymatique du précurseur peptidique Fmoc-FFY-PO<sub>4</sub><sup>2-</sup> en Fmoc-FFY catalysée par la phosphatase alcaline.

L'originalité de cette seconde stratégie réside non seulement dans l'utilisation d'un procédé de gélification localisé en surface par voie enzymatique, mais surtout dans le développement d'une surface comme outil permettant le contrôle de l'auto-assemblage fibrillaire dans l'espace. En effet, la couche enzymatique est recouverte d'un revêtement polymérique qui présente une concentration surfacique en initiateurs peptidiques variable.

Cette couche est un outil d'ensemencement à l'origine d'un assemblage local des gélateurs sur la surface contrairement au système de l' $\alpha$ -chymotrypsine (Figure 8).

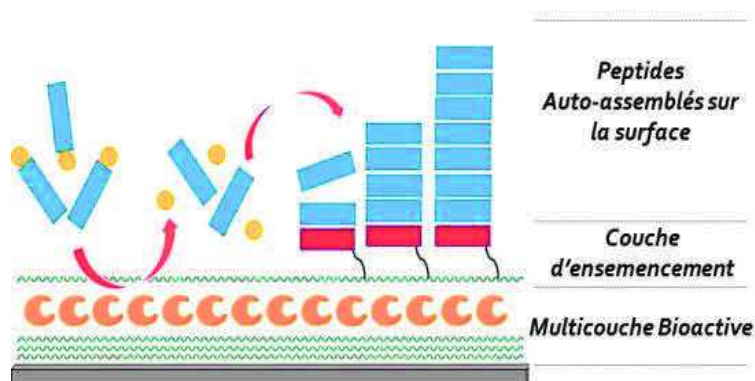


**Figure 8** : Représentation schématique d'un auto-assemblage peptidique induit par une réaction enzymatique qui s'opère en surface, proche d'une couche d'ensemencement.

Afin d'immobiliser la PA, la multicouche PEI-(PAA/PAH)<sub>3</sub> (PAA : poly(acide acrylique) chargé négativement et PAH : poly(allylamine hydrochloride) chargé positivement) a été construite. Après adsorption de la PA, deux polymères d'ensemencement ont été synthétisés : le premier est un polymère *initiateur*, PAA-CFF-Fmoc, correspondant à l'acide polyacrylique fonctionnalisé à 5% par des fonctions peptidiques gélifiant. Son rôle est d'augmenter la densité locale de peptides gélifiants lorsqu'il est adsorbé en surface. Le second polymère, PAA-CGGG-Fmoc, est également un dérivé d'acide polyacrylique mais modifié par un peptide non gélateur, incapable de s'auto-assembler avec le peptide Fmoc-FFY. Le mélange de ces deux polymères, PAA-CFF-Fmoc et PAA-CGGG-Fmoc, à différents ratios (r) d'ensemencement, permet de contrôler la densité surfacique en peptide initiateur. Une fois la multicouche enzymatique construite PEI-(PAA/PAH)<sub>3</sub>/PA/PAH/(PAA-CFF-Fmoc/PAA-CGGG-Fmoc) sur un substrat, celle-ci est mise en contact avec le peptide précurseur Fmoc-FFY-PO<sub>4</sub><sup>2-</sup>. La proportion de peptides actifs Fmoc-FFY générée depuis la surface, additionnée à celle provenant de la couche d'ensemencement permet d'atteindre une concentration (*critique*) locale telle que la gélation se produit exclusivement depuis la surface du matériau modifié. Sans la présence de la couche d'ensemencement, aucune gélation n'est observée.

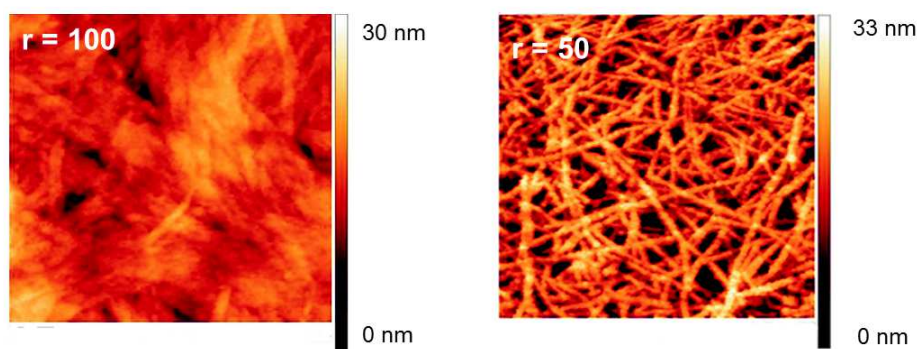


**Figure 9** : Images AFM de la surface après injection de  $Fmoc-FFY-PO_4^{2-}$  à différents taux d'ensemencement  $r$  ( $r = 50\%$  et  $r = 100\%$ ).

La vitesse de croissance de fibres de peptides, leur morphologie ainsi que leur degré d'enchevêtrement peuvent être modulés par la densité surfacique de sites d'ensemencement et/ou d'enzymes. Les images de microscopie à force atomique (AFM) montrent qu'à un ratio  $r = 50\%$  équivalent en PAA-CFF-Fmoc et PAACGGG-Fmoc, le réseau de fibres est beaucoup moins dense que pour une surface uniquement fonctionnalisée avec PAA-CFF-Fmoc ( $r = 100\%$ ) (Figure 9).

## Conclusion

La recherche dans le domaine des systèmes chimiques auto-assemblés se focalise sur la conception d'architectures complexes organisées depuis la surface. C'est dans ce contexte que nous avons développé deux types de revêtement de surface capable d'initier un contrôle dans le temps et dans l'espace d'interaction chimiques entre des gélateurs chimiques et leur environnement. Nous avons conçu et développé deux types de nanofilms enzymatique en surface grâce à la méthode du « couche par couche ». Ce film enzymatique précurseur peut induire la transformation chimique de peptides en composés pouvant s'auto-assembler. En ajustant la composition de ces films précurseurs enzymatiques, il est possible d'influencer le procédé de nucléation, la croissance et la structure de l'hydrogel, exclusivement à la surface.

Depuis octobre 2013, j'ai pu développer deux approches basées sur le procédé d'auto-assemblage de peptides assisté par une enzyme. Dans une première approche, j'ai décrit l'auto-assemblage de peptides assisté par l' $\alpha$ -chymotrypsine immobilisée en surface

via des interactions électrostatiques et des liaisons hydrogènes. Ce stimulus enzymatique localisé catalyse la condensation de peptides *KLOEt* pour former des oligomères  $(KL)_nOEt$ . Ces oligomères sont graduellement libérés depuis la surface et s'auto-assemblent sous forme de nanofibres croissants depuis la surface. Cette stratégie permet d'ajuster l'amplitude et la cinétique d'auto-assemblage en modifiant la concentration initiale de *KLOEt* ou la densité d' $\alpha$ -chymotrypsine immobilisée en surface.

Dans une deuxième partie, j'ai développé un film regroupant les propriétés catalytiques d'une enzyme et la capacité d'ensemencement de peptides hydrogélateurs initiant leur auto-assemblage exclusivement en surface. Cette multicouche bioactive d'ensemencement est chargée en alcaline phosphatase et catalyse la formation du peptide gélateur Fmoc-FFY à proximité de la surface. Une séquence Fmoc-FFC dite « initiatrice » est également greffée sur un polymère pour ensuite être déposée à la surface du film enzymatique. Cette couche d'amorce a été utilisée pour créer un motif local d'agrégation. Le film enzymatique assure continuellement la transformation chimique de peptide en hydrogélateur et la couche d'ensemencement, le contrôle spatiale de la nucléation de l'auto-assemblage. En l'absence de la couche d'ensemencement, aucun phénomène de gélation n'a été observé. Par conséquent, nous avons développé un revêtement bioactif intelligent qui induit l'auto-assemblage d'un réseau de fibres permettant son contrôle spatiotemporel. Ces travaux pourront apporter une contribution significative à l'élaboration de nouveaux matériaux intelligents nanostructures toujours plus sophistiqués.

## Bibliographie

1. Decher, G. Fuzzy nanoassemblies: Toward layered polymeric multicomposites. *Science* **1997**, 277 (5330), 1232.
2. Rydzek, G.; Parat, A.; Polavarapu, P.; Baehr, C.; Voegel, J.-C.; Hemmerlé, J.; Senger, B.; Frisch, B.; Schaaf, P.; Jierry, L.; Boulmedais, F. One-pot morphogen driven self-constructing films based on non-covalent host-guest interactions. *Soft Matter* **2012**, 8 (2), 446.
3. Bowerman, C. J.; Nilsson, B. L. Review self-assembly of amphipathic  $\beta$ -sheet peptides: Insights and applications. *Peptide Science* **2012**, 98 (3), 169.
4. Zhang, S.; Holmes, T.; Lockshin, C.; Rich, A. Spontaneous assembly of a self-complementary oligopeptide to form a stable macroscopic membrane. *Proceedings of the National Academy of Sciences* **1993**, 90 (8), 3334.
5. Lee, N. R.; Bowerman, C. J.; Nilsson, B. L. Effects of Varied Sequence Pattern on the Self-Assembly of Amphipathic Peptides. *Biomacromolecules* **2013**, 14 (9), 3267.
6. Yang, Z.; Xu, B. A simple visual assay based on small molecule hydrogels for detecting inhibitors of enzymes. *Chem. Commun. (Cambridge, U. K.)* **2004**, (21), 2424.
7. Qin, X.; Khuong, A. C.; Yu, Z.; Du, W.; Decatur, J.; Gross, R. A. Simplifying alternating peptide synthesis by protease-catalyzed dipeptide oligomerization. *Chemical Communications* **2013**, 49 (4), 385.
8. Yang, Z. X., Keming; Guo, Zufeng; Guo, Zhihong; Xu, Bing. Intracellular enzymatic formation of nanofibers results in hydrogelation and regulated cell death. *Adv Mater* **2007**, 19, 3152.
9. Vigier-Carrière, C.; Garnier, T.; Wagner, D.; Lavalle, P.; Rabineau, M.; Hemmerlé, J.; Senger, B.; Schaaf, P.; Boulmedais, F.; Jierry, L. Bioactive Seed Layer for Surface-Confined Self-Assembly of Peptides. *Angewandte Chemie International Edition* **2015**, n/a.

# Contrôle de l'auto-assemblage de peptides par une surface modifiée

## Résumé:

*Mots clés : Peptides, Auto-assemblage, Hydrogel, Enzyme, Confinement en Surface, Couche-par-couche*

Depuis quelques années, la modification de surface est une méthode efficace qui permet de contrôler les interactions entre un matériau et son environnement. Ce domaine de recherche ouvre la voie au développement de nouvelles surfaces « intelligentes » aux propriétés fonctionnelles. Dans ce manuscrit, nous présentons la conception d'un revêtement capable de contrôler l'auto-assemblage de peptides exclusivement à la surface d'un matériau. L'auto-assemblage est initié par un stimulus enzymatique localisé à la surface qui permet la transformation de peptides précurseurs en peptides gélateurs, ayant la propriété de s'auto-assembler pour former des structures fibrillaires enchevêtrées bases d'hydrogels. Les surfaces enzymatiques ont été obtenues par adsorption d'enzyme spécifique en utilisant la méthode « couche par couche ». Dans une première approche, la croissance du réseau de fibres est initiée par accumulation d'oligopeptides  $(KL)_nOEt$  confinés sur le film enzymatique d' $\alpha$ -chymotrypsine. Ce processus d'hydrogélation peut être contrôlé dans le temps (en ajustant le temps de latence) en changeant la concentration en peptides  $KLOEt$  et la densité de surface en enzyme. Dans une deuxième approche, le film multicouche bioactif contenant l'alkaline phosphatase a été fonctionnalisé par une couche d'ensemencement composée d'acide poly(acrylique) modifié par une séquence peptidique Fmoc-FFC aux propriétés gélatrices. La modification de la densité de peptides gélatrices en surface a permis de contrôler le processus d'auto-assemblage du peptide gélateur Fmoc-FFY depuis la surface. Lorsque le film bioactif est mis en contact avec le peptide précurseur, i.e. Fmoc-FFY( $PO_4^{2-}$ ) substrat de l'alkaline phosphatase, le peptide gélateur se forme et s'auto-assemble sous forme de nanofibres à partir de la surface. Grâce à ces deux études nous avons démontré qu'un film précurseur enzymatique ou une couche bioactive d'ensemencement sont des matériaux permettant d'initier et de contrôler l'auto-assemblage de peptides en surface afin de former un hydrogel.

## Abstract:

*Keywords: Peptides, Self-Assembly, Hydrogel, Enzyme, Surface Confined, Layer-by-layer*

Since the middle of the last century, the functionalization of surfaces has emerged as a convenient method to control interactions between a material and its surrounding environment. This recent research field paves the way to the design of surfaces bearing original “smart” functionalities. Herein, we present the design and control of peptide self-assembly taking place exclusively at or near a surface in response to an enzymatic stimulus. The *localized enzyme-assisted self-assembly* (LEASA) of peptides led to the growth of micrometric hydrogels from the surface. The enzymatic surface was obtained by adsorption of specific enzymes using the layer-by-layer method. In a first strategy, we developed the growth of fibrillary networks resulting from the accumulation of oligopeptides  $(KL)_nOEt$  produced from a confined enzymatic layer of  $\alpha$ -chymotrypsine at the interface. This process of gelation was tuned in time (lag time) by controlling the peptide  $KLOEt$  concentration and the enzymatic surface density. In a second strategy, alkaline phosphatase was embedded into a multilayer film to obtain a bioactive surface on which a *seed-layer*, i.e a poly(acrylic acid) covalently modified with a hydrogelator peptide, was adsorbed. This layer allows to control the self-assembly of the fiber network by changing the peptide density anchored on the seed layer. When this *bioactive and seeding film* is brought into contact with the peptide substrate, i.e. Fmoc-FFY( $PO_4^{2-}$ ), of alkaline phosphatase, an efficient self-assembly of Fmoc-FFY is obtained leading to nanofibers growing from the surface. We demonstrated that an enzymatic precursor film or a more sophisticated bioactive seeding layer can self-instruct the self-assembly of small peptides sequences and influence buildup of a micrometric hydrogel from the surface.